Estimation of waves and ship responses using onboard measurements

Montazeri, Najmeh

Publication date:
2016

Document Version
Publisher's PDF, also known as Version of record

Technical University of Denmark

Estimation of waves and ship responses using onboard measurements

Najmeh Montazeri

Technical University of Denmark
Department of Mechanical Engineering
Section of Fluid Mechanics, Coastal and Maritime Engineering

Preface

This thesis is submitted as a partial fulfilment of the requirements for the degree of Doctor of Philosophy in Mechanical Engineering at the Technical University of Denmark (DTU). The research was conducted at the Section of Fluid Mechanics, Coastal and Maritime Engineering, Department of Mechanical Engineering between March 2013 and March 2016 under the supervision of Associate professor Ulrik Dam Nielsen and Professor Jørgen Juncher Jensen.

The project was financed by DTU and NK classification society. Class NK also supported the project providing full-scale data and hydrodynamic data for an in-service container ship. Their interest, discussions and support throughout the project are gratefully acknowledged.

I wish to thank Associate professor Ulrik Dam Nielsen for his valuable guidance and good support. It was also my honour to work with Professor Jørgen Juncher Jensen during the three years. My gratitude goes to him for his precious advice, inspiring discussions, and for being always approachable.

Many thanks to the very good colleges at DTU, especially Sopheak Seng, Ingrid Marie Vincent Andersen, Mostafa Amini Afshar, Ju-hyuck Choi and Robert Read, for discussions and their assistance, and also Yasaman Mirsadraee, Stavros Kontos and Pelle Bo Regener. With their positive attitudes and support, they all made my working environment very friendly.

I would like to acknowledge the TULCS project partners, the Maritime Research Institute Netherlands (MARIN) and the Bureau Veritas. The in-house full-scale data and hydrodynamic data that I used in my thesis were provided by them.

I also appreciate my family's support and encouragement with regard to my studies and especially this PhD accomplishment.

Abstract

This thesis focuses on estimation of waves and ship responses using shipboard measurements. This is useful for development of operational safety and performance efficiency in connection with the broader concept of onboard decision support systems.

Estimation of sea state is studied using a set of measured ship responses, a parametric description of directional wave spectra (a generalised JONSWAP model) and the transfer functions of the ship responses. The difference between the spectral moments of the measured ship responses and the corresponding theoretically calculated moments formulates a cost function. A set of wave parameters, characterising the directional wave spectrum, is estimated through an optimisation problem using global search basin with proper constraints. This approach applies a sequential partitioning procedure, which is able to classify swell and wind sea events using wind information.

The model is tested on simulated data based on known unimodal and bimodal wave scenarios. The wave parameters in the output are then compared with the true wave parameters. In addition to the numerical experiments, two sets of full-scale measurements from container ships are analysed. Herein, the validation of the estimation method is assessed by comparing the results with the wave data from other tools, such as wave radar data and hindcast data. The results show that the developed method is reasonably accurate.

Automatic selection of a set of responses to be used for wave estimation is also studied using a sensitivity analysis of the wave parameters. This selection depends on the waves and the operational condition of the ship. Therefore, the method can be utilised based on initial knowledge about the waves and the operational condition in a specific location.

A dynamic trend model is proposed for tracking the evolution of the wave parameters during the voyage. This provides a prediction of the wave parameters, e.g. 20 minutes ahead of the measurements. Given the predicted parame-

ters, a wave spectrum model and the transfer functions, forecasts of different wave-induced responses are made. The predicted variances of the responses are compared with actual measurements. The relatively good agreement in this comparison validates the model and the optimisation method. Finally, an uncertainty analysis of the presented approach is implemented to assess the reliability of the method.

Resume

Nærværende rapport omhandler estimering af bølger og skibes respons ved hjælp af ombordmålinger foretaget på det aktuelle skib. Denne viden kan/skal bruges til udvikling af (drifts)sikkerhed og optimering af ydeevne, eksempelvis samlet i et integreret beslutningsstøttesystem.

Estimering af søtilstanden undersøges ved hjælp af et sæt af målte skibesrespons, en parametrisk beskrivelse af et retningsbestemt bølgespektrum (en generaliseret JONSWAP model) og overføringsfunktioner for skibes respons. Forskellen mellem de spektrale momenter af de målte skibsrespons og de tilsvarende teoretisk beregnede momenter udgør en cost-funktion. Et sæt af bølgeparametre, der karakteriserer det retningsbestemte bølgespektrum er blevet estimeret gennem en optimering ved hjælp af global søgning. Denne fremgangsmåde anvender en sekventiel partitionering procedure, som er i stand til at klassificere dnninger og vindbølger ved hjælp af vind oplysninger.

Modellen testes på simuleret data genereret ud fra kendte unimodale og bimodale bølgescenarier. De estimerede bølgeparametre i outputtet bliver så sammenlignet med de sande bølger. Udover de numeriske eksperimenter, analyseres to sæt fuldskalamålinger fra containerskibe. I denne analyse vurderes valideringen af modellen ved at sammenligne resultaterne med bølgedata fra andre værktøjer, eksempelvis data fra bølgeradar og hindcast studier. Resultaterne viser, at den udviklede metode giver tilfredsstillende estimeringer med god effektivitet.

Automatisk valg af responskombination skal bruges til bølgeestimering. Dette emne studeres ved hjælp af en sensitivitetsanalyse af bølgeparametre over for de forskellige respons. Dette valg afhænger af bølger og skibets operationelle tilstand. Derfor kan fremgangsmåden anvendes baseret på indledende viden om bølger og den operationelle tilstand på en bestemt placering.

En dynamisk trendmodel foreslås til sporing af udviklingen i bølgeparametre under skibets sejlads. Modellen tilvejebringer en forudsigelse af bølgeparametre,

f.eks 20 minutter forud for målingerne. Ved at bruge af de forudsagte parametre, et givent bølgespektrum og overføringsfunktioner, kan forskellige bølgeinducerede respons forudsiges. De predikterede responsvarianser sammenlignes med faktiske målinger. Den relativt gode overensstemmelse i denne sammenligning validerer modellen og optimeringsmetoden. Endelig implementeres en usikkerhedsanalyse af den præsenterede metode for at vurdere pålideligheden af modellen.

Contents

Chapter 1

Introduction

1.1 Objective of Decision Support Systems

Operational performance management of ships is one of the main concerns in the shipping industry. Many newly-built vessels and marine structures are equipped with data collection systems that are able to provide engine and hull performance monitoring. These data, including actual fuel consumption, speed, loading condition, environmental data, propulsion power, etc., are being used for optimisation of operational conditions; i.e. engine setting, navigation and loading conditions. With increasing concerns about energy consumption and gas emissions from ships, decision support systems are nowadays available to advise on how to operate the ship within acceptable limits. Optimal ship operational performance and route optimisation are thereby ensured with minimised fuel costs within an acceptable time frame.

The effect of waves degrade a ship's operational efficiency to some extent. Added resistance due to waves enforce additional trust to achieve the desired speed. Moreover, accidents occur due to unexpected and dangerous sea states, which can make the crew unable to keep the ship under proper control. Therefore, besides optimising the ship for a minimum fuel consumption, safety of crew/passengers, cargoes and the ship itself should be considered. For these purposes, in addition to the above-mentioned data, a performance system needs collection/estimation of environmental data, typically sea state information.

Continuous measurement of ship responses (autologging) and making a monitoring system available are recommended for decision support systems. A set of accelerometers and strain gauges can be installed onboard the ship to measure

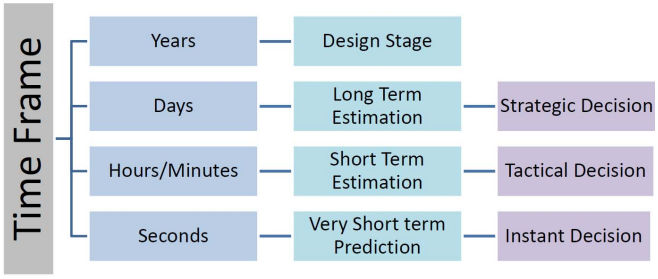

Figure 1.1: Categories of decision support based on time frames.

motions and structural loads. The advantage of those measurements will be discussed further in this chapter.

The decisions must be made in such a way that a reasonable safety level is ensured while the costs are minimised. This is, of course, an extremely complex task because of the large number of scenarios to be considered and the large uncertainty associated with each scenario. In order to establish a more efficient system, definition and quantification of the associated risks are helpful. The decision making can then be carried out under a consideration of risk acceptance criteria.

The concept of decision support systems for ships can be categorised based on the time frame of the estimations/predictions. Those categories are outlined in Figure 1.1 and explained in the following sections. They may, however, have overlap in actual performance analysis.

1.2 Decision Support in Design Stage

At the design stage, the time frame is usually the intended design life of ships. Full-scale measurements of ships are useful for controlling the validity of the theoretical models and the assumed conditions for response calculations, and for assessing the accuracy of pre-operational predictions.

Response data provide the classification society with valuable insight into the ship's behaviour under realistic conditions. This information could be useful for modification of design parameters according to the actual operational profiles. A very important issue in this category is the rule requirement for hull girder strength capacity as the size of container ships are increasing and global

hydroelastic structural responses could be critical. In this regard, Andersen [2] has analysed several sets of full-scale measurements of strain in different container ships. The influence of wave-induced hull girder vibrations on vertical bending moment and fatigue damage is investigated in that study. Avoiding overall failure, such as hull girder damage or capsizing, is the main goal in the design stage.

1.3 Long-Term Decision Support

For long-term decision support, the time frame for estimations or predictions is usually between several days to a couple of months, depending on the type of operational guidance. The current ship performance systems in the industry dominantly provide long-term decision support. The associated strategic decisions relate to route planning, cleaning of hull and propeller, optimising propulsion power, operational draft, trim, etc. The system is developed to integrate the operational data with the wave data.

Therefore, the input in the long-term decision support is long-term information about waves and also full-scale records of ship responses. Probability distribution of sea state parameters and extreme value prediction of responses are accomplished. In an advanced system, the output plots could be basically similar to meteorological maps, which show geographical regions with dangerous zones and provide warning system based on probability analysis. This kind of information is useful for the majority of merchant ships and offshore structures.

Monitoring of propulsion, wave-induced motions and loads during voyages also provides valuable input to ship structural monitoring systems and determination of long-term ship operational profiles.

1.4 Short-Term Decision Support

1.4.1 Motivation

During the operations, various risks are faced due to rough waves. Probable hazards include parametric rolling, fatigue damage, loss or damage of cargo, seasickness, etc. Therefore, care should be taken not to face operational conditions with high risks of those accidents. This issue increases the motivation to provide ships with real-time operational guidance systems, the time frame of which is between 20 minutes to several hours depending on the operational

type. Expansion of decision support systems to include short-term navigational aid during the ship voyage could improve the efficiency and safety of voyages.

In the aforementioned short-term decision support, which is emphasised in this study, the trend of response measurements can be analysed to predict future risk events. However, the effect of changing operational parameters (speed, draft, course, ...) should be included. Therefore, on-site wave estimation is also required, according to which prediction of wave-induced responses such as longitudinal hull girder loading, fatigue damage, seakeeping performance (i.e. dynamic responses of the ship in a seaway) is accomplished. Moreover, prediction of weather changes in the near future can make the risk evaluations more reliable.

In addition to safety aspects, real-time wave information can become useful for prediction of added resistance, as mentioned before. Therefore, the excess fuel consumption and the propulsion of the ship can be estimated more accurately and consequently, the cost-effectiveness of the ship performance system can be improved as well.

1.4.2 Onboard wave estimation

Wave field data can be obtained using instruments, visual observations, or hindcast methods, i.e. numerical analysis of historical wave data. The average wave parameters i.e. the significant wave height, the peak period, the mean wave direction, and sometimes information about swell, can be obtained by these methods. Instrumental data can be collected by wave buoys or surface piercing instruments. Floating wave buoys are primary tools that are widely used for wave measurements, and they can provide rather accurate and reliable data. However, they are not practical for ship operations that may require precise sea state information in real-time and at the actual positions. Wave information can also be supported by satellite observations. Several investigations carried out in recent years indicate very promising results that support use of satellite data. According to investigations, over the range of significant wave heights 1-8 m, satellite altimeter-derived significant wave heights have been nearly as accurate as those obtained from surface buoy measurements [63]. Nevertheless, this method is near real-time and it is not financially efficient yet.

Due to the above-mentioned reasons, a delicate and fundamental part of decision support systems is onboard or so called ship-based estimation of the sea state at the exact position of the ship in the ocean. There are basically two methods for onboard wave estimation: Wave radar systems and estimation based on ship responses. Wave radars (e.g. WAVEX, WAMOS) provide directional wave spectra but infer wave height indirectly. Although this method is believed to

be an accurate method, the motions and the forward speed of the ship insert uncertainties to their estimates compared to using them from a fixed platform. Moreover, the estimate of wave period by wave radars can be compromised due to limitations in antenna revolution speed and image resolution. Those systems for recording the sea surface are under continuous development.

As an alternative to wave buoys, the ship itself can act as a wave rider buoy where response measurements are processed to give the sea state. This method, which is also known as Wave Buoy Analogy (WBA) has been recently explored in many research projects. It facilitates onboard estimations that require simple instrumentation and hardware including an ordinary set of accelerometers and possibly strain gauges connected to a PC. Thus, this method is less complicated and less expensive for wave estimation compared to other tools such as radar systems and satellites.

Numerical wave modelling produces output in the form of an energy spectrum. This energy spectrum is usually assigned a significant wave height calculated from the amount of energy in the spectrum, a peak (or zero upcrossing) period and a mean or dominant wave direction; which are all obtained from analysis of the energy spectrum. Those definitions describe the overall properties of the sea state. A general form of hydrodynamic models for analysis of different ship responses are usually represented in the frequency domain. Therefore, having the frequency-wise wave energy spectrum is very helpful for short-term analysis of ship responses.

1.4.3 The system framework

Figure 1.2 shows a logical architecture of short-term decision support. The main modules are the data processing and analysis module and the sea state estimator module. The data processing and analysis module can include data quality control, fault diagnosis, calibration, and filtering. Monitoring of the measurements can be available for arbitrary positions on the ship.

The above mentioned response-based wave estimation (WBA) provides the sea state estimation module in Figure 1.2. The fundamental input to this module is a set of filtered and digitised response signals in segments of several minutes, and the pre-calculated response functions (hydrodynamic data). These inputs set up equations, which relate the measured ship responses, on one side, with the wave energy spectrum through response functions, on the other side. From this relation, the principle is to minimise the difference between the two sides in terms of the least squares method. This concept and the formulations are explained in Chapter 2.

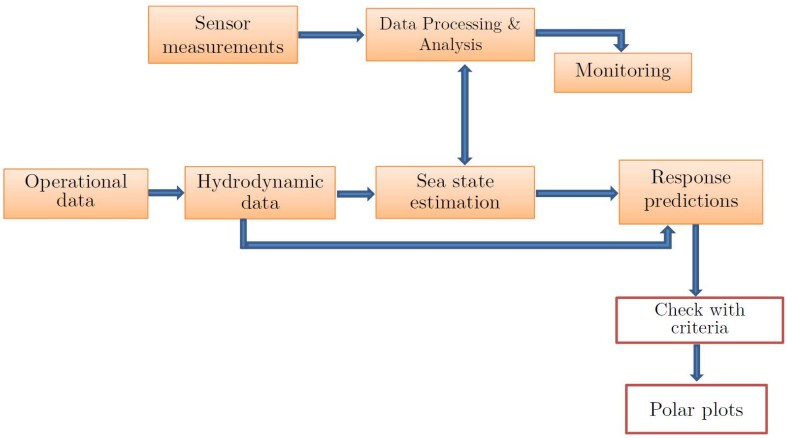

Figure 1.2: Short-term decision support.

The proper response functions are used again for prediction of the response spectra. The predicted responses are checked against predefined operational criteria. This comparison results in the construction of a polar plot, on which the areas with dangerous combinations of ship course and speed are indicated. The user is able to visualise danger zones for different phenomena by pressing the respective buttons on the user interface. It is also possible to raise a warning if the vessel is in a region with a critical wave induced extreme response, e.g. undue bending moment, excessive local accelerations, green water, etc. By changing the ship's course or speed, effective countermeasures can be identified and initiated to avoid potential hazards. In addition to course and speed changing, ballasting, and activating/deactivating motion control devices could be other risk control options to improve the efficiency.

For an efficient and reliable in-service monitoring system, it is important that the user interface is user-friendly and easily perceptible. A Danish joint project 'SeaSense' applied a decision support system on several in-service ships with monitoring system and graphical user interface. For more information about the project and sample polar plots see [35].

1.5 Very Short-Term Decision Support

Real-time prediction of responses on the order of seconds ahead of measurements is important for various offshore operations, e.g. crane operations for shifting cargo between ships or mobile platforms, and helicopter landing. Another

application of this category may be instant decisions for operations of navy vessels.

Andersen et al. [3] have implemented prediction of stress signals in 5-15 seconds in advance. The procedure is applied on time series of full-scale strain measurements. Data processing and analysis are explained using different methods e.g. conditional processes, the autoregressive predictor method, and also a method based on superposition of sinusoidal components. The results are then compared to the actual measurements, which are generally fair for predictions 5-10 seconds in the future.

Note that in this category, although the responses are induced by waves, the analysis is implemented independently of the wave spectrum. This is because the time intervals are short and non-stationary, and wave spectra cannot be used. The criteria here could be related to the absolute strength of the vessel or local accelerations (or motions) at any arbitrary point on the vessel e.g. helicopter deck. Considering these criteria, different risk control options can be used depending on the type of operation. This category of decision support is, however, not studied in this project.

1.6 Present Contribution

This thesis focuses on real-time wave estimation to be used for short-term decision support. The estimation method that is used in this approach is based on measured ship responses onboard the ship. The problem is formulated using a standard JONSWAP wave spectrum. The wave parameters inside the spectrum are estimated through an optimisation. The method is capable of categorising wind-sea and swell systems using onboard measurements. The proposed method is tested using both simulated data and full-scale measurements of container ships. Automatic selection of response combination, to be used for wave estimation, is also studied using a sensitivity analysis.

In addition to wave estimation, prediction of waves and different responses in the near future can be upgraded using a mathematical model for tracking the evolution of wave parameters during the voyage. This method can improve the reliability and efficiency of decision support systems onboard ships. Finally, an uncertainty analysis of the wave estimation and the response prediction approaches is implemented.

Chapter 2

Model Description

2.1 Introduction

In moderate and mild waves, the wave-induced six degrees of freedom motion of a ship and associated structural loads are linear with the incident waves, meaning that the amplitudes of those responses are proportional to the wave amplitudes in regular waves. As a consequence of this linear theory, the responses can be quantified in irregular waves by adding together results from regular waves with different amplitudes, wavelengths and propagation directions. The amplitude of a response to an incident wave of unit amplitude or unit wave slope is called the transfer function or "Response Amplitude Operator" (RAO), which is expressed in the range of wave frequencies and wave directions relative to the ship. Apart from the relative amplitude of the response, the phase angle is also calculated, which represents the phase relationship between the response and the wave. Thus, the transfer functions are expressed as complex quantities.

In the response-based wave estimation, in addition to the above mentioned linearity consideration, the following assumptions are made: First, the sea waves are random and stationary, in a stochastic sense, within a certain period of response records at each estimation sequence. Second, the speed and the course of the ship are almost constant in that period.

The measured ship responses are used to obtain the response spectra. The combination of this data and the pre-calculated transfer functions (RAOs) are utilised to estimate the encountered wave spectrum. This estimation is implemented using an optimisation model, which is described in this chapter. Figure 2.1 shows a schematic of this procedure for estimation of directional

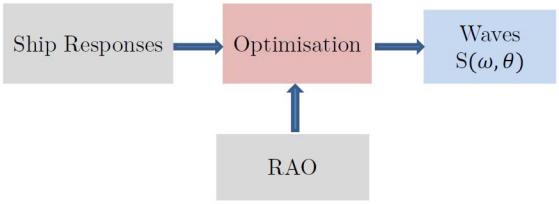

Figure 2.1: Response-based wave estimation system.

wave spectra.

2.2 Basic Equation

The theoretical relationship between the cross-spectral density of the i^{th} and j^{th} responses, $\Phi_{ij}(\omega)$, and the directional wave spectrum, $S(\omega, \theta)$, is given by:

$$\Phi_{ij}(\omega) = \int_{-\pi}^{\pi} H_i(\omega, \theta) H_j^*(\omega, \theta) S(\omega, \theta) d\theta, \tag{2.1}$$

where ω is the wave frequency and θ is the relative wave direction. For convenience, the ship course can be considered as the reference for wave direction so that the true wave direction and the relative direction to the ship are equal. $H(\omega, \theta)$ in Eq. (2.1) denotes the complex-valued transfer function and * is the complex conjugate. The responses are measured with respect to the moving reference frame of the ship and, hence, they should be considered in the encounter-frequency domain. The relation between encounter frequency and wave frequency in deep water is as follows:

$$\omega_e = \omega - \frac{V}{g}\omega^2 cos(\theta). \tag{2.2}$$

In this equation, V is the ship speed and g is the gravitational acceleration. Eq. (2.1) can be written in the form:

$$\bar{\Phi}_{ij}(\omega_e) = \int_{-\pi}^{\pi} H_i(\omega, \theta) H_j^*(\omega, \theta) S(\omega, \theta) \left| \frac{d\omega}{d\omega_e} \right| d\theta. \tag{2.3}$$

The left- and right-hand sides of Eq. (2.3) are the measured and the calculated cross-spectral density of responses, respectively. Hence, this equation can be considered as a cost function relating the measured and theoretical responses. Spectral analysis is applied on the measured time series of responses using e.g. Fast Fourier Transformation (FFT). Therefore, the spectral and cross spectral densities, i.e. $\bar{\Phi}_{ij}(\omega_e)$ in Eq. (2.3), are derived.

2.3 Literature Studies

Various studies have been performed so far for wave estimation using Eq. (2.3). They can be classified as parametric and non-parametric methods. In both of the methods, Eq. (2.3) is considered as a cost function for the whole range of frequencies. So, for N responses and M frequencies, $N^2 * M$ equations are present.

In the parametric approaches, the estimated wave spectrum is assumed to follow a standard parametrised wave spectrum so that the associated wave parameters are to be estimated. As examples, one can refer to Nielsen and Stredulinsky [46], and Tannuri et al. [58]. Bayesian method, on the other hand, is a non-parametric method that yields the wave spectral density at a number of discretised points of the wave field. This method uses prior information in terms of second order derivative equations to be minimised, making the directional wave spectrum smooth and realistic. The so-called hyperparameters are used to control the amount of smoothing in the spectrum. Iseki and Terada [21] proposed this method for wave estimation using one hyperparameter. Nielsen [40] increased the number of hyperparameters to make the spectrum smooth with respect to direction as well as frequency.

Both aforementioned methods (parametric and Bayesian) have been successful to some extent; see also [39, 57]. However, numerical problems might occur since the optimisation deals with response magnitudes close to zero for some combinations of discretised frequencies and directions. Therefore, strategies should be applied to overcome this problem.

Another non-parametric method is also formulated in [51], using the Kalman filter, which is able to merge data from different sources. However, this method is only studied on vessels with zero forward speed and further investigations are required to assess its capability for ships during their voyages. In this thesis, the parametric approach is pursued with an updated optimisation model as described below.

2.4 Moment-Based Cost Function

Apart from Eq. (2.3), another cost function that could be implemented is formed using the equivalence of the amount of variance (or covariance) between the measured and the theoretical responses. This equation can be derived by integration of the two sides of Eq. (2.3) with respect to encounter frequency.

Thus, the following equation is achieved:

$$\int_{\omega_{e_l}}^{\omega_{e_h}} \bar{\bar{\Phi}}_{ij}(\omega_e) d\omega_e = \int_{\omega_l}^{\omega_h} \int_{-\pi}^{\pi} H_i(\omega,\theta) H_j^*(\omega,\theta) S(\omega,\theta)\, d\theta d\omega. \tag{2.4}$$

Indexes l and h correspond to lower and higher frequency limits, respectively. Calculation of those limits and the method used to derive the moments are dealt with in Chapter 3 through partitioning of the spectrum. Iseki and Terada [22], and Nielsen [36] have used Eq. (2.4) for individual responses ($i = j$) as an additional cost function to Eq. (2.3). However, in the current study, Eq. (2.4) is considered exclusively. It can be observed that the term $\left|\frac{d\omega}{d\omega_e}\right|$ is not needed in this cost function.

Using this variance-based cost function makes the optimisation simpler than the traditional formulation mentioned in Section 2.2, since the number of governing equations in the system will be decreased to N^2. Thus, the optimisation becomes faster. Moreover, errors due to smoothing and interpolation in the spectral analysis of measured signals on the left side of Eq. (2.3) can be removed by integration. Additionally, since the whole areas below the response spectra are considered, numerical problems due to periods with transfer functions close to zero are less probable. Note that a bandpass filter should be applied on the load signals in order to remove high frequency vibrations that are not wave-induced responses of the rigid body but might occur due to hydro-elasticity of the ship as a consequence of springing and whipping. This filtering is carried out here in the frequency domain using the FFT and inverse FFT.

In addition to Eq. (2.4), the higher order moments of individual response spectra ($i = j$) with respect to encounter frequency should be equal between the measured and the theoretical values. This provides a more generic set of cost functions as

$$\int_{\omega_{e_l}}^{\omega_{e_h}} \omega_e^n \bar{\bar{\Phi}}_i(\omega_e) d\omega_e = \int_{\omega_l}^{\omega_h} \int_{-\pi}^{\pi} \omega_e^n \left|H_i(\omega,\theta)\right|^2 S(\omega,\theta)\, d\theta d\omega, \quad n = 0, 1, 2, ... \tag{2.5}$$

where n is the order of the moment. The second and the fourth moments of a response spectrum outline, respectively, the variance of the rate and the acceleration of that response as will be explained in Section 4.3.

2.5 Parametric Model

In order to study the sea state variability in time and space, parametrisation of directional wave spectra is very useful. Because the variations can be tracked through integral parameters. Different formulations have been proposed for

modelling of spectral density of irregular waves since 1955. These theoretical formulations describe average shapes expected to occur in the presence of a known wind speed, or in a state of known significant wave height and peak period. However, describing spectra by simplified models such as two-parameter spectra results in a considerable scatter around the shape of the spectra, particularly in the case of bimodal seas. In other words, there can exist a wide range of spectral shapes for a known combination of significant wave height and wave peak period. The scatter is most clearly evident for the low frequency part of the spectrum, where the swell components are located. This deviation of spectral shapes can be overcome by increasing the number of parameters, making the model sufficiently flexible to describe various sea states in different locations. In addition to the significant wave height and the mean period of waves, some shape factors have been used to describe the sea state [18, 61].

In most applications of modelling and description of waves, three or more free parameters are fitted to the measured spectrum using a regression algorithm. It should be noted that initialisation of the parameters are critical to the convergence of the algorithm, especially in cases of spectra with more than three parameters. This has also become an important issue in the response-based wave estimation. Because numerical conditioning of the nonlinear minimisation problem is poor and it is important to start with adequate parameter estimates.

Parametric representation of waves is also advantageous for decision support. While the ship is moving, the spectral shape of the wave energy is exposed to variations with location changes. The interpretation and evolution of these variations would be easier with the use of spectral parameters. In addition, because of data storage limits onboard ships during a voyage, it is more efficient to archive datasets of integral parameters rather than the whole spectra. For these reasons, in some of the non-parametric approaches for real-time wave estimation, a parametric form is eventually fitted to the estimated spectrum using the least squares method. This makes the parameters readily available and brings the model towards a smooth spectral shape. See e.g. [50, 60].

Another advantage in the parametric approach is that a full wave spectrum within a wide range of frequencies will be estimated. As a consequence, even though high frequency waves may have been filtered out by the ship, the high frequency tail of the estimated spectrum is formed in such a way that the whole spectrum is adjusted to a standard spectral shape.

The most common model of a unidirectional unimodal spectrum for developing seas is the family given by [9]:

$$S(\omega) = \alpha g^2 \omega^{-r} exp(-\beta\omega^{-n}) \gamma^{exp[\frac{-(\frac{\omega}{\omega_p}-1)^2}{2\sigma^2}]}. \tag{2.6}$$

Eq. (2.6) is a generalisation of a lot of well known spectral approximations, where α, β, r, n and γ are free positive-valued parameters. The parameters α and β are the scale and the location coefficients, respectively, which depend on the wave height and period. The parameters r and n control the shape of the spectrum, and ω_p is the peak frequency of the waves; i.e. the frequency at which the spectral peak occurs. This peak frequency is related to the peak period by

$$\omega_p = \frac{2\pi}{T_p}. \tag{2.7}$$

In Eq. (2.6), γ is the peakedness factor, which is always greater than or equal to one ($\gamma \geq 1$). The spectral width parameter, σ, is usually taken as

$$\sigma = \begin{cases} 0.07, & \omega < \omega_p \\ 0.09. & \omega \geq \omega_p \end{cases}$$

To simplify the model for describing the sea state, some of the parameters can be fixed. Fixing $r = 5, n = 4$ and $\gamma = 1$, yields the Pierson Moskowitz spectrum that is proposed for fully developed wind seas. The JONSWAP spectrum is a more generalised form of Pierson Moskowitz that is basically used for developing seas, where γ is other than 1, to represent fetch limited wind seas:

$$S(\omega) = \frac{\alpha g^2}{\omega^5} exp[-\frac{5}{4}(\frac{\omega_p}{\omega})^4]\gamma^{exp[\frac{-(\frac{\omega}{\omega_p}-1)^2}{2\sigma^2}]}. \tag{2.8}$$

Although this JONSWAP model was designed for the North sea, it is used almost anywhere because the bandwidth can be adjusted by changing its peakedness parameter. The value of α depends on wind speed, but there is an empirical formulation as a function of the significant wave height, H_s, the peak period, T_P and the peakedness factor, γ:

$$\alpha \approx 5.061 \frac{H_s^2}{T_p^4}[1 - 0.287ln(\gamma)]. \tag{2.9}$$

Another generalisation of the Pierson Moskowitz model that is commonly used is the Gamma spectrum:

$$S(\omega) = \frac{(\frac{4\lambda+1}{4}\omega_p^4)^\lambda}{\Gamma(\lambda)} \frac{H_s^2}{\omega^{4\lambda+1}} exp\Big[-\frac{4\lambda+1}{4}\Big(\frac{\omega_p}{\omega}\Big)^4\Big], \tag{2.10}$$

with λ being the shape factor, which is related to r by $r = 4\lambda + 1$. The peakedness and the width of the spectrum in Eq. (2.10) are controlled by this parameter. It is noteworthy that uncertainty in the form of decay in the high frequency tail of the spectrum is still an issue in wave spectral modelling [8].

Although the literature in the field of ocean waves mostly deals with one dimensional wave spectra, it is very important in ship operations to have the full directional wave spectrum available as a two-dimensional model. Because

the sea waves, in reality, are short-crested and their directionality has an impact on ship responses. Therefore, a wave spectrum is defined as a product of the frequency-wise spectrum and a spreading function, D, that outlines directional characteristics:

$$S(\omega, \theta) = S(\omega)D(\omega, \theta), \tag{2.11}$$

under the condition

$$\int_{-\pi}^{\pi} D(\omega, \theta)d\theta = 1. \tag{2.12}$$

The most frequently used spreading function in engineering practice is [15]:

$$D(\omega, \theta) = N(s)cos^{2s}(\frac{\theta - \mu}{2}), \tag{2.13}$$

where

$$N(s) = \frac{2^{2s-1}}{\pi}\frac{\Gamma^2(s+1)}{\Gamma(2s+1)} \tag{2.14}$$

is a normalisation constant, s is the spreading parameter and μ is the dominant or mean direction of wave propagation. The dependence of wave spreading on frequency can be described as

$$s = \begin{cases} (\frac{\omega}{\omega_p})^5 s_{max}, & \omega < \omega_p \\ (\frac{\omega}{\omega_p})^{-2.5} s_{max}. & \omega \geq \omega_p \end{cases} \tag{2.15}$$

Here, s takes a maximum value around the spectral peak frequency and it decreases for frequencies lower and higher than the peak frequency. The parameter s_{max} varies between 5 and 30 for wind waves, being a function of wind speed [62].

2.6 Spectral Partitioning

2.6.1 Modelling of a combined sea sate

Apart from local wind generated waves, there are also series of surface gravity waves that are not generated by the immediate local wind, but by distant wind that blows for a duration of time over a fetch of water. These wave systems that are called swell, often have long periods and can propagate faster than the generating wind field. Swell systems may add to the locally-generated wind sea and create double- or multiple-peak spectrum. The various systems in a combined sea usually have different peak frequencies and different directions of propagation. This event is called an omnidirectional system, and the spectrum in such conditions is rather complicated to estimate, since it can be the result of several swell systems in addition to locally generated waves.

Based on some observations in the North Atlantic, Kerbiriou et al. [27] have found that one-system configurations (one swell or one wind sea) account for about 37% of the observed cases. This means that the simplified unimodal sea state description is erroneous 63% of the time. In general, the probability of double peak wave spectra is reported as about 25-30%, both in open ocean and coastal areas. Those spectra are most often made up of one swell and one wind sea. [27, 64].

Integral parameters properly describe a single-peaked wave spectrum, but when the waves are composed of more than one wave system, the mean integral parameters for the whole spectrum are less meaningful and less accurate, unless they refer to individual wave components. In order to increase the validity of the spectral shape estimates, each wave system should be modelled individually even though the model dimension will increase. Spectral partitioning and identification of wind sea and swell is very important for structural assessments, marine operations and, especially, safety of ships performances.

Typical combinations of wind sea and swell in an omnidirectional sea state may lead to critical ship behaviour. For instance, a combined wave system can result in simultaneous significant roll motion and vertical acceleration, that may cause cargo to shift. In a study by Ewans et al. [14], response estimates of a FPSO for individual components of wind and swell are performed in order to examine the effects of spectral description of the individual sea states on the ship responses and, thereby, to improve the operability. On the other hand, for onboard estimation of sea state, assessment of spectral components is favourable for tracing the evolution of those wave systems throughout the operational period. Spectral partitioning is also beneficial in data assimilation for meteorological purposes.

A common representation of a combined sea is simply to add two directional spectra [9]:

$$S(\omega, \theta) = S_w(\omega, \theta) + S_{sw}(\omega, \theta), \tag{2.16}$$

where $S_w(\omega, \theta)$ is the wind-sea spectrum and $S_{sw}(\omega, \theta)$ is the swell spectrum, which itself could be a combination of several swell systems. However, standard engineering calculations often deal with spectra that are described in terms of two components (bimodal spectra) at most. For instance, in [14], the vessel responses are analysed in some areas in the South Atlantic and west of Namibia. It is shown in this study that the correlation coefficients between the parameters of bimodal models and the measured waves are close to one, even in multi-modal conditions. Additionally, based on various statistical plots of responses and wave parameters, it is indicated that the results from the multimodal data are very close to those from bimodal data except in low sea states. Accordingly, it is concluded that decomposition of spectra into a maximum of two components provides an adequate description of the sea state in terms of the integrated

parameters, i.e. basically significant wave height, mean wave period and mean wave direction.

Parametric modelling of combined waves is proposed in several studies. Ochi and Hubble [49] have formulated a double peak spectral model as a sum of two Gamma spectra, Eq. (2.10) [55]. Torsethaugen and Haver [61] proposed a model that is used for design purposes in Norwegian waters. It is based on a fitting of two JONSWAP models to the measured waves in that area, and the parameters are adjusted accordingly. It should also be mentioned that in the response-based wave estimation, Nielsen and Iseki [42] use a fifteen-parameter trimodal spectrum that is capable of modelling a combined sea consisting of up to three systems.

2.6.2 System classification of wave spectra

For modelling of measured ocean wave spectra, a pre-processing step is usually implemented, which separates the components of a combined sea state. The procedure involves identification of the peak frequencies of the spectral components. The algorithm finds a matrix of locally largest neighbours. The solution may have many isolated spectral peaks that are not a proper realisation of the ocean waves. So, the number of peaks should be reduced. This can be done using a smoothing parameter in the routine and finally merging the close peaks. The criterion to merge adjacent peaks is based on the value of both peak period and mean direction of components. An energy threshold for each component is also applied. See e.g. [9, 13, 19, 53].

The second step is identification of swell and wind-sea peaks. In general, wind seas are more irregular and short-crested, respond quickly to wind variations, so they are characterised by a rather broad spectrum, the energy of which is concentrated at higher frequencies (between 0.1 and 0.4 Hz). Swell systems, however, are more complicated to model since no single self-similar form exists as for wind driven waves. Swell events consist of reasonably regular long-crested waves that are not strongly affected by the wind. As the wind drops or when waves leave the generation area, long waves travel faster than short waves and their steepness reduces due to frequency and direction dispersion. As a consequence, the swell system looses its high frequency components becoming more peaked and narrow. In other words, for the same initial spectrum in the storm area, the shape of the swell spectrum depends on the distance travelled. The swell frequencies usually lie between 0.03 and 0.2 Hz [53].

For the sake of system classification in wind sea or swell, most methods rely on determination of a separation (splitting) frequency, ω_s, for a particular spectrum. Waves with frequencies higher than ω_s are mostly generated by local winds,

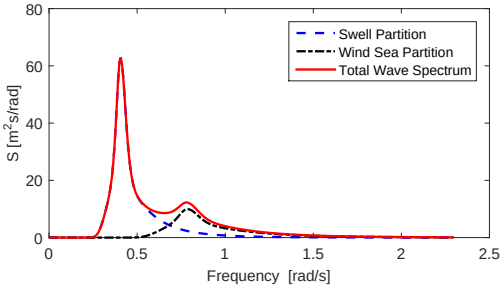

Figure 2.2: Spectral partitioning and fitting.

and wave components at frequencies lower than ω_s correspond to swell. After separating the spectrum into low- and high-frequency partitions, a standard (e.g. JONSWAP) model is fitted around each component. For each partition, the wave parameters are extracted. The summation of the components should describe the whole spectrum. This method has been applied on both frequency (1 dimensional) spectrum and directional (2 dimensional) spectrum [13]. Figure 2.2 shows an example of spectral partitioning in a frequency spectrum.

In the wave buoy analogy based on non-parametric methods, the above mentioned peak identification procedure can be implemented. This has been employed for wave estimation using the Bayesian method [38, 60]. The study based on the Kalman filter [50] is also capable of separating wind sea and swell. In the present study, however, the partitioning is introduced based on a parametric approach. The procedure is quite different from the above-mentioned algorithms in the sense that neither the spectral shape nor the sea state parameters are known. Thus, identification of wind sea/swell and estimation of associated parameters are accomplished simultaneously.

Since a swell system results from a wind sea that propagates away from the generation area, it is commonly described by the same spectral model as wind sea. However, modelling such narrow peaks using a JONSWAP spectrum requires the peak enhancement factor to take much higher values than the commonly used range ($1 < \gamma < 7$). A JONSWAP spectrum with $7 < \gamma < 10$ have been found to be adequate for swell modelling [9, 13, 15].

The proposed partitioning procedure in this thesis is similar to the Torsethaugen approach, [61], mentioned in Section 2.6.1, which splits the energy into a swell component and a wind-sea component. However, the Torsethaugen model is not widely adopted outside the Norwegian Continental Shelf. For the goal of onboard decision support, it is important that the spectral model is generic enough, which covers an acceptable range of actual waves in various areas. Therefore, a sum of two generalised JONSWAP models is used herein. However,

the choice of models can vary depending on the local site.

For a fully-developed sea, the peak frequency of the Pierson-Moskowitz (PM) spectrum, denoted by ω_{PM}, is calculated from:

$$\omega_{PM} = 0.82\frac{g}{U_w}, \tag{2.17}$$

where U_w, the mean wind speed (in m/s), is usually measured at 10 m elevation. This quantity can continuously be measured onboard the ship. However, in the Torsethaugen spectrum, the spectral peak frequency for a fully-developed sea is obtained using the measured significant wave height because the wind speed may be unknown in many applications.

A simple way is to set a constant splitting frequency or period, which should be predetermined. A common value in practice is $\omega_s = 0.2\pi$ rad/s associated with $T_p = 10$ s [12]. A more general representation of the splitting frequency is based on the assumption that this frequency is close to the spectral peak of the PM spectrum, Eq. (2.17). So, the separation frequency in rad/s is defined as [53]:

$$\omega_s = \frac{g}{C_s U_w}, \tag{2.18}$$

where C_s is an empirical constant, usually chosen between 1.3 and 1.5. This small difference between the separation frequency and the PM peak frequency is due to uncertainty of sea state or the angular shift between wind and wave. Eq. (2.18) is used in this thesis for approximation of the separation frequency.

The spreading parameter defined in Section 2.5 also varies for wind sea and swell. Goda [15] proposed $s_{max} = 10$ for wind waves, $s_{max} = 25$ for swell with short decay distance, and $s_{max} = 75$ for long decay distance. In the current study, this parameter is also taken to be fitted in the optimisation.

As a conclusion of this chapter, the JONSWAP model will be substituted in the cost function in Eqs. (2.4) and (2.5) for each partition. Thus, the variable space involves 10 “fit parameters” as follows:

$$\begin{cases} H_{s,wind} \\ H_{s,swell} \\ T_{p,wind} \\ T_{p,swell} \\ \mu_{wind} \\ \mu_{swell} \\ \gamma_{wind} \\ \gamma_{swell} \\ s_{max,wind} \\ s_{max,swell} \end{cases} \tag{2.19}$$

Chapter 3

Optimisation

3.1 Introduction

The problem formulated in Chapter 2 will be solved using an optimisation method. In this chapter, two different methods from the MATLAB optimisation toolbox are used. Implementation of the procedure and the constraints used for partitioning approach are described. The contents of this chapter and Chapter 4 are included in [34].

3.2 Discretisation of the Cost Function

In order to solve Eq. (2.4) numerically, the integrals must be discretised with respect to frequency and direction. Then, the cost function can be expressed as

$$R_{ij} = \delta\theta\delta\omega \sum_{k=1}^{K}\sum_{l=1}^{L} H_i(\omega_k,\theta_l)H_j^*(\omega_k,\theta_l)S(\omega_k,\theta_l), \quad i,j \in [1,2,...,N] \qquad (3.1)$$

where R_{ij} is the covariance between the i^{th} and the j^{th} responses. K and L are the number of frequencies and wave directions, respectively, and N is the number of responses to be used for wave estimation. The variables $\delta\omega$ and $\delta\theta$ are the increments between the discrete frequencies and directions. In order to implement the optimisation, the residuals are evaluated as the difference between the two sides of Eq. (3.1), normalised by R_{ij}. Therefore, the sum of

squared residuals, SSR, is expressed as:

$$SSR = \sum_{i=1}^{N}\sum_{j=1}^{N} \frac{1}{(R_{ij})^2}[R_{ij} - \delta\theta\delta\omega \sum_{k=1}^{K}\sum_{l=1}^{L} H_i(\omega_k, \theta_l)H_j^*(\omega_k, \theta_l)S(\omega_k, \theta_l)]^2. \quad (3.2)$$

Estimation of the wave parameters in Eq. (2.19) are carried out by the least squares approach, which minimises the SSR in Eq. (3.2). The number of equations can be adjusted to increase the speed of the optimisation and also to obtain more reliable results. This is discussed further in Chapter 4.

3.3 Global Optimisation Methods

Minimisation of Eq. (3.2) can be solved using gradient-based methods. For instance "fmincon" from the MATLAB is widely used when linear and/or nonlinear constraints exist. This function begins from an initial guess, iterates according to a given update scheme, and finishes when a stopping criteria is met. The final iteration constitutes a local minimum if the conditions are fulfilled and the Hessian[1] is positive definite.

Through the optimisation, a large number of local minima may be present and the computation is highly dependent on the initial values. To compensate, a global search basin can be used rather than local minimisation in the least squares analysis as also mentioned in [52]. However, it may decrease the speed of optimisation. In this thesis, the process to get global minima is accomplished by the "MultiStart" class and the "Genetic Algorithm" from the MATLAB optimisation toolbox. Both methods are well suited to solve the current constrained nonlinear optimisation problem. Multistart, as the name implies, runs fmincon from multiple starting points using a sequential quadratic algorithm. The results of each fmincon run is stored in a vector, and in the end, the best result is selected as the global minimum.

The genetic algorithm, on the other hand, is a method based on natural selection, the process that drives biological evolution. This method is a part of the group of Evolutionary Algorithms (EA), which has been applied in many research areas (e.g. [50]) to increase the robustness of the optimisation. The algorithm repeatedly modifies a population of individuals representing possible solutions of the task. At each step, it selects individuals at random from the current population to be parents. This selection is based on their fitness. The parents are then used to produce children for the next generation by making random changes. The direction and the step length of those changes satisfy the

[1] Hessian is the square matrix of the second partial derivatives of a function.

bounds and constraints. Over successive generations, the population evolves toward an optimal solution that minimises the cost function.

The genetic algorithm differs from the classical derivative-based optimisation algorithms in the following ways: First, the genetic algorithm generates a population of points at each iteration and the best point in the population approaches an optimal solution, whereas the classical algorithms generate a single point at each iteration and the sequence of points approaches an optimal solution. Second, in the genetic algorithm, the next population is selected by using random number generators; whereas in the classical methods, the next point in the sequence is selected by a deterministic computation. Third, contrary to the gradient-based methods, the genetic algorithm uses the objective function information rather than derivatives or other auxiliary knowledge.[2]

3.4 Computation Procedure

3.4.1 General constraints

The global optimisation is not efficient unless some constraints are applied to the fit parameters. The following boundaries are generally valid in ocean waves:

$$0 \leq H_s \leq 15, \quad [m] \tag{3.3}$$

$$6 \leq T_p \leq 20. \quad [s] \tag{3.4}$$

Another constraint is associated with the global steepness limit of waves [25]:

$$11.4\sqrt{\frac{H_s}{g}} < T_p, \tag{3.5}$$

because very steep waves will break. The above restrictions provide a proper conditioning for estimation of H_s and T_p. But initialisation and limits of the mean wave direction are also necessary to reach an accurate estimate. In real applications of onboard wave estimation, a range of initial populations for wave direction can be provided by using observations or other estimation tools. Prior information about wave direction may also be provided by "Blind estimation" introduced by Nielsen and Iseki [43].

[2] http://se.mathworks.com/help/gads/index.html

3.4.2 Identification of the dominant system

A wave spectrum is categorised as wind- or swell-dominated sea as follows. The primary (dominant) peak frequency of the wave spectrum is extracted by fitting a single wave model to the measured responses. The parameters γ and s_{max} are fixed to 3.3 and 20 here, respectively, for simplification. It is noteworthy that the estimated parameters are spectrally averaged values in this pre-estimation level, and they are not expected to be accurately calculated. Particularly, the average direction is meaningless when the wave spectrum is omnidirectional.

The estimated peak frequency is compared with the PM peak frequency, which is approximated by Eq. (2.17). A similar criterion to the Torsethaugen spectrum [61] is used. Accordingly, if $\omega_p < \omega_{PM}$, the waves are considered as swell dominated and if $\omega_p > \omega_{PM}$ they are wind dominated.

The above mentioned classification should finally conform with the following criterion based on the relative ratio of zero-order spectral moments of swell and wind-sea systems [55]:

$$\xi = \frac{m_{0_{ws}}}{m_{0_{sw}}}, \tag{3.6}$$

where the subscripts ws and sw stand for wind-sea and swell partitions, respectively. The moments, m_0, are given by

$$m_0 = \int S(\omega) d\omega. \tag{3.7}$$

Wave fields with ξ smaller than one represent swell-dominated waves, and those with ξ greater than one correspond to wind-dominated waves. After identifying the dominated system, a more accurate estimation of the parameters is obtained through the partitioning approach.

3.4.3 Fitting of swell and wind Sea

As mentioned in Section 2.6, the wave spectrum should be split into low-frequency and high-frequency parts using the separation frequency, Eq. (2.18). The fitting procedure is applied first, on the dominant system and then, on the secondary system. The value of the separation frequency determines the integral bounds in Eq. (2.4) for each partition. For the swell part, $\omega_l = 0$ and $\omega_h = \omega_s$, whereas for the wind part, $\omega_l = \omega_s$ and ω_h is equal to the upper bound of the spectrum; e.g. 2 rad/s.

The left-hand side of Eq. (2.4) is integrated with respect to encounter frequency. The lower and upper limits, i.e. ω_{e_l} and ω_{e_h} respectively, should be tuned

properly so that they precisely represent the corresponding wave frequency bound between ω_l and ω_h on the right hand side. Given ω_s, Eq. (2.2) is employed to calculate the corresponding separation frequency of encounter used to split the response spectra:

$$\omega_{e_s} = \omega_s - A\omega_s^2, \quad A = \frac{V}{g} cos(\mu), \tag{3.8}$$

However, this transformation is not straightforward since the mean wave direction is unknown. So, a range of mean wave directions is considered to initiate the encounter splitting frequency. The optimisation is then carried out conditional on the difference between the estimated mean wave direction and the initial value not being larger than 20 deg. Then, the optimum solution is the one with minimum SSR over the entire range.

For the swell part, Eqs. (3.3) to (3.5) are used as constraints. The separation frequency of encounter is derived as

$$\omega_{e,(s,swell)} = max \begin{cases} \omega_e(\mu_0) \\ \omega_e(\mu_0 - \epsilon) \\ \omega_e(\mu_0 + \epsilon) \\ \omega_{e(s,wind)}, & \text{if wind dominated} \end{cases} \tag{3.9}$$

where μ_0 is the initial mean wave direction and ϵ implies a deviation from this quantity that is associated with short-crestedness of waves. The magnitude of this interval depends on the spreading factor, but a fixed value of $\epsilon = \pi/9$ rad is considered here for simplicity. In the case of wind-dominated waves, the separation frequency of wind-sea part, $\omega_{e(s,wind)}$, is also considered to avoid any gap between the two partitions in the encounter frequency domain. In other words, the splitting of response spectra should be chosen in such a way that the upper limit in the swell part is equal to or greater than the lower limit in the wind-sea part, because an overlap between the two components can be present.

Apart from short-crestedness of waves, using the exact value of ω_{e_s} from Eq. (3.8) in following sea condition, may cause errors in the estimations. As seen in Figure 3.1, in all relative directions between 90° and 180°, transforming from the wave frequency to the encounter frequency is direct because as the frequency increases, the encounter frequency increases as well. In following sea or stern-quartering sea conditions, where $0 < \mu < 90$, the encounter frequency limit between 0 and ω_{e_s} does not correctly match the wave frequency limit between 0 and ω_s and so on for the high frequency partition. Thus, this encounter frequency bound should be slightly expanded. The above mentioned intervals may compensate for this problem.

Similar to the swell part, a deviation from the mean direction is applied for

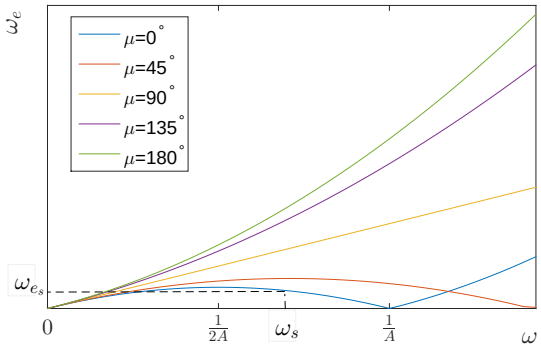

Figure 3.1: Calculation of separation frequency in the encounter domain. (The position of $\frac{1}{2A}$ and $\frac{1}{A}$ is only shown for $\mu = 0°$).

the high frequency parts of the response spectra:

$$\omega_{e(s,wind)} = min \begin{cases} \omega_e(\mu_0) \\ \omega_e(\mu_0 - \epsilon) \\ \omega_e(\mu_0 + \epsilon) \\ \omega_{e(s,swell)}, \qquad \text{if swell dominated} \end{cases} \tag{3.10}$$

This deviation is assumed a bit larger than swell ($\epsilon = \pi/6$ rad) since wind generated waves are more short-crested as explained in Chapter 2.

For wind-sea partition, estimation is more complicated than swell. The responses of a large ship with a large inertia filter out the high frequency part of the spectrum and using the same conditions as swell estimation may be insufficient. To overcome, additional constraints to Eqs. (3.3)-(3.5) are used to upgrade wind-sea estimates. For instance, in JONSWAP models, an empirical lower bound is considered for the steepness of wind-generated waves [62]:

$$T_p < 15.7\sqrt{\frac{H_s}{g}}. \tag{3.11}$$

Another condition commonly used for a system to be identified as wind sea is that the mean direction of the wave train must be at most 90° apart from the wind direction, θ_w, that is measured onboard the ship [19]:

$$|\theta_w - \mu| \leq \pi/2. \tag{3.12}$$

Otherwise, the estimate cannot belong to the present wind sea.

In partially-developed seas, wind generates random pressure fluctuations at the sea surface that produce small waves with shorter periods than fully-developed

sea. The peak frequency of the wind sea in the JONSWAP spectrum is an empirical function of both wind speed and fetch length. Since information about the fetch length is not usually available, a so-called wave age criterion can be used [19]:

$$c_p \leq C_s U_w \left| cos(\theta_w - \mu) \right|, \tag{3.13}$$

where c_p is the phase speed of wind sea, defined as the speed of waves at the peak. This value is calculated by

$$c_p = \frac{g}{\omega_{PM}} \tag{3.14}$$

in deep water. The parameter θ_w in Eq. (3.13) is the wind direction and μ is the mean wave direction as defined before. The inequality in Eq. (3.13) applies to cover partially- as well as fully-developed sea states. In terms of the peak frequency of the wind sea, Eq. (3.13) becomes

$$\omega_p \geq \frac{g}{C_s U_w \left| cos(\theta_w - \mu) \right|}. \tag{3.15}$$

Eq. (3.15) can be useful for estimation of wind-sea direction. However, it is observed in this study that using this inequality as a constraint can mislead the convergence of the optimisation. So, this equation is merely helpful to estimate the wave direction, fixing the estimated peak period.

In the last step of optimisation, the significant wave height of the secondary peak is adjusted by fitting the whole measured response spectra to a double-peaked wave model fixing the other estimated parameters. This can avoid the total energy of the waves to be overestimated since the wind part may have an overlap with the swell part, particularly for waves with closely located peaks. The following dimensionless parameter related to spectral peaks of swell and wind-sea systems is used in [55].

$$ID = \frac{\omega_{p_{ws}} - \omega_{p_{sw}}}{\omega_{p_{ws}} + \omega_{p_{sw}}} \tag{3.16}$$

that is called “Intermodal Distance”. The peak frequencies of wind-sea and swell parts are $\omega_{p_{ws}}$ and $\omega_{p_{sw}}$, respectively. Wave fields with ID values close to zero correspond to sea states with swell and wind-sea peaks very close to each other. When the ID value is closer to one, wind-sea and swell peaks are located far from each other in the spectrum.

A flowchart overview of the optimisation procedure, explained in this chapter, is shown in Figure 3.2.

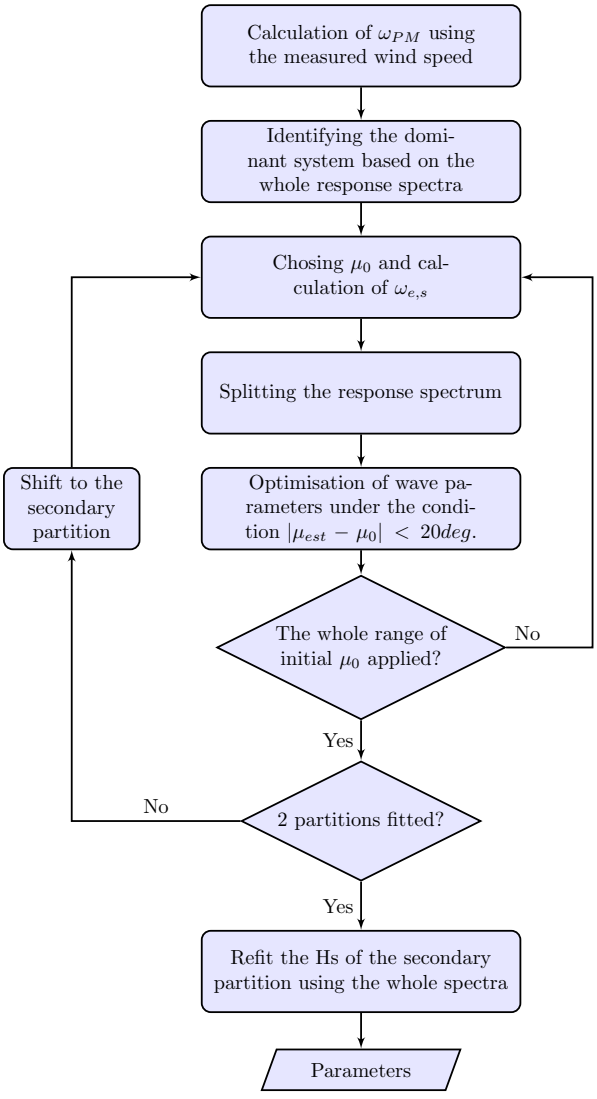

Figure 3.2: Flowchart of the optimisation procedure.

Chapter 4

Numerical experiments

4.1 Introduction

To investigate the applicability of the proposed wave estimation method, numerical simulations are carried out for a container ship, which could represent sensor measurements. The simulations are based on known standard directional wave spectra that provide stationary stochastic time series of waves and different ship responses. In this chapter, the wave estimation procedure is applied on the generated data. In this numerical study, the capability and efficiency of the method can be assessed properly, since the waves in the input are known.

4.2 Sample Ship

The CMA-CGM 9400 TEU container ship, Rigoletto, that has been under investigation during several years for the TULCS project[1] is considered as a case study in this project. The main characteristics of the vessel and the typical operational condition used in this chapter are given in Table 4.1.

[1]Grant No. 234146

Table 4.1: Ship characteristics and operational condition.

Properties	Values
LOA (Overall length) [m]	349.0
B (Beam) [m]	42.8
T (Draft) [m]	14.5
Maximum Capacity [TEU]	9415
DWT (Dead weight)[ton]	113,000
V (Speed) [kn]	20

Figure 4.1: The CMA-CGM container ship, Rigoletto.

4.3 Response Amplitude Operators

For wave estimation purposes based on short-term responses, sufficient resolution of the transfer functions is very important. In addition, the transfer functions must cover a proper range of wave periods, especially in the region with the highest wave energy. Otherwise, the wave spectrum may be poorly estimated. Depending upon natural frequencies, some responses might not be able to capture the high frequency part of the spectrum, whereas some others can do. Therefore, to get more accurate estimations, several responses should be used simultaneously to make sure that the entire spectrum has been covered. Moreover, since the method is based on spectral moments, i.e. Eqs. (2.4) and (2.5), the number of responses taken into account should provide at least a number of equations equal to the fit parameters (Eq. (2.19)).

Selection of the best combination of responses is very important. It is often seen that shifting between different responses may influence the estimations remarkably. The optimum selection of responses may not be identical for all

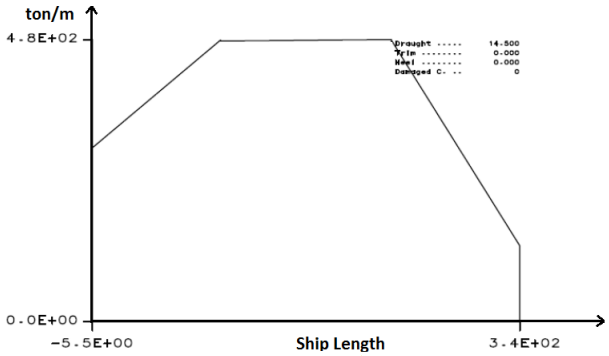

Figure 4.2: Approximated weight distribution along the ship.

ships and even not for all of the operational conditions of one specific ship. Therefore, this choice should be made based on prior knowledge about the transfer functions of a particular ship in different operational conditions. This is investigated in Chapter 7.

The transfer functions of the motions of Rigoletto are provided by BUREAU VERITAS using HydroStar software, which is based on linear potential theory. The transfer functions are calculated at frequencies from 0.06 rad/s to 1.8 rad/s with 0.06 rad/s intervals and in different directions from 0° (following sea) to 180° (head sea) with 10° intervals. The transfer functions of roll motion were found to be unrealistic since the orders of roll magnitudes that they give are far different from the full-scale measurements from this ship. Therefore the roll transfer function used in this study is calculated using the in-house software, Iship, based on linear strip theory.

The complex-valued transfer functions of wave induced vertical bending moment at midship section are also calculated using Iship. It is clear that the weight distribution should be reproduced for this calculation. The actual longitudinal weight distribution is approximated by combination of a midship rectangle with forward and aft trapezoids as shown in Figure 4.2.

Figure 4.3 shows the amplitudes of the transfer functions for the particular operational condition in Table 4.1. As seen in this Figure, the amplitude of each response varies with wave frequencies and wave directions. In general, most response amplitudes are relatively large within the low frequency band. However, in head sea and following sea conditions, roll and sway responses are zero. In the high frequency region, the response amplitudes are somewhat lower than in the low frequency region.

Heave and pitch are known as the most reliable responses in terms of hydrody-

namic calculations. The transfer functions of these motions can be calculated with a good accuracy based on strip theory, panel methods or experiment. So, these motions are widely used for wave estimation. The behaviour of these two motion components in waves depends on the wave length in relation to the ship length. In other words, the ship length determines the wave length, and correspondingly the frequency, up to which head waves can be sensed by heave and pitch motions [51]. It can be seen in the figure that for Rigoletto, in head seas and following seas, the amplitudes of these motions mostly become close to zero at around 0.8 rad/s associated with 98 meter wave length. As the ship length increases, this limiting wave length that can be estimated by heave and pitch becomes larger.

In addition to heave and pitch, roll or sway is usually included as well in the response combination due to their asymmetric characteristics. This means that the phase angles of roll and sway response functions are not identical for waves entering from port and starboard sides of the ship. Therefore, those responses are theoretically capable of recognising the sign of relative directions. Note that positive values correspond to waves entering on the starboard side, whereas negative values correspond to waves entering on the port side.

Sway does not have a restoring force, so the error in calculation of this response may be quite large. On the other hand, the assumption that roll motion is linear is questionable at higher excitations. Uncertainties of transfer functions will be discussed further in Chapter 8. Those inaccuracies in transfer functions for roll and sway might result in considerable uncertainties in the wave estimations. To compensate, the selected responses can be weighted non-uniformly. This will be discussed in Section 4.5. Regarding the choice between sway and roll, Simos et al. [57] suggest sway motion since the transfer functions of this motion are less sensitive to the loading condition and also because of non-linearity in roll motion. Nielsen [37], however, finds this justification difficult. According to a primary study on Rigoletto, which was carried out by the author, [33], it was found in the optimisation procedure that adding roll motion to the response combination, results in large outliers in the magnitudes of the residuals compared to other responses. For this reason, and also due to the findings in [30], sway motion is used in this thesis instead of roll.

Wave-induced vertical bending moment is another response that can be utilised for wave estimation [47]. As seen in Figure 4.3, this response is significant for a wide range of wave frequencies, which is quite beneficial for estimation of the wave spectrum as discussed above. This response is proportional to the wave height if the ship tends to be wall sided near the operational draft. But in case of small block coefficient or large wave heights, the wall-sided assumption is not valid any longer and the vertical bending moment becomes a non-linear function of wave height [17]. It is also clear in the figure that the maximum vertical bending moment occurs in head seas and following seas and its amplitudes

decrease toward beam sea condition.

In general, transfer functions of accelerations have a slower decay than motions at high frequencies and, hence, a combination of displacements and accelerations (or rates) is recommended to be used in order to improve the estimates at both low and high frequencies [51]. It is well known that the complex-valued transfer functions of a response rate, H_{rat}, and acceleration, H_{acc}, can be evaluated by single and double differentiation of displacement, H_{disp}, respectively. Thus, the amplitudes of transfer functions for rates and accelerations will be

$$|H_{\mathrm{rat}}(\omega,\theta)| = \omega_e \, |H_{\mathrm{disp}}(\omega,\theta)| \,, \tag{4.1}$$

and

$$|H_{\mathrm{acc}}(\omega,\theta)| = \omega_e^2 \, |H_{\mathrm{disp}}(\omega,\theta)| \,, \tag{4.2}$$

respectively. Correspondingly, their equations in the cost function are provided by the second and the fourth moments of the response spectrum in Eq. (2.5), respectively.

4.4 Response Generation

Different wave scenarios characterised in Table 4.2 are considered. The JONSWAP spectrum, Eq. (2.8), combined with the spreading function just as Eq. (2.13) is used. The ship course is considered as the reference for wave direction so that the relative direction represents the true wave direction. The wind speeds are chosen based on statistical wave plots for the chosen periods.

In Table 4.2, cases A through H represent unimodal wave spectra and cases I through L are bimodal sea states with separately-located peaks, whereas cases M through P represent bimodal waves with closely-located peaks. As pointed out in Section 2.6, superposition of two JONSWAP spectra will be used to simulate bimodal waves.

For a given operational condition, the time series for a response can be calculated using the amplitude of the transfer function as a function of the encounter frequency and the encounter angle [26, 36, 43]:

$$\xi(t) = \sum_{n=1}^{N_0} \sum_{m=1}^{M_0} a_{mn} \, |H(\omega_{e,mn}, \theta_m)| \, cos(\omega_{e,mn} t + \phi_{mn}), \tag{4.3}$$

where the directional wave spectrum is discretised into N_0 frequencies and M_0 directions. The variables $\omega_{e,mn}$ and a_{mn} are the encounter frequency and the wave amplitude, respectively, corresponding to the n^{th} discrete frequency

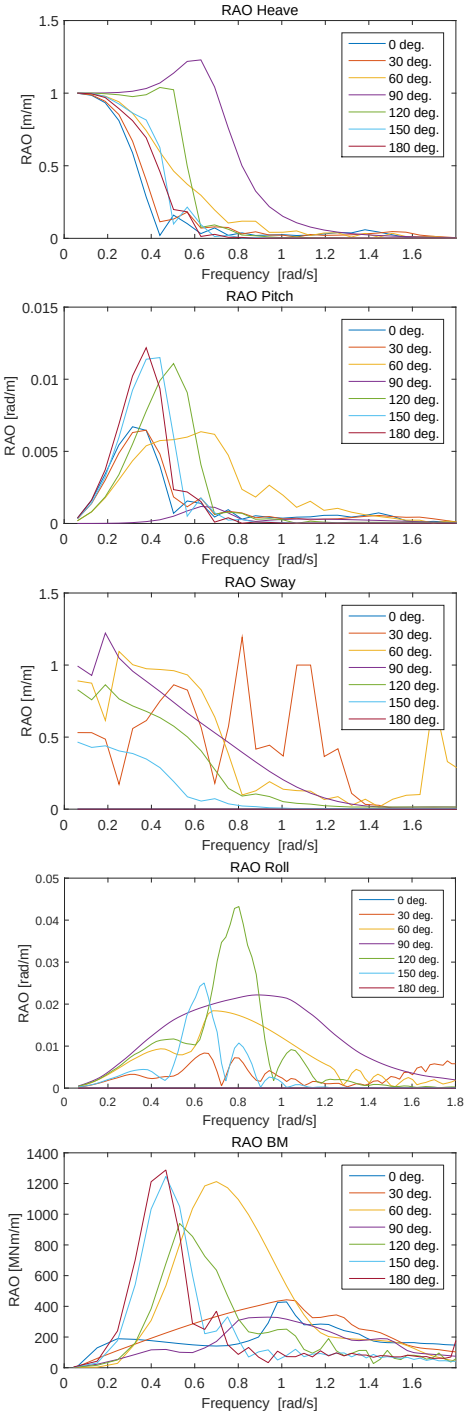

Figure 4.3: Amplitudes of RAO for different responses, V=20 kn, T=14.5 m.

Table 4.2: The main parameters of the studied wave cases.

Cases	Wind sea					Swell					Wind Speed
	H_s(m)	T_p(s)	μ(deg.)	s_{max}	γ	H_s(m)	T_p(s)	μ(deg.)	s_{max}	γ	U_w(m/s)
A	3	8	45	10	2	0	—	—	—	—	14
B	3	8	90	10	2	0	—	—	—	—	14
C	3	8	135	10	2	0	—	—	—	—	14
D	3	8	180	10	2	0	—	—	—	—	14
E	0	—	—	—	—	5	15	45	25	4	5
F	0	—	—	—	—	5	15	90	25	4	5
G	0	—	—	—	—	5	15	135	25	4	5
H	0	—	—	—	—	5	15	180	25	4	5
I	3	8	45	10	2	5	15	-135	25	4	14
J	3	8	-90	10	2	5	15	90	25	4	14
K	3	8	135	10	2	5	15	45	25	4	14
L	3	8	90	10	2	5	15	180	25	4	14
M	3	8	45	10	2	2	12	-135	25	4	14
N	3	8	-90	10	2	2	12	90	25	4	14
O	3	8	135	10	2	2	12	45	25	4	14
P	3	8	90	10	2	2	12	180	25	4	14

and the m^{th} discrete angle; ϕ_{mn} are phase lags. As the wave records and the responses are assumed to be Gaussian processes, Eq. (4.3) can be written as

$$\xi(t) = \sum_{n=1}^{N_0} \sum_{m=1}^{M_0} [u_{mn} c_{mn}(t) + \bar{u}_{mn} \bar{c}_{mn}(t)], \tag{4.4}$$

where the variables u_{mn} and $\bar{u}_{mn}$ are uncorrelated zero-mean normally distributed variables. The coefficients $c_{mn}(t)$ and $\bar{c}_{mn}(t)$ are deterministic and given by

$$c_{mn}(t) = \sigma_{mn} \, |H(\omega_n, \theta_m)| \, cos(\omega_{e,nm} t + \epsilon_{mn}), \tag{4.5a}$$

$$\bar{c}_{mn}(t) = -\sigma_{mn} \, |H(\omega_n, \theta_m)| \, sin(\omega_{e,nm} t + \epsilon_{mn}), \tag{4.5b}$$

with

$$\sigma_{mn}^2 = S(\omega_n, \theta_m) \delta\omega_n \delta\theta, \tag{4.5c}$$

where $\delta\omega_n$ and $\delta\theta$ are the increments between the discrete frequencies and directions, respectively. In this study, the wave direction is discretised from $-\pi$ to π rad with $\delta\theta = \frac{\pi}{18}$ rad ($M_0 = 36$). The variables u_{mn} and $\bar{u}_{mn}$ in Eq. (4.4) are related to the wave amplitude through [26]:

$$a_{mn} = \sigma_{mn} \sqrt{u_{mn}^2 + \bar{u}_{mn}^2}, \tag{4.6}$$

and the phase angle in Eq. (4.5) is

$$\epsilon_{mn} = tan^{-1}\Big(\frac{Im[H(\omega_n, \theta_m)]}{Re[H(\omega_n, \theta_m)]}\Big). \tag{4.7}$$

The frequency band is taken from 0.06 to 2 rad/s with non-equal random $\delta\omega_n$ to avoid repeating signals [38]:

$$\omega_{n+1} = \omega_n + c.p_n, \tag{4.8}$$

with c as a small factor and p_n as a random variable with values between 0 and 1. With the above simulation technique, wave heights vary statistically meaning that any wave record has a significant wave height which, in most cases, is not exactly equal to the H_s of the actual wave spectrum [38].

The transfer functions from Section 4.3 are used to simulate the sensor installations. So, the ship speed is 20 kn in all cases. Note that the transfer functions are interpolated and extrapolated for the above mentioned range of random frequencies. Fifteen sets of realisations, 3600 seconds long, are generated for the considered responses, i.e. vertical motion at port (at midship section, 19.25 m from centreline); pitch and sway at the centre of gravity; and vertical bending moment at the midship section. Such long time series ensure that the actual energy of the response record is preserved and the risk of statistical outliers is minimised.

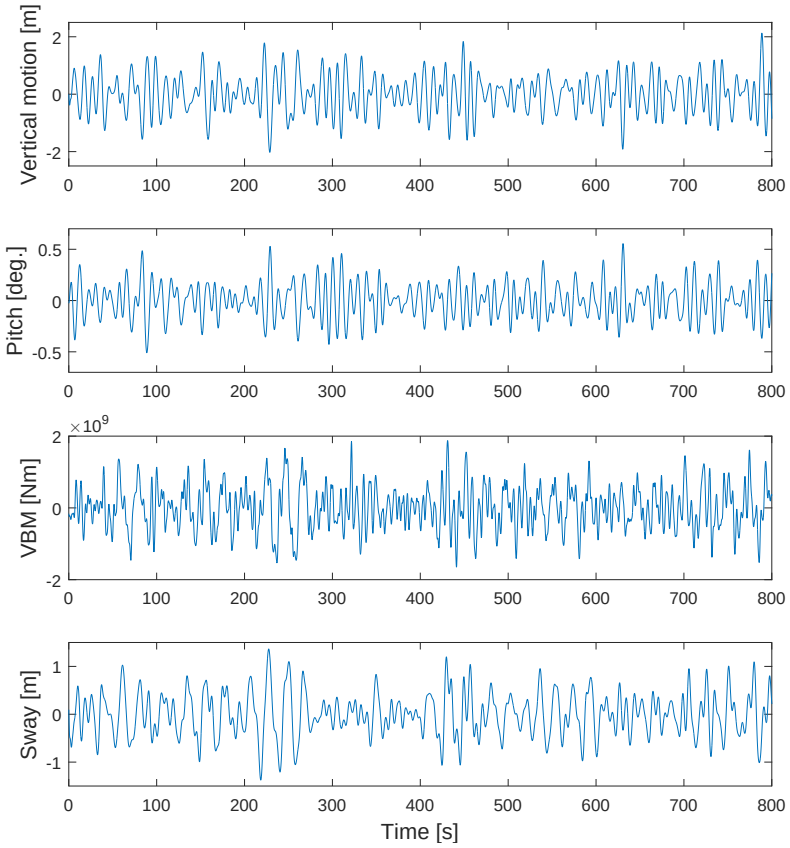

Figure 4.4: Sample of time history simulations for vertical motion, pitch, vertical bending moment and sway.

The aforementioned response combination is chosen based on the literature. As discussed in Section 4.3, this selection covers a sufficiently wide range of frequencies. It is noteworthy that roll motion is not used directly but only as a contribution to vertical motion on the port side. So, both sway and vertical motion provide asymmetric characteristics. Figure 4.4 shows samples of time history simulations.

4.5 Implementation of the Program

The Matlab toolbox, "WAFO" [62], is used for spectral analysis of responses and moment calculations. Apart from the displacements of the specified responses,

the rates of vertical motion, pitch and bending moment are also used in the swell part. In the wind-sea part, accelerations are used instead of rates as wind-generated waves are related to high frequencies.

Since the sway motion deals with hydrodynamic uncertainties addressed in Section 4.3, it is not given the same weight as other responses in such a way that the diagonal ($i = j$) equations of this motion are neglected. In other words, this response is only used for cross-spectral terms to identify whether the waves are entered from port or starboard.

Moreover, in the current spectral moment-based method, numerical problems i.e. large magnitudes of residuals can be experienced during the optimisation because the areas under the cross-spectral curves are relatively small. In addition, smoothing of cross-spectra adds uncertainty to the model. Therefore, the cross-spectral calculations, which correspond to off-diagonal components ($i \neq j$) in Eq. (3.2) are limited to pitch and sway motions in this study. The Matlab built-in function "cpsd" is used to evaluate cross-spectral densities. This function uses Welch's averaged, modified periodogram method of spectral estimation. The output is validated using an in-house algorithm based on multivariate autoregressive modelling (MAR)[36]. For the imaginary parts of the cross-spectral densities, the absolute values are taken into account for moment calculations on both the measured and the theoretical sides to facilitate the optimisation. For simplification, the peakedness factor of wind-sea partition is fixed to a constant value of 1 as in many other studies, e.g. [56].

In this project, regardless of knowing whether the wave spectrum is unimodal or multipeaked, the optimisation procedure, explained in Chapter 3 is applied to all wave cases in Table 4.2. The results from the gradient-based method (Multistart) and the genetic algorithm approach were found to be very similar except a few cases where the genetic algorithm shows a higher stability in terms of initialization and convergence. On the other hand, the computational time of multistart is approximately 8-10 minutes for estimation of the whole spectrum; whereas the genetic algorithm is 2-3 times slower. The computer system was intel(R) Core(TM) i7 with CPU 2.40 GHz and 8 Gb of memory.

Based on the current study, it was not possible to determine which algorithm is more efficient for the optimisation problem of this method. Justification of this choice requires further studies. Only the results from genetic algorithm are shown here.

Table 4.3: Parameters of unimodal spectrum (Wind Sea).

Case		H_s(m)	T_p(s)	μ(deg.)	s_{max}
A	real	3	8	45	10
	mean	2.1	7.2	63	15
	std	0.19	0.36	15	4.4
B	real	3	8	90	10
	mean	3.9	7.6	81	18
	std	0.4	0.2	12.5	5
C	real	3	8	135	10
	mean	3.5	6.7	136	16
	std	0.43	0.35	10	4
D	real	3	8	180	10
	mean	4	7.2	-176	12
	std	0.64	0.6	2	10

4.6 Results

The estimated parameters are compared with the real values in Tables 4.3-4.5. The average values and the standard deviations correspond to the fifteen sets of realisations as discussed in Section 4.4. As the results show, this number of data sets seems to be sufficient since the standard deviations are mostly small. For illustration of the results in Tables 4.3-4.5 please see Figures 8.3-8.5.

It can be seen in Tables 4.3 and 4.4 that for both swell-dominated and wind-dominated unimodal waves, the estimations reasonably match the true waves particularly in terms of the significant wave height, the peak period and the mean wave direction. The highest wave direction error is 25 deg. in case H.

For the pure wind seas, when a secondary spectrum is fitted to the low frequency part, the algorithm often converges giving a small magnitude of significant wave height. However, modification of this secondary peak through the fitting of the whole spectrum in the final step, which was explained in Section 3.4.3, always results in a significant wave height very close to zero. This implies that the secondary peak can be correctly neglected in this case.

For the pure swell events, the wind speed is quite low, 5 m/s according to Table 4.2. So, the separation frequency becomes a large value and, consequently,

Table 4.4: Parameters of unimodal spectrum (Swell).

Case		H_s(m)	T_p(s)	μ(deg.)	s_{max}	γ
E	real	5	15	45	25	4
	mean	4.9	14.6	43	27	5
	std	0.34	0.52	7	19	2.26
F	real	5	15	90	25	4
	mean	4.8	14.8	90.8	23	6
	std	0.5	0.32	1.3	4	1.8
G	real	5	15	135	25	4
	mean	5.5	15.9	135	52	6
	std	0.5	0.37	2	14.4	0.9
H	real	5	15	180	25	4
	mean	6	15	155	61	6
	std	0.4	0.5	2.5	12	0.6

the high frequency range to be fitted to the secondary spectrum is narrow. As a result, the program does not converge or it converges to a point outside the range of wind-sea frequencies. As expected from the true wave, it can be concluded that no wind-generated peak is recognised in the spectrum.

According to Table 4.5 for bimodal wave spectra, the partitioning approach precisely estimates the significant wave heights and the peak periods. The results of both swell and wind-sea parts in all wave scenarios are promising even in the case of closely-located peaks, where the two systems are overlapping. The error of the mean wave direction in wind seas does not exceed 21 deg. However, the standard deviation is quite large in case P. For the mean wave direction in the swell part, the errors are not significant except in case P, where the direction is 48 deg. lower than the true value.

Among all of the studied cases, the maximum errors in H_s and T_p are 1 meter and 2 seconds, respectively. The estimations, relatively, follow the accuracy requirements for the wave estimator given by the World Meteorological Organisation, WMO, [6]. The error limit in that source is $\pm 20\%$ for the significant wave height and ± 1.0 s for the average wave period.

It is also observed in this study that the estimated spreading parameter is critical to the initial guess, particularly in the wind-sea systems. In the swell systems, this parameter is usually overestimated, which conforms with the

Table 4.5: Parameters of bimodal spectrum.

Case		Wind sea				Swell				
		H_s(m)	T_p(s)	μ(deg.)	s_{max}	H_s(m)	T_p(s)	μ(deg.)	s_{max}	γ
I	real	3	8	45	10	5	15	-135	25	4
	mean	3.1	8.8	66	15	5.2	15	-160	33	1.5
	std	0.7	0.49	10	0	0.65	0.58	12	5.8	0.6
J	real	3	8	-90	10	5	15	90	25	4
	mean	3.2	8.6	-106	18	4.4	16.6	98	27	4.4
	std	0.57	0.75	22	2	1.3	1	7.6	14	2.9
K	real	3	8	135	10	5	15	45	25	4
	mean	2.3	7.3	120	12	5.5	13	49	65	6
	std	0.5	0.8	13	0	0.4	0.15	14	20	4
L	real	3	8	90	10	5	15	180	25	4
	mean	3.6	9.12	89	15	5.3	16	174	49	4.8
	std	0.5	0.17	2	0	0.93	2.7	4	28	2.1
M	real	3	8	45	10	2	12	-135	25	4
	mean	2.7	8.3	56	19	2	13.9	-140	39	7
	std	0.5	0.8	18.6	3.5	0.3	1.4	31	13	2
N	real	3	8	-90	10	2	12	90	25	4
	mean	2.7	9.5	-102	21	2.6	13	110	38	5.2
	std	0.66	1.28	17	3.8	0.19	1.7	25	22	4.3
O	real	3	8	135	10	2	12	45	25	4
	mean	4	8.7	132	15	2.3	11.2	50	30	6.8
	std	0.6	0.9	15	0	0.18	0.95	9.3	7	2.4
P	real	3	8	90	10	2	12	180	25	4
	mean	3.8	8.1	96	15	2.2	12.8	132	53	5.6
	std	0.37	1	34	4	0.3	0.4	6	11	2.1

outcome of other response-based estimation studies e.g. [59]. However, it is found that the estimates of the three basic parameters (H_s, T_p, μ) are relatively independent of the spreading parameter, and also the peakedness factor. This confirms that the current method, where only the moments of spectra are fitted, deals with the main integral parameters of each system, and it might not be correct to evaluate the spectral shape of waves based on this approach. Example polar plots and frequency spectra for cases I and N are illustrated in Figures 4.5 and 4.6, which show the influence of the differently-estimated spreading factors and peakedness factors on wave spectral shapes. For more figures see Appendix A.

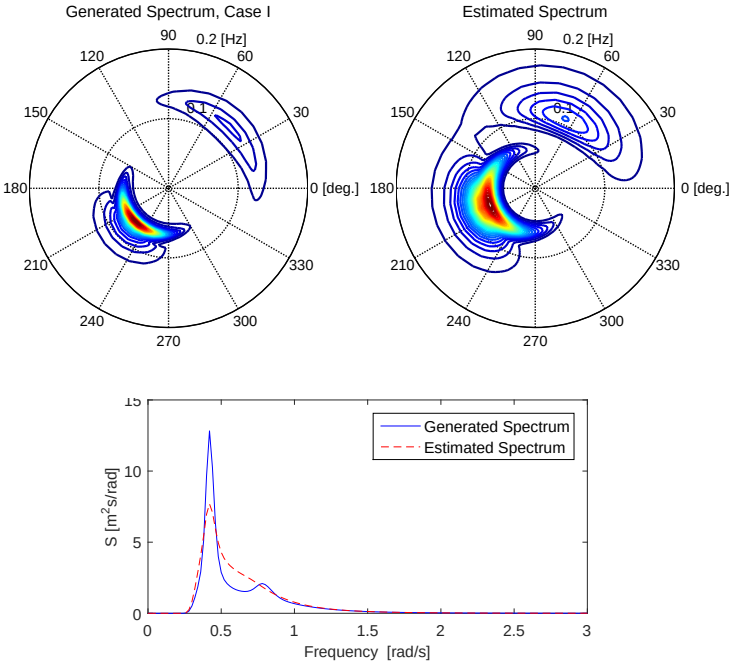

Figure 4.5: Directional wave spectrum in Case I.

4.7 Conclusion

The method based on a parametric model of wave spectra and the partitioning procedure, presented in Chapters 2 and 3, are evaluated by numerical tests. The results show that this method can successfully estimate the underlying sea state used for generation of the responses. In both wind-sea and swell wave

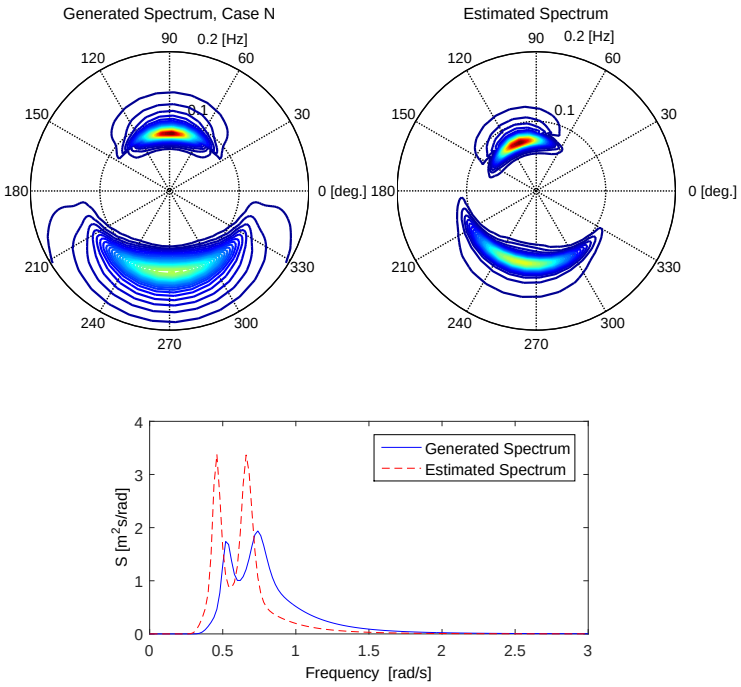

Figure 4.6: Directional wave spectrum in Case N.

scenarios, not only the the significant wave heights and the wave peak periods, but also the estimated mean wave directions are quite accurate.

Although high-frequency wind seas may not be sensed by large ships because of filtering effects, this can be overcome to some extent by the additional constraints applied to the optimisation problem in the wind-sea partition. As the results show, for the specific ship studied here, this strategy is efficient enough to estimate waves with a peak period of 8 seconds or longer. However, when the actual peak period is very low, e.g. 6 seconds, the current method is not expected to be reliable since all the responses are close to zero at frequencies greater than 1 rad/s as seen in Figure 4.3. Nevertheless, it is noteworthy that with the goal of decision support for operational safety, the complete and accurate wave energy distribution with frequency and direction may not necessarily be important. Because the ship may not respond to the high frequency excitations at all, and only the frequency range that the ship responds to is important.

Chapter 5

Estimation Based on Full-Scale Measurements

5.1 Introduction

In order to assess the validity and the robustness of the presented wave estimation method, besides numerical experiments, full-scale measurements of ships should be examined. In this chapter, two container ships with different sizes are studied. As stated before, the wave elevation is a random and stationary process. Thus, the time series of responses are assumed to be stationary and ergodic so that the statistical properties can be estimated from one realisation of responses.

In order to analyse the estimations based on full-scale data, the measured data should be checked first. Among the available time series, some responses look distorted in a specific period, meaning that the time series are unstable or spectral analysis results in unexpected shapes. Those responses should be discarded. In an ideal case, as already applied in many applications, the signals are recorded as digital processes for a specific period, and the time series are calibrated. A data control regarding format errors, information errors and non-physicality is carried out. The time series accepted as correct should be stored to be used for wave estimation. Lajic [30] has introduced concepts for a fault tolerant system that can automatically detect and discard faulty signals. However, the data control process is not carried out herein.

Table 5.1: Operational conditions.

Cases	Dates	Mean Draft [m]	Speed [kn]	Location
I	12/08/2011	14.2	21.0-23.5	Gulf of Aden
II	16/09/2011	14.0	17.0-18.0	Gulf of Aden
III	20/09/2011	14.0	11.5-13.5	South of India
IV	2/10/2011	15.0	9.5-14.0	Off Hong Kong

5.2 9400 TEU Container Ship

5.2.1 Measurement systems

Full-scale data from the container ship characterised in Chapter 4 is considered here. The ship is equipped with both accelerometers and strain gauges. Accelerations are captured by three degrees of freedom acceleration sensors on both port and starboard sides along the ship. Those accelerometers are calibrated for ±5g and the rate of turn sensors for ±150 deg/s. The strain measurements amidships are obtained using two sets of long-base strain gauges mounted in the passageways just below the deck at midship section.

During the TULCS project, the ship traded on a route between the North Sea in Europe and the Sea of China. Four sets of 24-hours data in 2011, which are provided by MARIN, are considered in this study for wave estimation. The operational conditions and the geographical locations are specified in Table 5.1. The same data were used by Andersen [2].

The time series of vertical motion at forward (151 m from midship section) and port side of the ship, pitch, sway and strain at midship section are used. The rates and displacements are also provided, which are derived by integration. The sampling rate is 20 Hz after anti-aliasing filtering have been applied. Besides the response measurements, ship speeds, ship headings, mean wind speeds and mean wind directions are also available.

The relation between the mean wave direction relative to north and this quantity relative to ship heading is calculated from

$$\mu = 180 - (\theta_{wave} - \theta_{Sh}), \tag{5.1}$$

where μ is the relative mean wave direction, θ_{wave} is the mean wave direction and θ_{Sh} is the ship heading relative to north. A head sea is, thus, represented by $\mu = 180°$. In a similar way, the wind direction relative to the ship heading, ν can be calculated from the measured wind direction.

As a sample, 800-second time series of responses in case I are shown in Figure

5.1. The strain is converted into stress using a modulus of elasticity of 210 GPa corresponding to normal ship building steel. The average of stresses at port and starboard is taken to be converted to vertical bending moment in order to exclude possible contributions from horizontal and torsional stress components. The maximum wave-induced vertical bending moment, VBM, at the location of the strain gauge at midship section can be found from Naviers formula:

$$VBM = \frac{\sigma I}{z_{sg}}, \tag{5.2}$$

where σ is the stress associated with pure vertical bending, I is the sectional

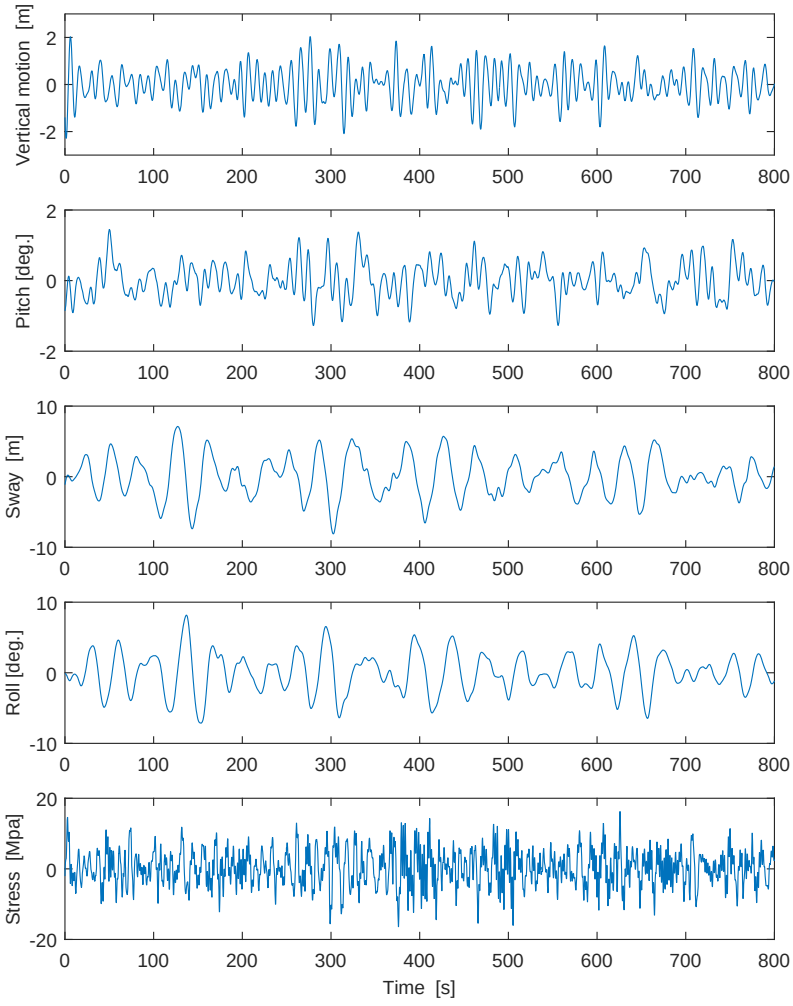

Figure 5.1: Sample time series of different responses.

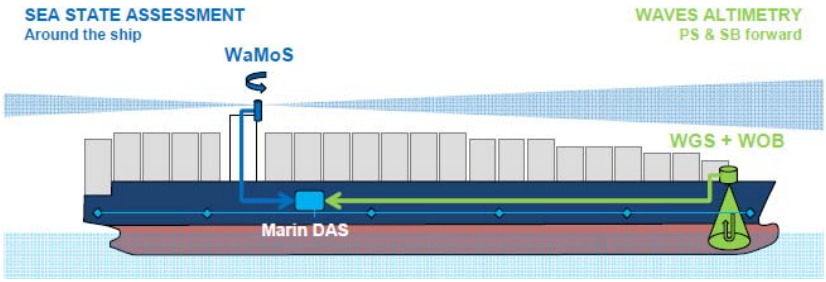

Figure 5.2: Equipments onboard Rigoletto for wave estimation.

moment of inertia of the hull and z_{sg} is the vertical distance from the neutral axis to the strain gauge.

As shown in Figure 5.2, there are two other systems already installed onboard the Rigoletto to estimate the sea state: 1) an X-band radar system (Wave Monitoring System or WaMoS), which scans the sea surface and gives the sea state parameters (zero upcrossing period, peak period, significant wave height and mean wave direction), and 2) a wave guide system by a Dutch company, Radac, which is installed in the bow of the ship and consists of two radar sensors. This system prepares time-varying signals proportional to the distance from the sensor at the ship bow to the water surface. This is converted to the instantaneous water surface position by the difference with the time-varying vertical position of the sensor. This position signal is obtained by using a double integration of vertical acceleration signal from an accelerometer in the same location as the radar unit. It should be mentioned that the latter system is not able to indicate the orientation of the waves. Moreover, the peak periods from the Radac are estimated by implementing spectral analysis based on the measured sea surface elevations in the encounter domain. Transformation of these data to the 'true domain' needs information about the relative direction of waves, which is not available from the Radac itself. In this study, the wave direction data from the WaMoS are used to obtain the true wave periods of the Radac.

For both systems, the parameters are computed every 30 seconds for observation period of 20 minutes. The swell and the wind-generated components are separated by the WaMoS based on the estimated peak periods. For the analysis in the TULCS project, the separation period is set to the arbitrary fixed value of 10 s, as mentioned also in Chapter 2. If the estimated peak period is less than this value, the sea state is set to wind driven and if the peak period is greater than or equal to this value, the sea state is set to swell.

Hindcast data are also available from Deutscher Wetterdienst for the GPS positions corresponding to the considered voyages. The data include wind

speed and direction, current speed and direction, and also the significant wave height, peak period and direction of wind-sea and swell components. The wave data from the above mentioned three sources, averaged every hour, are used in this chapter for comparison with the estimated sea states based on ship responses.

5.2.2 Wave estimation procedure

In practice, wave systems are assumed to be stationary in a duration of the order of 20-60 minutes. In this chapter, as the geographical location of ship is subject to change continuously, the optimisation is implemented based on a 20-minute long data as a stationary period for wind waves; however, swell events seem to be stationary for a longer period. Estimation of swell partition is applied on 1 hour data herein. The mean values of the time series are set to zero to remove the variation in the still-water level, temperature effects, etc. Average wind speed and average wind direction within the corresponding periods are used. This is valid as the wind is also assumed to be stationary over one hour [8]. The wave estimations are carried out in segments of 20 minutes to fulfil real-time conditions.

Following the same procedure as in Chapter 4, the number of peaks is investigated using the separation frequency, which is calculated from the measured wind speed. First, a single wave spectrum is fitted to the measured data using the accelerations and the displacements of the responses. Then, the estimated peak frequency is compared to the peak of the PM spectrum. After charactering the waves as swell or wind dominated, partitioning is applied by separating the high-frequency wind sea part from the low-frequency swell part. As explained in Chapter 3, the measured wind direction with an interval $\pm 90^\circ$ is used to restrict the wave direction estimates in wind seas.

Another approach to determine the mean wave direction is proposed by Davis et al. [24] and [11] using the relative magnitudes of the measured pitch, roll and the vertical velocity of the vessel's center of gravity. This is based on the fact that strong motions occur for relatively long waves and RAOs for these motions become close to unity. Considering the upward heave denoted by x_2, downward roll to starboard by x_4 and bow up pitch by x_6, the magnitude of the angular slope of the deck, x_s can be obtained from

$$sin^2(x_s) = \frac{tan^2(-x_6) + tan^2(x_4)}{1 + tan^2(-x_6) + tan^2(x_4)}. \tag{5.3}$$

The direction of the resultant inclination (the relative wave direction) is given

by

$$tan(x_{5w}) = \frac{tan(x_4)}{tan(-x_6)}. \tag{5.4}$$

Therefore, the instantaneous roll and pitch values are taken to compute the apparent relative wave direction. In addition, the instantaneous heave velocity, (dx_2/dt), is calculated. The values of x_{5w}, for which the latter product is negative, and $|x_s|$ has significant or maximum values, indicate the dominant sea direction, which can be approximately considered as the relative mean wave direction, μ, in the current study.

This criterion seems interesting to exert a limit on direction estimations for swell-dominated waves. The output of the above mentioned method can also be utilised as an initialisation. This initialisation was examined in the current cases in this section through a local optimisation and the results were mostly close to the global search procedure. This is advantageous as the computation speed is increased by local optimisation. However, it is stated in [24] that this method is generally only efficient in head seas and bow-quartering seas. Since the case studies here are mostly estimated as bow-quartering seas, further studies are needed to evaluate the efficiency and robustness of the aforementioned method. This is out of the scope of this thesis and the results are not included herein.

5.2.3 Results and discussions

The results for the peak periods, the significant wave heights and the relative wave directions are shown in Figures 5.3 to 5.6 for individual cases in Table 5.1. The values here are based on the multistart optimisation. The estimated parameters are compared with the estimated values from the WaMoS, Radac and Hindcast data. Since there is no comparative information about the spreading factor and the peakedness factor, the results for these two parameters are not presented in this chapter.

The directional wave radars are generally believed to be quite precise in estimating the wave direction and period. However, the estimates of significant wave heights by wave radar can be less reliable since accurate calibration of this system is important. A significant wave height of 3-5 m is stated to be the most reliable region for the WaMoS onboard the TULCS ship [2]. Initial data analysis of WAVEX, which is a similar system to the WaMoS, shows that this system may significantly overestimate wave heights for swell-dominated conditions [63].

All waves in this section were identified as unimodal. Moreover, bimodal systems from the hindcast data do not seem to be valid in most cases, as will be discussed below. For this reason, the total significant wave heights of the

hindcast data are only shown in the figures for comparison purposes. This quantity is derived by:

$$H_s = \sqrt{H_{s,swell}^2 + H_{s,wind}^2}. \tag{5.5}$$

The same cases as Table 5.1 are also investigated by Nielsen et al. [48], using the traditional parametric method (applied based on Eq. (2.3)) and the Bayesian method. The associated results, which are derived using heave, pitch, roll and sway are also presented in the figures for comparison. For details about the calculation procedures of these estimates, please refer to [48]. The red curves with the 'Parametric' label show the results of the current method based on spectral moments.

In general, the magnitudes and the trends of the significant wave heights and the peak periods conform well with the WaMoS estimates. The peak periods from the Radac are not believed to be reliable as they have large deviations and unrealistic values that are out of scale.

In case I, the estimated peak frequencies are always greater than the peak of the PM spectrum, indicating that the waves are wind dominated. Applying the partitioning procedure, no swell event is identified in this case. As seen in Figure 5.3, this is consistent with the estimates of the WaMoS and the other response-based methods, but in contrast to the hindcast data that show bimodal waves containing both wind sea and swell. Nevertheless, it can be observed that the hindcast peak periods of swell and wind sea are very close together in the first half of the day and the magnitudes of the wind-sea peak periods are unrealistically low between hours 17:00 and 23:00. Therefore, this bimodality in the hindcast data is likely to be a fault.

Among the three response-based estimation methods, the wave parameters from the current parametric method is, in average, closest to the WaMos in this case. Between hours 0:00 and 12:00, the significant wave heights are about 1 meter lower than the WaMoS and the Radac data. This is quite similar to the outcome of the Bayesian method, whereas in the traditional parametric method, the difference is somewhat larger. In the second half of the day, a drop in the energy of waves can be observed in all methods and the quantities of H_s are very close to each other. According to the direction estimates, almost all methods consistently identify bow-quartering/beam sea from the port side throughout the entire day. However, in a couple of estimates, the difference between the current parametric method and the WaMoS becomes considerable.

Figure 5.4 shows the estimated parameters for case II. In this case, from the beginning of the day until 19:00, the first fit implies a swell-dominated spectrum since the estimated peak frequency is always lower than the corresponding peak of the PM spectrum. No secondary peak is distinguished by the current

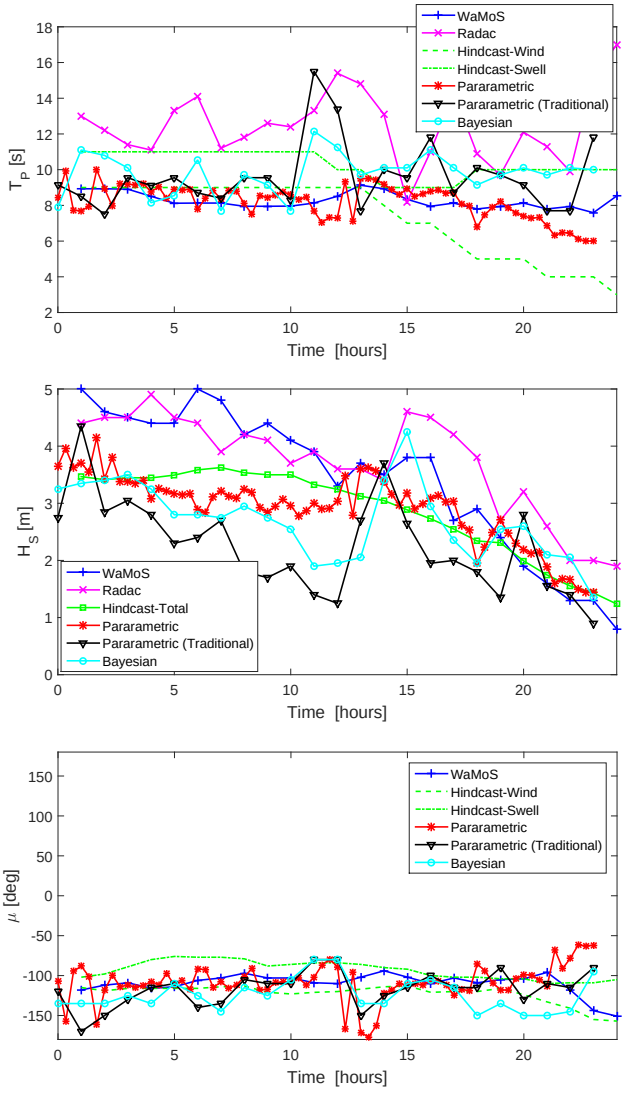

Figure 5.3: Comparative wave parameters using different methods, case I.

estimation method as the estimated peak frequencies of the wind parts always fall below the separation frequencies. In the hindcast data, the second peak is hardly true between hours 0:00 and 18:00, as the peak period is too low. This indicates a pure swell system during this period.

In the last hours of the day, i.e. hours 19:00 to 23:00, where the sea state seems to be moderate according to the estimated significant wave heights, the dominant peak periods are very close to the PM peak periods. It is thereby

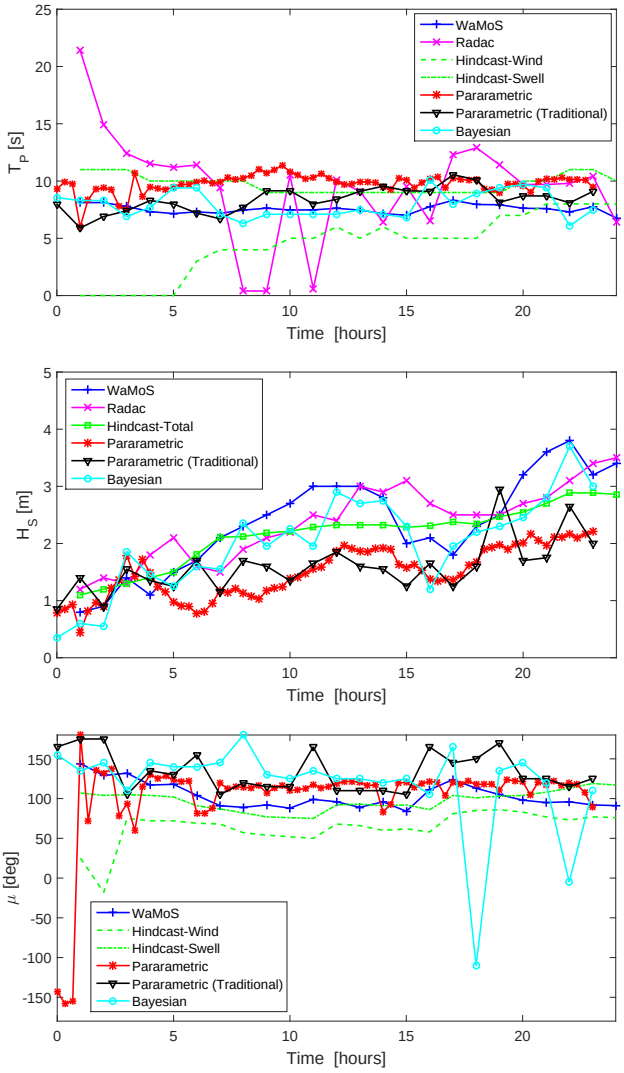

Figure 5.4: Comparative wave parameters using different methods, case II.

reasonable to identify the sea state in this period, as a fully-developed sea. By implementing the partitioning approach in the next step, the estimated peaks in the two partitions are very close together, which conforms with the hindcast data. Hence, the two peaks are merged and a single peak model is used for the whole day.

The significant wave heights in case II comply to some extent with the traditional parametric method. The trends are quite similar to the other sources as well.

However, the magnitudes fall 0.5 to 1.5 meter lower than the WaMoS and the Radac after the first quarter of the day. The peak periods are rather steadily larger than WaMoS, but relatively close to the hindcast swell data. In this case, in terms of the significant wave heights and the peak periods, the Bayesian method gives values closer to the WaMos and the Radac compared to the parametric methods. For direction estimation, except a few initial differences in the direction signs, the estimated values agree reasonably with the WaMoS and the hindcast swell, representing a bow-quartering sea from the starboard side.

In case III, the waves during the whole day are also distinguished as swell dominated. The measured wind speed is very low so that the separation frequency is very high and, thus, no wind sea is identified. As seen in Figure 5.5, the significant wave heights estimated by the current method are mostly in-line with the Bayesian and WaMoS estimates, representing steadily a moderate sea. However, the Radac data are slightly off compared to the other methods.

Similar to case II, the estimated peak periods are systematically greater than the WaMoS. The Bayesian method, on the other hand, has estimated the peak periods rather closely to the WaMoS and hindcast swell. In this case also, the estimated wind sea from the hindcast is not reliable because of very low peak periods. The estimated relative wave directions from all methods imply a steady bow-quartering sea. Notwithstanding, a few outliers are present in the beginning of the day. It is believed that those outliers in cases II and III can be eliminated by improving conditioning of the optimisation by using other sources, or the trend analysis that is introduced in Chapter 6.

Figure 5.6 corresponds to case IV, where the relatively high significant wave heights imply a severe sea state especially in the second half of the day. The waves are distinguished to be wind dominated since the estimated peak frequencies are always well above the peak frequency of PM spectrum. The estimation procedure identifies only one wave system because the estimated peak frequencies for the swell partitions are too low (around 0.05 Hz) with only small amounts of energies (H_s less than $0.1m$).

The significant wave heights from the current method follow the tendency and the magnitudes of the outcome of other response-based methods, to some extent. However, in the second half of the day, the discrepancy between the estimates and the Radac becomes up to 6 meters and the hindcast data are below the other methods. The Radac values seem to be overestimated in such severe sea states. This can be justified due to bow waves, sprays or local wave-hull disturbances, etc.

The peak periods and the relative wave directions from the current method, match well with the WaMoS and the hindcast wind sea in this case. The current

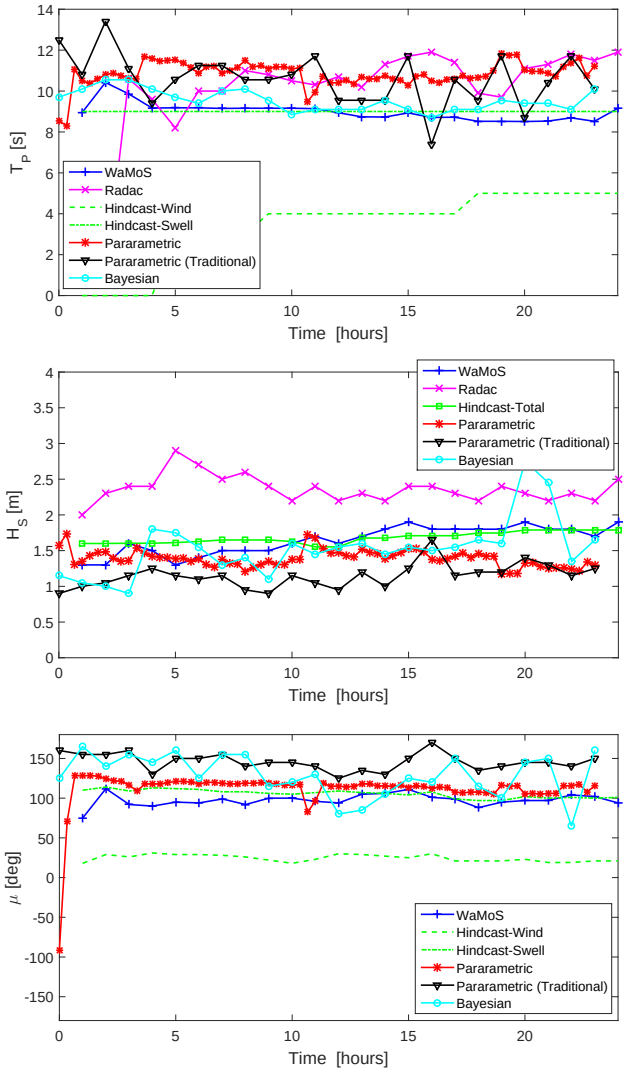

Figure 5.5: Comparative wave parameters using different methods, case III.

method seems to be more promising than the other response-based methods in terms of the time variations and the magnitudes of the peak periods and the mean wave directions. This fact is more pronounced compared to the Bayesian method with large deviations and instability in direction estimates.

All in all, it can be inferred from the above figures and interpretations that the study of considered full-scale data of the specific ship supports its numerical results in Chapter 4. This validates the applicability of the proposed wave

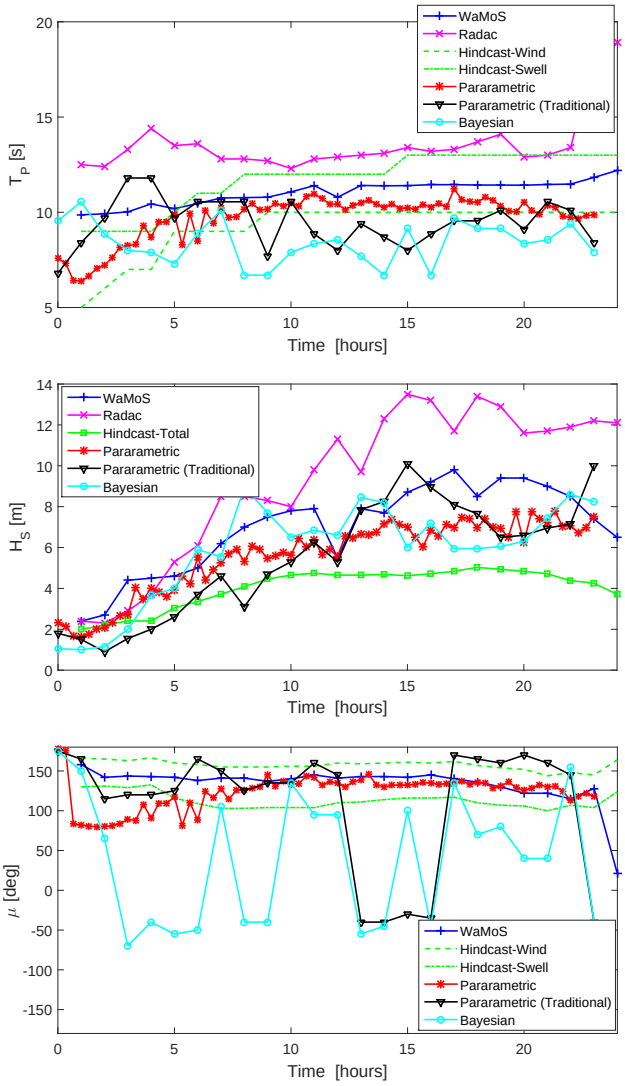

Figure 5.6: Comparative wave parameters using different methods, case IV.

estimation method. Moreover, comparing the results with a couple of previous response-based wave estimation methods (Wave buoy analogy) in the literature, the estimation of wave direction seems to be generally improved.

In wind-sea cases, in general, estimations of peak periods and mean directions look more reliable compared to other methods. Because the scatters are lower and the values are generally closer to WaMoS and hindcast. This is probably due to the additional constraints applied on the wind-sea optimisation by using

wind data. However, in swell-dominated cases, the significant wave heights estimated by the current method fall systematically lower and the peak periods are higher than the other sources. This can be a shortcoming of the parametric models since the results from the traditional parametric method deviate in a similar way. This lack was not significantly realised in the numerical calculations in Chapter 4 because the responses are simulated from the same wave spectral model. The Bayesian method seems more powerful in the associated estimates in those swell cases.

5.3 6800 TEU Container Ship

Full-scale measurements of a 6800 TEU container ship are available from the NK classification society. Table 5.2 shows the main characteristics of this ship. The time series of pitch, roll, heave acceleration, and sway accelerations are available at the center of gravity. The stresses are also provided at the midship section, on the upper deck level, which can be easily converted to vertical bending moments. The data are sampled at 10 Hz for periods of 20 minutes every 2 hours.

Hindcast data are also available, which are used for comparison with the estimations keeping in mind that these data do not show the accurate wave parameters at the specific location of the ship. Moreover, wind-sea and swell data are not available separately. The wave periods are presented as significant wave period, T_s, which is defined as the average period of the one-third highest waves. To be able to compare the results, these periods are converted to peak periods with the following relation [32]:

$$T_p = 1.0574 T_s. \tag{5.6}$$

A couple of 24-hour days that have relatively low gaps in time series of responses, hindcast and GPS data are chosen for wave estimation. The operational conditions of the studied cases are presented in Table 5.3. As the measurements are not calibrated, those time series that are unstable or have significant outliers

Table 5.2: Ship characteristics.

Properties	Values
Overall Length [m]	293.87
Beam [m]	40
Maximum Draught [m]	14
Maximum Speed [kn]	29
DWT [ton]	75,000

Table 5.3: Operational conditions for the studied cases.

Cases	Dates	Mean Draft [m]	Average Speed [kn]	Location
I	12/08/2002	12	23	East China Sea
II	24/07/2003	11	24	Gulf of Aden
III	28/09/2003	11	21	East China Sea
IV	23/11/2003	11	22	East China Sea
V	29/11/2003	9	24	East China Sea
VI	10/01/2004	12.7	24	Arabian Sea
VII	26/05/2004	11.5	23	Arabian Sea
VIII	05/09/2004	10	20	East China Sea

are disregarded. As a sample, 800 seconds of time series of responses in case V are shown in Figure 5.7.

The operational speeds and also the headings of the ship are calculated from the GPS data using the following formula[1], based on the coordinates of two points (1 and 2):

$$\begin{aligned} x_1 &= R_E cos(\phi_1) cos(\varphi_1), \\ y_1 &= R_E cos(\phi_1) sin(\varphi_1), \\ z_1 &= R_E sin(\phi_1), \end{aligned} \tag{5.7a}$$

$$\begin{aligned} x_2 &= R_E cos(\phi_1) cos(\varphi_1), \\ y_2 &= R_E cos(\phi_1) sin(\varphi_1), \\ z_2 &= R_E sin(\phi_1), \end{aligned} \tag{5.7b}$$

where ϕ and φ represent the latitude and longitude in rad, respectively. $R_E =$ 6371000 m is the mean earth radius. The angle between the two points can be calculated using the dot product and R_E:

$$\theta_{12} = acos\Big(\frac{x_1 x_2 + y_1 y_2 + z_1 z_2}{R_E^2}\Big). \tag{5.8}$$

The great-circle distance between the two points is

$$D = R_E \theta_{12}, \tag{5.9}$$

and finally, the ship forward speed, V, is obtained by dividing the distance by the time travelled between the two points, Δt:

$$V = \frac{D}{\Delta t}. \tag{5.10}$$

[1] http://www.ridgesolutions.ie/index.php/2013/11/14/algorithm-to-calculate-speed-from-two-gps-latitude-and-longitude-points-and-time-difference/

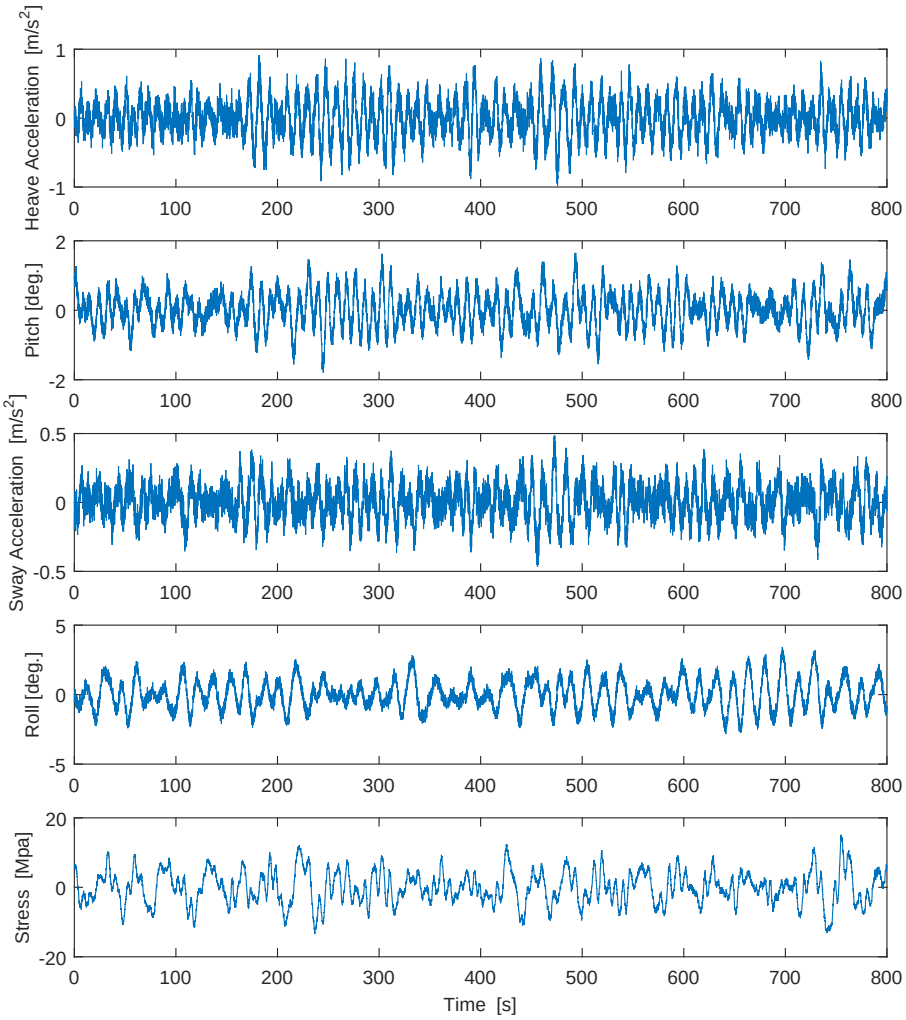

Figure 5.7: Sample time series of different responses in case V.

The ship heading, θ_{Sh}, can be derived using a straight line along a great-circle arc from the start point to the end point [2]:

$$\theta_{Sh} = atan\Big(\frac{sin(\varphi_2 - \varphi_1)cos(\phi_2)}{cos(\phi_1)sin(\phi_2) - sin(\phi_1)cos(\phi_2)cos(\varphi_2 - \varphi_1)}\Big). \tag{5.11}$$

It should be noted that the above calculations assume the speed through water equal to speed over ground. However, depending on the current speed, this

[2]http://www.movable-type.co.uk/scripts/latlong.html

may impose uncertainty to the estimations.

The transfer functions of heave, pitch, sway, roll and vertical bending moment at midship section are also provided by Class NK in several loading conditions. The amplitudes of those transfer functions for T=10 m and V=23 kn are shown in Figure 5.8. Comparing this figure with Figure 4.3 in Chapter 4, the amplitudes of RAOs in different directions show a very similar qualitative behaviour to Rigoletto in heave, pitch and sway motions. However, as expected because of the smaller size and the lower DWT of this ship, the amplitudes of heave and pitch are slightly larger than Rigoletto. For vertical bending moment, the maximum amplitude occurs at head sea condition similar to Rigoletto. However, the magnitudes are much lower in this smaller ship. The maximum amplitude of roll motion is 0.12 rad/m in beam sea condition, whereas in Rigoletto, the maximum magnitudes are quite a bit lower occurring in bow-quartering sea condition.

The response combination used here for wave estimation is similar to Section 5.2. Roll is not considered, but heave is used instead of vertical motion. The transfer functions are interpolated and extrapolated for the full range of directions with 5° intervals and also for different drafts that are not available. Cases with forward speeds far from the provided RAOs were not used.

Figures 5.9-5.16 show the estimated parameters from multistart method compared with the hindcast data. It can be seen in Figure 5.9 that in case I, a unimodal swell spectrum is estimated. The significant wave heights are 1-1.5 meters lower and the peak periods are up to 2 seconds longer than the hindcast data. It is also observed that at 20:00, the optimisation fails. The estimated wave direction in case I is very close to the hindcast data. However, deviations of $50 - 70^\circ$ are observed during the last hours of the day.

In case II (Figure 5.10), the estimated waves are swell dominated. Although the trend of the significant wave heights of swell mostly agrees with the hindcast, in common with case I, the magnitudes of H_s and T_p fall significantly below and above the hindcast values, respectively. However, the estimates become very close to the hindcast data in the last hours. The estimated mean swell directions show beam sea conditions during the whole day. This is in fair agreement with the hindcast data, where the waves vary from a beam sea toward a stern-quartering sea. The present method also estimates a wind-sea system during the early hours of this day. This wind sea enters from the bow, and diminishes later. In this period (between hours 0:00 and 6:00), the summation of the significant wave heights of wind sea and swell gives a value very close to the hindcast data.

In case IV, as shown in Figure 5.11, during the first third of this day, a pure swell system is estimated, the significant wave heights and the directions of

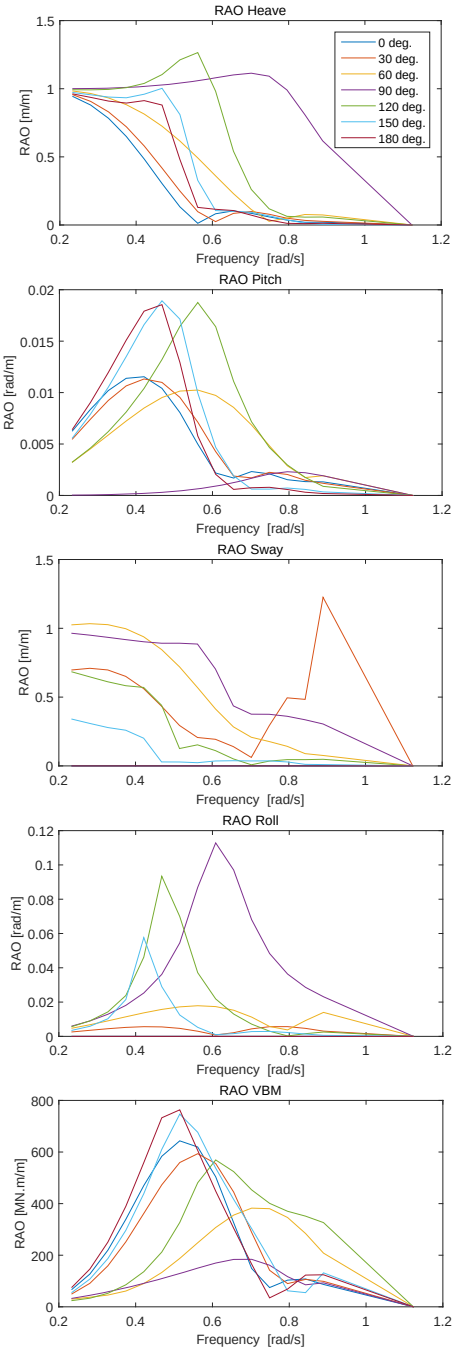

Figure 5.8: Amplitudes of RAO for different responses, V=23 kn, T=10 m (The legends are identical in all figures).

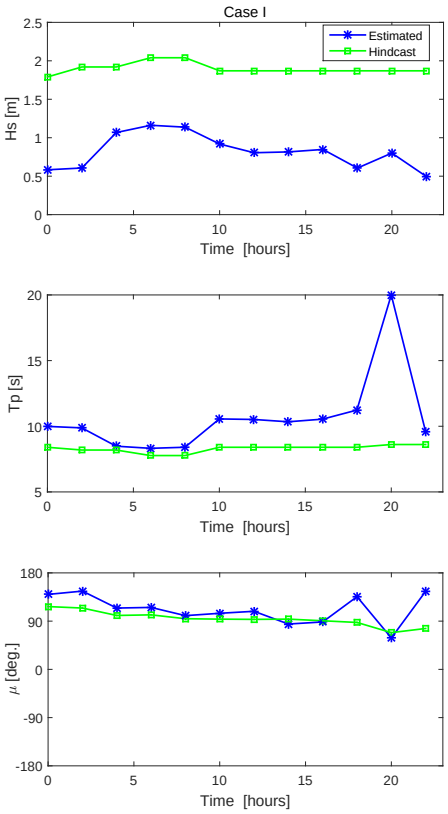

Figure 5.9: Estimated wave parameters for case I.

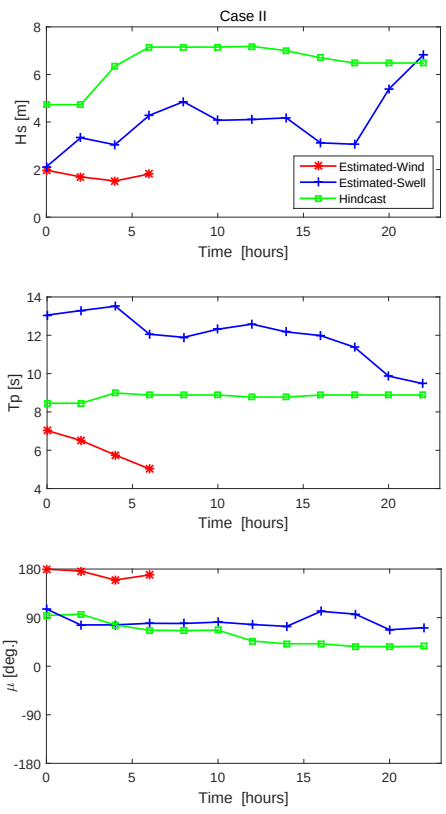

Figure 5.10: Estimated wave parameters for case II.

which match the hindcast data very well. However, the peak periods are much higher than the hindcast. During the rest of the day, the spectrum is estimated to be bimodal. The significant wave height of swell increases from 1 meter to 4 meters. The significant wave height and the period of wind sea is very close to the hindcast data in this case. However, the direction estimates indicate beam sea/bow-quartering sea conditions entering from the port side, whereas the hindcast shows bow-quartering sea/head sea from the starboard side. As mentioned before, there is no information on whether the hindcast data correspond to wind sea or swell, so it is not easy to judge whether or not the estimations are correct.

In case IV (Figure 5.12), the waves are wind dominated. The significant wave heights of swell are very low ($< 1m$) and become zero at 16:00. Compared to the hindcast data, the significant wave heights of the wind sea are underestimated by 1-2 meters during the first third of the day, but this difference becomes

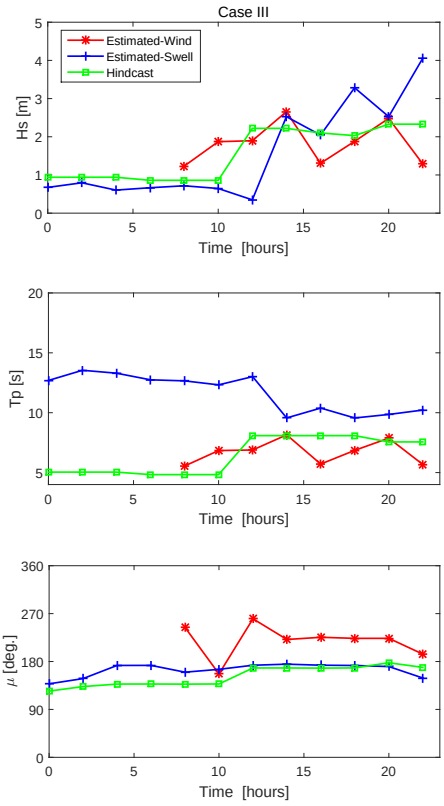

Figure 5.11: Estimated wave parameters for case III.

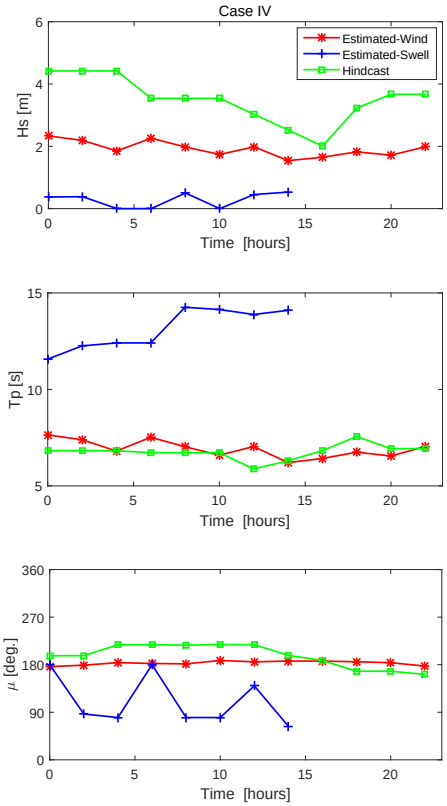

Figure 5.12: Estimated wave parameters for case IV.

rather low during the rest of the day. The estimated peak periods and directions of the wind sea are relatively consistent with the hindcast.

In Figure 5.13, in the early hours, the spectrum is estimated as unimodal swell. The significant wave heights are fairly close to the hindcast but the peak periods and the directions differ largely. During the rest of the day, the estimated spectrum is bimodal. Between 6:00 and 14:00, the significant wave heights of both wave components are 2-3 meters, superposition of which matches the hindcast. At 16:00, a jump is seen in the estimation of the significant wave height of swell, which seems questionable. After this point, the estimated significant wave heights are in line with the hindcast. However, the wind sea also has a considerable quantity that should be added to the swell. The direction of swell during the whole day is around beam sea and the wind sea is entering at bow-quartering. These directions are mostly far from the hindcast data.

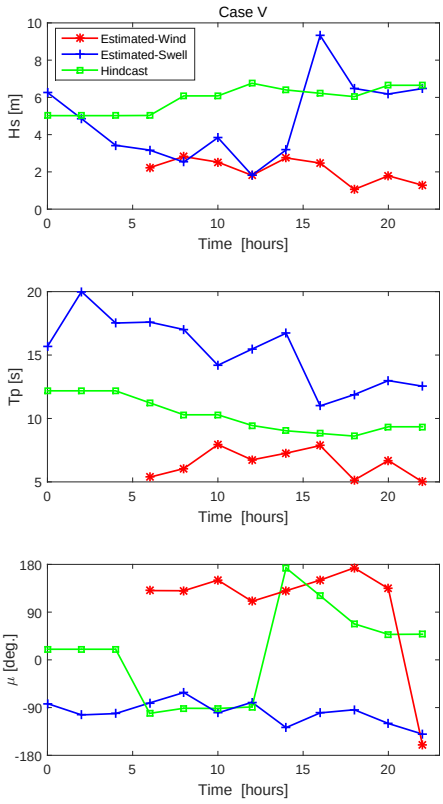

Figure 5.13: Estimated wave parameters for case V.

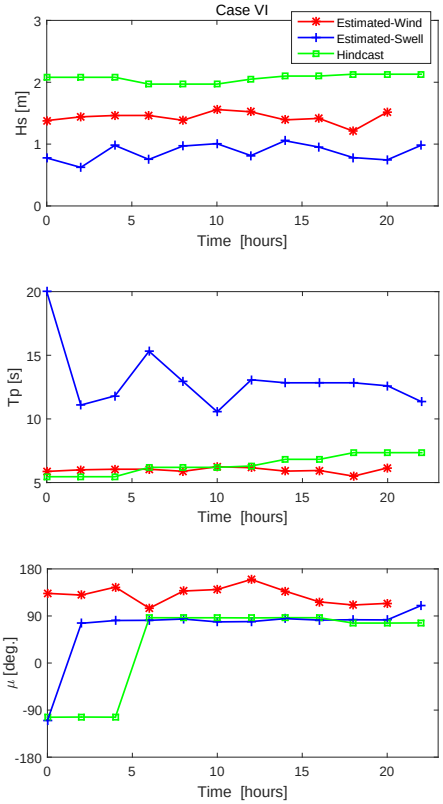

Figure 5.14: Estimated wave parameters for case VI.

In Figure 5.14, the first estimate at 0:00 is hardly correct since the peak period is too large compared to the further estimates. Other than this first point, both the estimates and the hindcast data consistently imply a steady sea state during the day. Superposition of the significant wave heights of wind sea and swell agrees with the hindcast data. The periods of wind-sea estimates conform very well with the hindcast data. The sea state is estimated to be wind dominated in bow-quartering conditions. However, the directions from the hindcast show a beam sea, which is more consistent with the swell direction estimates rather than the wind-sea quantities.

As seen in Figure 5.15, similar to case VI, case VII is also quite stable during the day and the summation of swell and wind sea is reasonably close to the hindcast. The wind-sea estimates are very close to the hindcast data in terms of both the peak periods and the directions. In Figure 5.16, the estimations characterise a swell system with parameters quite different from the hindcast. However,

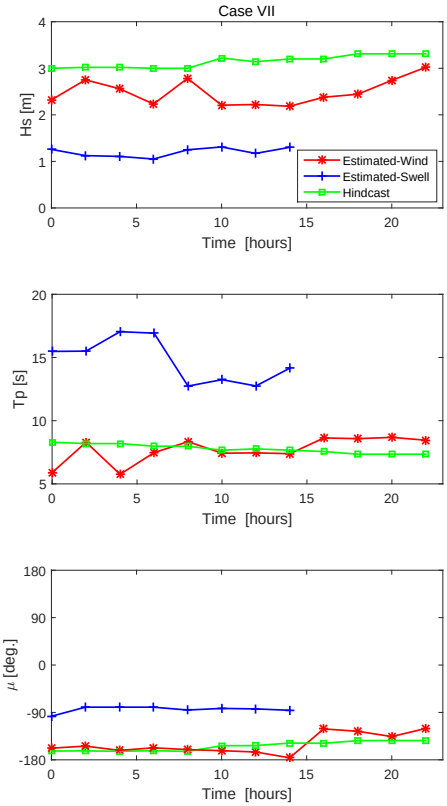

Figure 5.15: Estimated wave parameters for case VII.

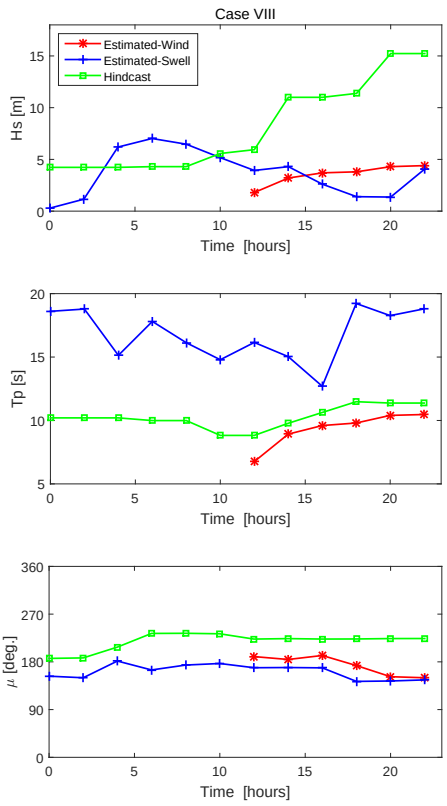

Figure 5.16: Estimated wave parameters for case VIII.

in the latter half of the day, an additional wind-sea system is identified, the peak periods of which comply with the hindcast in terms of the trend and the magnitudes to some extent. This wind sea is estimated to be head sea, which is reasonably close to the hindcast data. The very large magnitudes in the significant wave heights of the hindcast in the last hours of the day are not reliable.

In general, the results for this 6800 TEU container ship show that the wind-sea estimates can be quite promising, but in the swell estimations, the significant wave heights and the peak periods persistently fall lower and higher than the hindcast data, respectively. This result is consistent with the observations from the 9400 TEU container ship as mentioned in Section 5.2.3.

5.4 Conclusion

The presented wave estimation approach is tested using full-scale data for two container ships. Although the true wave parameters are unknown, comparing the results with other wave information sources strengthens the validity of the method in general. Moreover, comparisons between the current moment-based parametric method and the previous response-based wave estimation methods in a few available case studies are made. Progress is observed in the current method, especially compared to the usual parametric approach. This could be due to the fact that integrated response spectra are used rather than spectral densities and this can smooth the results. The applied constraints in the optimisation procedure or the different response combination that is used could be helpful as well. Swell estimations based on the parametric method seem to be less accurate compared to wind seas, which is likely to be due to uncertainty in swell modelling as mentioned in Chapter 2. Additional constraint on swell systems may be useful in the optimisation procedure. This information can be provided from meteorological trends at the actual position of the vessel. A capability to merge data from different methods, can also improve the efficiency of onboard wave estimation. For instance, Iseki et al. [23] have proposed a hybrid Bayesian method that combines wave information from radar and wave buoy analogy.

Chapter 6

Trend modelling of wave parameters

6.1 Introduction

In order to provide a more efficient usage of estimated wave parameters, an automatic dynamic model is introduced in this chapter to evaluate the trend of these parameters during the voyage. This type of result is of interest to upgrade onboard response predictions. In addition, the trend analysis could provide proper conditioning information to be utilised as input to the sea state estimation model. This information could be used as initial values or some constraints to limit the parameters to be estimated. In addition to operational purposes, time evolution of wave systems onboard ships can be useful for global meteorological purposes, for instance, to find out the geographical sources of swell systems. In this regard, it should be mentioned that ship-based observation of waves is already used as a source of data in climatological studies [63].

6.2 Tracking and Prediction of Wave Parameters

6.2.1 Local regression trend model

Due to the variability of sea states over long periods, it is not easy to find a good adjustment for a coherent and consistent time-sequence modelling of evolution of wave parameters. Instead, a dynamic model is introduced, which can become updated according to the new available data. This model is also beneficial for data monitoring in onboard applications, where the location of the ship is continuously changing. The formulation in this section refers to [31]. The so-called trend model is a regression model, in which a certain function of time, $\boldsymbol{x_t}$, is taken as independent variable. A general form of linear regression model is:

$$Y_t = \boldsymbol{x_t}\boldsymbol{\theta} + \epsilon_t, \tag{6.1}$$

where Y_t is a dependent variable and $\boldsymbol{\theta} = (\theta_1, ..., \theta_p)^T$ is a vector of model parameters, which are called regression parameters hereafter to be distinguished from the wave parameters. The residual, ϵ_t, is a random variable with $E[\epsilon_t] = 0$ and $Var[\epsilon_t] = \sigma^2$. Although both time and location change during a voyage, only time variations of wave parameters are considered here. Therefore, the time index t (an integer number) denotes the independent variable and $\boldsymbol{x_t}$ is a certain function of t, $\boldsymbol{x_t} = \boldsymbol{f}^T(t)$, which produces a known vector. Amongst the mathematical functions, polynomial models are widely used for this function [29, 31]. Quadratic model is applied here, $\boldsymbol{f}(t) = (1, t, \frac{t^2}{2})^T$, with $p = 3$ parameters. Therefore, Eq. (6.1) is written as:

$$Y_t = \theta_0 + \theta_1 t + \theta_2 \frac{t^2}{2} + \epsilon_t. \tag{6.2}$$

If the residuals do not follow normal distribution, p should be increased. When N observations (wave parameter estimates) are available, the model equation for those observations is written as:

$$\boldsymbol{Y} = \boldsymbol{x_N}\boldsymbol{\theta} + \boldsymbol{\epsilon}, \tag{6.3a}$$

$$\boldsymbol{Y} = (Y_1, ..., Y_N)^T, \tag{6.3b}$$

$$\boldsymbol{x_N} = (\boldsymbol{f}^T(-N+1), ..., \boldsymbol{f}^T(0))^T, \tag{6.3c}$$

$$\boldsymbol{\epsilon} = (\epsilon_1, ..., \epsilon_N)^T. \tag{6.3d}$$

The vector of regression parameters is estimated by a least squares method given the observations $Y_1, ..., Y_N$. A local trend model is used, where the observations in the distant past are given less weight than the recent observations for

estimation of the regression parameters. This is implemented by considering a forgetting factor, λ, $(0 < \lambda < 1)$, which determines the discount of past observations. The sum of squared residuals are expressed as:

$$SSR(\boldsymbol{\theta}; N) = \sum_{t=0}^{N-1} \lambda^t [Y_{N-t} - \boldsymbol{f}^T(-t)\boldsymbol{\theta}]^2. \tag{6.4}$$

The vector of regression parameters at time step N, $\widehat{\boldsymbol{\theta}}_N$, is the $\boldsymbol{\theta}$ that minimises $SSR(\boldsymbol{\theta}; N)$ in Eq. (6.4). By using a weighted least squares method, this vector is obtained by [31]:

$$\widehat{\boldsymbol{\theta}}_N = \boldsymbol{F}_{\boldsymbol{N}}^{-1} \boldsymbol{h}_{\boldsymbol{N}}, \tag{6.5}$$

with

$$\boldsymbol{F}_{\boldsymbol{N}} = \sum_{t=0}^{N-1} \lambda^t \boldsymbol{f}(-t)\boldsymbol{f}^T(-t), \tag{6.6}$$

and

$$\boldsymbol{h}_{\boldsymbol{N}} = \sum_{t=0}^{N-1} \lambda^t \boldsymbol{f}(-t) Y_{N-t}. \tag{6.7}$$

Estimation of the parameters is updated at each wave estimation segment, when the next observation is available. The forgetting factor is applied here as $\lambda = 0.85$. The prediction of Y given the observations at time step N, $\widehat{Y}_{N+1|N}$, is calculated by:

$$\widehat{Y}_{N+1|N} = \boldsymbol{f}^T(1)\widehat{\boldsymbol{\theta}}_N. \tag{6.8}$$

An interval is usually assigned to the predicted value as a confidence level or a coverage probability, which is called the prediction interval. A $100(1-\alpha)\%$ prediction interval is computed as:

$$\widehat{Y}_{N+1|N} \pm t_{\alpha/2}(N-p)\sqrt{Var[e_N]}, \tag{6.9}$$

where $t_{\alpha/2}$, as a function of $N-p$, is the $\alpha/2$ quantile in the Student's distribution that can be obtained from Table B.1 in Appendix B. e_N is the prediction error as:

$$e_N = Y_{N+1} - \widehat{Y}_{N+1|N}, \tag{6.10}$$

and the variance of this error in Eq. (6.9) is:

$$Var[e_N] = \sigma^2[1 + \boldsymbol{f}^T(1)\boldsymbol{F}_{\boldsymbol{N}}^{-1}\boldsymbol{f}(1)], \tag{6.11}$$

with an estimate $\widehat{\sigma}^2$ of σ^2 as follows:

$$\widehat{\sigma}^2 = \frac{\boldsymbol{\epsilon}^T\boldsymbol{\epsilon}}{N-p}. \tag{6.12}$$

For more details on the mathematical model see [31].

6.2.2 Application on the 9400 TEU container ship

As a case study, the full-scale data of Rigoletto from Section 5.2 are used to model the trends of the estimated wave parameters. The same cases as Table 5.1 are considered. The model uses 20-minute distant estimates from Section 5.2.3. Since the application is real-time, the predictions are also made 20 minutes ahead of the current time. The predictions are started when 3 hours of data are available.

Figures 6.1-6.3 show the estimated wave parameters together with the predictions during the 24-hour days. The dashed lines show 90% confidence interval. The predictions are compared with the WaMoS data. Note that the trend modelling should be applied on the wave parameters and not on the encounter parameters because the ship course can affect the model. For this reason, in Figure 6.3, the ship heading is subtracted from the relative directions so that the mean wave directions towards the north are tracked.

It can be seen, in general, that besides the capability of making predictions 20 minutes ahead of estimations, the trend analysis provides smooth evolution curves for wave parameters. In this way, probable erroneous outliers in the estimations can be compensated, since the local sea state changes relatively slowly in space and time. This can be implemented through a proper initialisation, which is quite important in the optimisation of the wave parameters, as mentioned before. Moreover, the prediction intervals can be used as constraints to avoid erratics that are observed e.g. in the first few hours in Figures 6.1 and 6.3. It can be seen that as the number of estimates used for the trend model increases, the prediction intervals become slightly narrower, meaning that the predictions are more reliable.

As mentioned in Chapter 2, tracing the evolution of individual wave components (swell and wind sea) separately would be advantageous. However, it is not studied in this thesis as the case studies of Rigoletto were all identified as unimodal waves. For the 6800 TEU container ship that was studied in Section 5.3, although some of the wave spectra are estimated to be bimodal, the recorded data in this ship are provided for only 20 minutes within every 2 hours. Thus, trend analysis may be inefficient for those long-distant estimates.

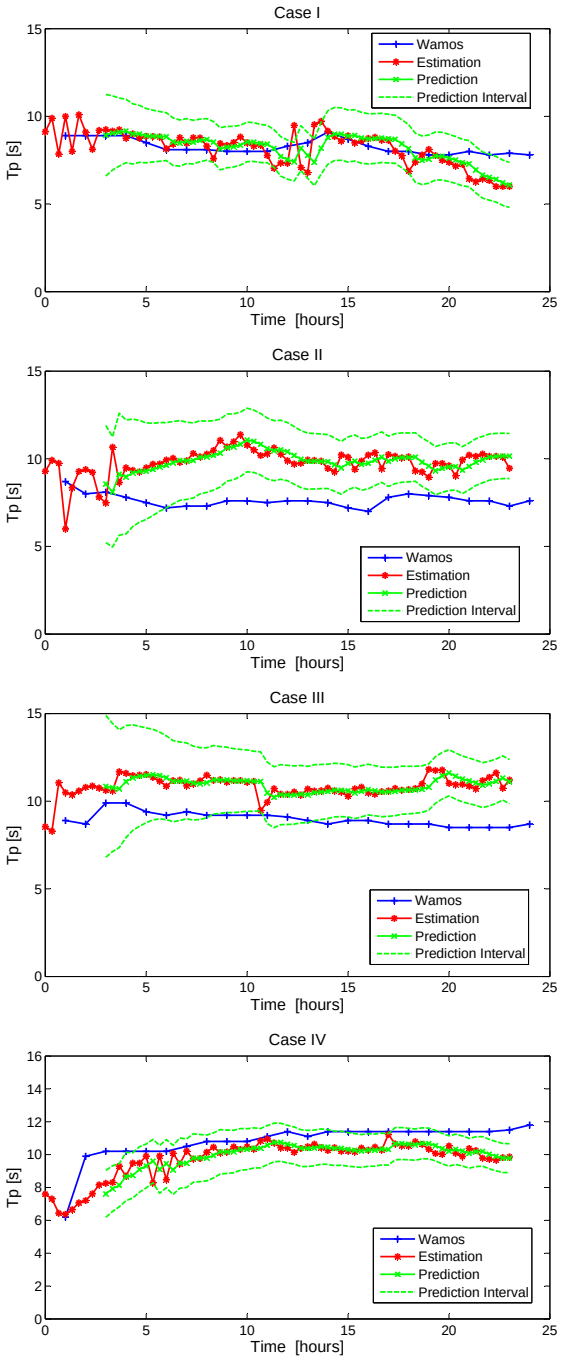

Figure 6.1: Wave peak period.

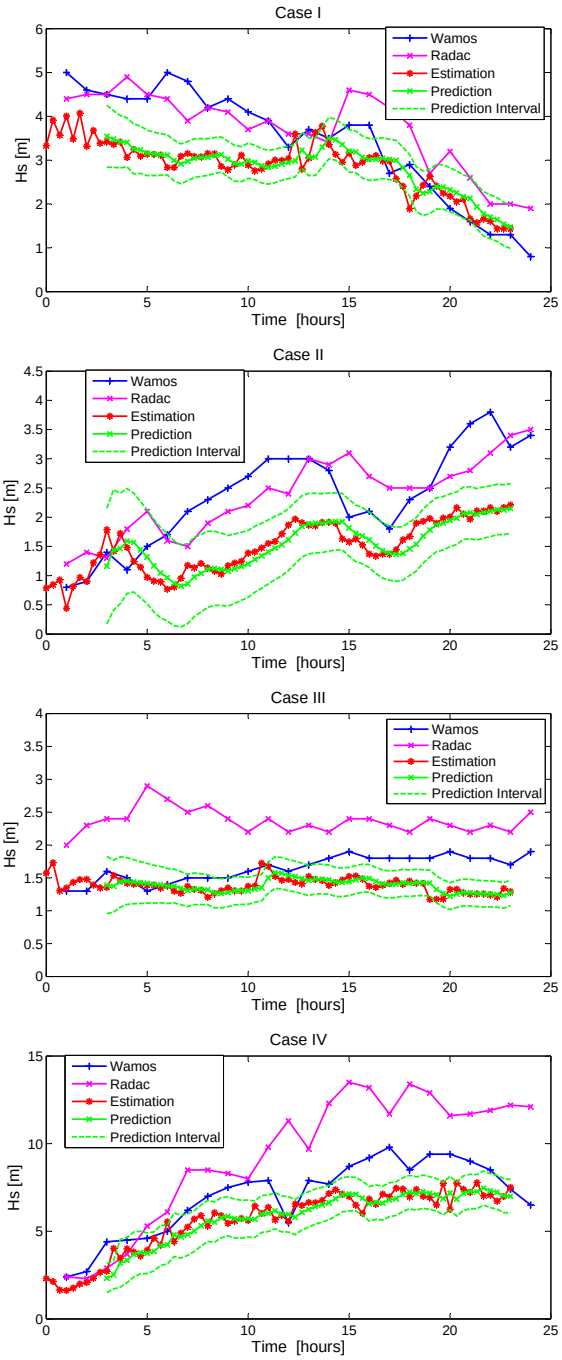

Figure 6.2: Significant wave height.

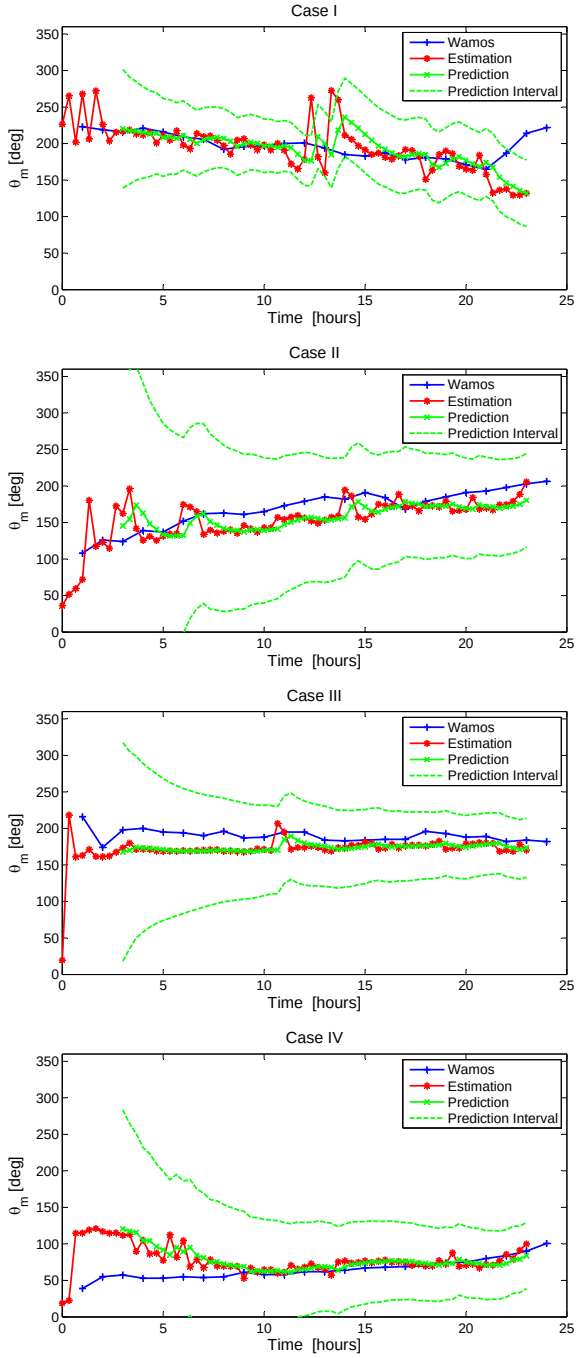

Figure 6.3: Mean wave direction.

6.3 Response Prediction

In decision support systems onboard ships, predictions of seakeeping performance, structural loads, fatigue damage and drift force of the ship are of interest. Moreover, upcrossing rate of whipping can also be estimated using wave data. The idea of seakeeping and load prediction is based on combination of wave estimations with the transfer functions of the response to be predicted. The outcome is the reproduced response statistics to be visualized on the user interface. The response variance, R, that represents the energy amount of the response is usually used:

$$R = \int_0^\infty \int_{-\pi}^{\pi} |H_l(\omega, \theta)|^2 \, S(\omega, \theta) \, d\theta d\omega, \tag{6.13}$$

as taken from Eq. (2.4). Typically, real-time estimation of responses, say 20-60 minutes ahead of measurements, assumes the sea state to be stationary in the corresponding time frame. Therefore, the wave estimates at the present time step together with information about possible changes in operational parameters (vessel speed and heading) are taken into account for response predictions. As shown and discussed by Nielsen and Iseki [44], these assumptions are, however, not necessarily valid. Therefore, they make a hypothesis, based on which the prediction of a response in the forward time step is scaled using the comparison between the measured and the calculated standard deviations, *std*, (square root of the variances) in the present step. So, the scaling factor reads:

$$\lambda_R = \frac{std_{\text{msr}}}{std_{\text{cal}}}, \tag{6.14}$$

In this thesis, in order to improve the precision and reliability of response predictions, it is suggested to adopt the predicted magnitudes of the wave parameters from the trend analysis in Section 6.2. This procedure is applied here to predict vertical bending moment at the midship section, roll and forward vertical acceleration, on the port side of the ship in the case studies in Table 5.1. The latter response is a combination of heave, pitch and roll accelerations. A JONSWAP wave model with the predicted parameters from Section 6.2.2 together with the proper transfer functions are used to obtain the response variances.

The predicted standard deviations of the aforementioned responses are compared with the real measurements. The results are shown in Figure 6.4-6.6. The predictions in this section are also made 20 minutes ahead of the measurements. The blue curves show the estimated responses based on the WaMoS wave parameters using also a JONSWAP model.

The relative differences between the measurements (the black curves) and the current method predictions (the green curves) determine the accuracy of wave

Table 6.1: The average values of e_{msr} within 24 hours.

Cases	VBM		VA		Roll	
	e_{msr}	e_{wamos}	e_{msr}	e_{wamos}	e_{msr}	e_{wamos}
I	0.20	0.34	0.13	0.26	0.55	0.12
II	0.13	0.54	0.13	0.29	0.45	0.28
III	0.05	0.09	0.07	0.06	0.17	0.34
IV	0.09	0.54	0.11	0.35	0.55	0.07

estimations and the estimation model. The error between the two is expressed as:

$$e_{\mathrm{msr}} = \Big| \frac{std_{\mathrm{msr}} - std_{\mathrm{cal}}}{std_{\mathrm{msr}}} \Big|. \tag{6.15}$$

In [44], this relative difference is used as an uncertainty measure. Note that for those responses that have been used for wave estimations (vertical acceleration, pitch, vertical bending moment and sway), e_{msr} cannot address the impact of measurement errors on the estimations.

On the other hand, the relative differences between the predictions (the green curves) and the WaMoS-based estimates (the blue curves) are also derived as:

$$e_{\mathrm{wamos}} = \Big| \frac{std_{\mathrm{cal}} - std_{\mathrm{wamos}}}{std_{\mathrm{cal}}} \Big|. \tag{6.16}$$

The average values of e_{msr} and e_{wamos} over the 24 hours are shown in Table 6.1 for the different responses in all cases. As seen in this table and figures 6.4 and 6.5, the magnitudes and the trends of the predicted bending moments and vertical accelerations are, in general, in good agreement with the real measurements. In other words, e_{msr} is quite low for these two responses. For evaluation of response variances, the same quantities as estimated values are used for the peakedness factor and the spreading parameter. Considering the inaccuracies in the estimations of those shape factors that was discussed in Chapter 4, the low values of e_{msr} show that those parameters are not very important for response variance predictions. Since vertical acceleration and wave bending moment are used for wave estimation, the good agreements with the measurements can be inferred as a validation of the estimation model and the optimisation procedure.

The predictions of vertical acceleration mostly conform with the WaMoS-based estimations as well. However, in case IV, where the waves contain relatively large amounts of energy according to Figure 5.6, the discrepancy between the two sets of estimates is relatively higher, consistently. For the vertical bending moment, the trends of WaMoS-based estimations are in qualitative agreement

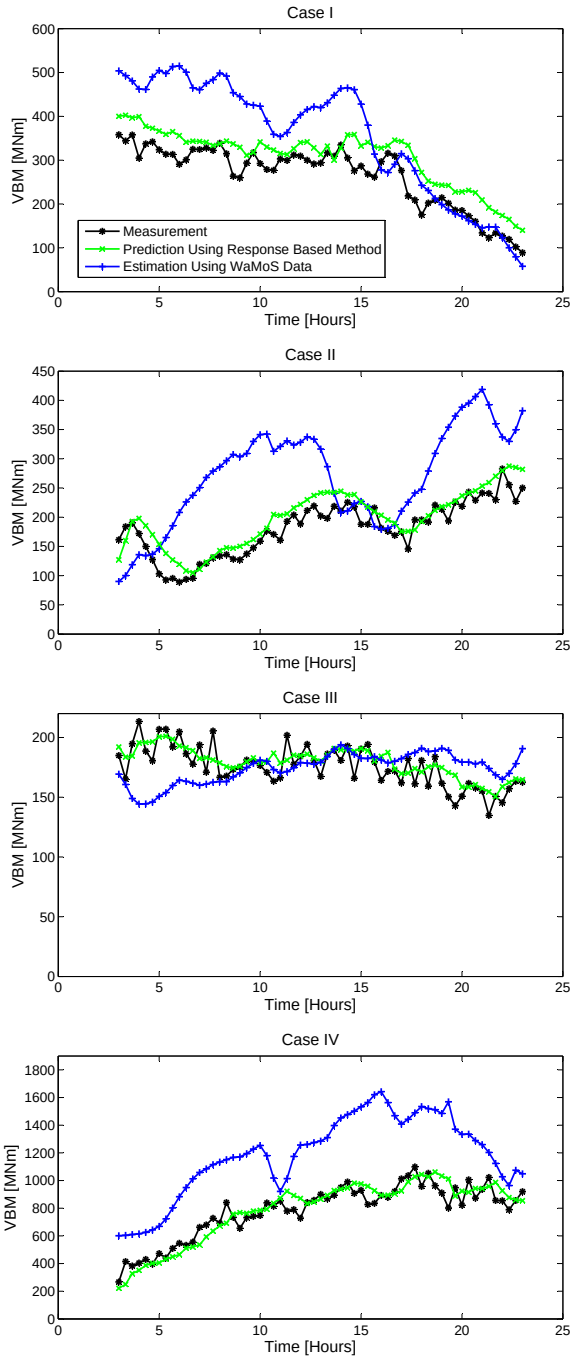

Figure 6.4: Standard deviation of Vertical Bending Moment (The legends are identical in all plots).

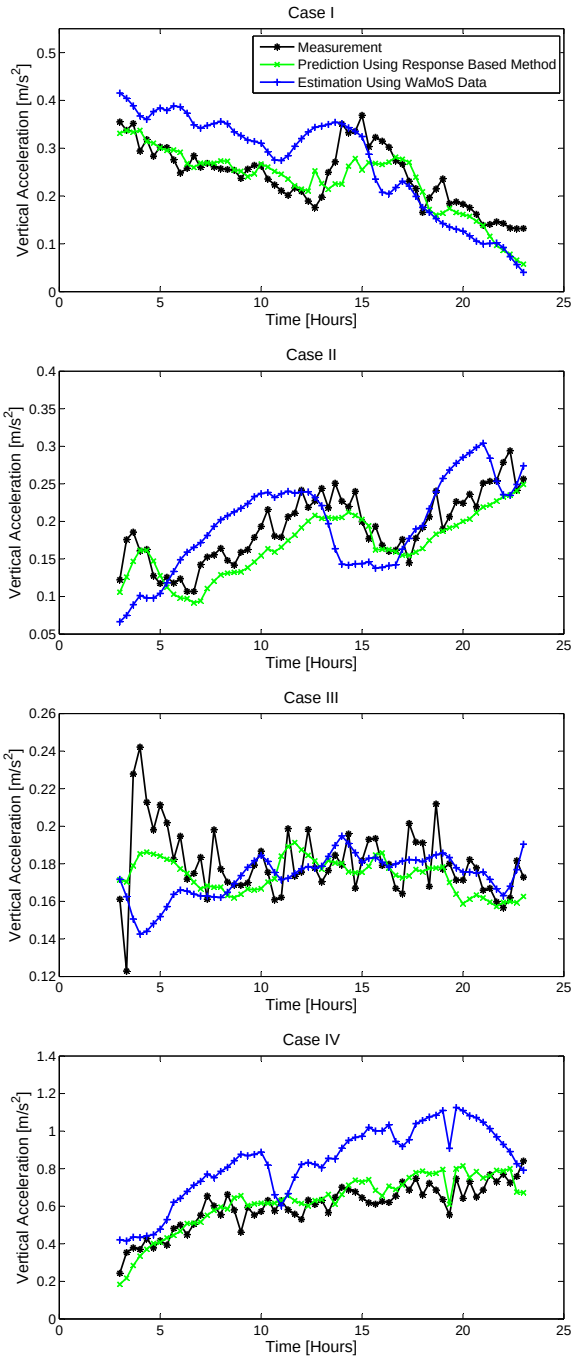

Figure 6.5: Standard deviation of Vertical Acceleration (The legends are identical in all plots).

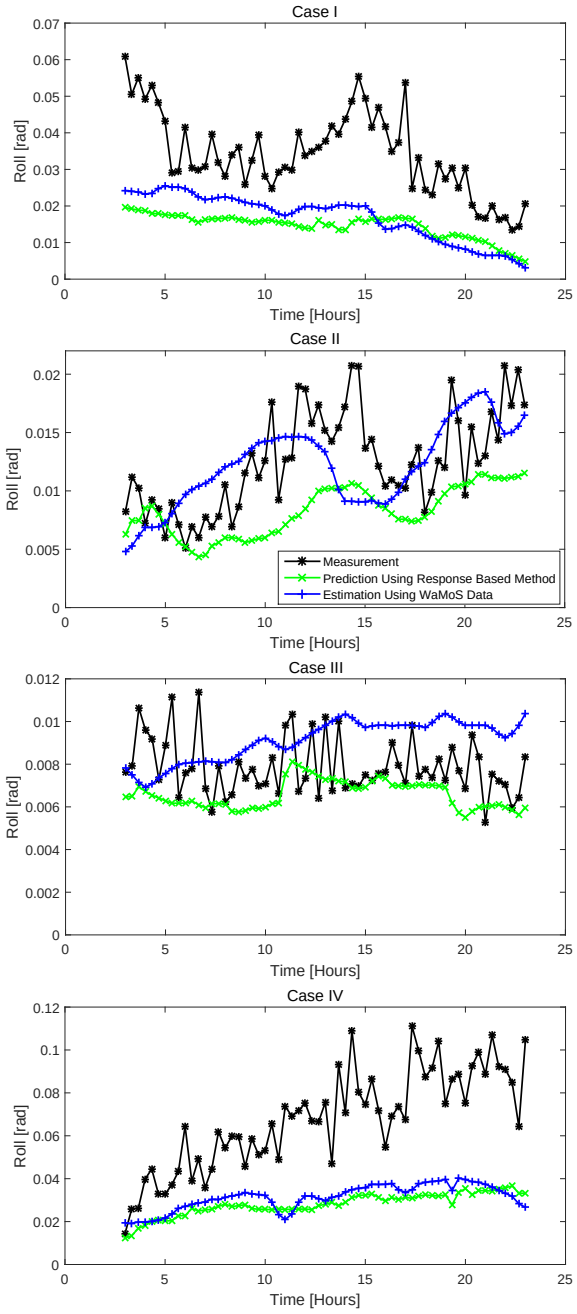

Figure 6.6: Standard deviation of Roll (The legends are identical in all plots).

with the predictions, but the values of e_{wamos} become large in cases II and IV. Those errors are mostly biased and they originate in the wave parameter estimates. It can be observed in Figure 6.4 that the shifts between the two sources follow the trends of discrepancies in the significant wave heights in Figures 5.4 and 5.6. Nevertheless, the errors are neither due to transfer function errors nor due to the spectral model inaccuracy since both sets of data have used the JONSWAP model and the same transfer functions. It should be noted that the influence of filtering of the ship on wave estimation cannot be realised from the above results either.

For roll motion, it can be seen in Figure 6.6 that the trends of predictions are fairly close to the measurements. In cases II and III, where the roll energy is quite low, the quantities of e_{msr} are small. It can also be inferred that WaMoS data sometimes overestimate the roll magnitudes in these cases. In cases I and IV, where the roll energy is relatively higher, an average error of $e_{\text{msr}} = 55\%$ is observed. However, the low differences between the predictions and WaMoS-based data in those two cases indicate that the relatively large values of e_{msr} are not necessarily due to wave parameter estimates, but can be due to transfer function errors or measurement errors.

6.4 Conclusion

A local regression trend model is proposed for prediction of sea state parameters. Although the moment-based wave estimation results from Chapter 5 are used here as a case study, the proposed trend model is applicable to any sea state data, no matter which estimation method is used. The predictions are made over a time horizon of 20 minutes. This trend model provides a smooth and consistent evolution of wave parameters, which is more realistic as the sea state varies quite slowly in time and space. The model can also associate confidence bands for the predictions.

The predictions are then used as input to estimate the future responses of the ship using a JONSWAP model, the updated operational condition, and the corresponding transfer functions. The results show a rather good agreement between the predictions and the actual measurements. This concept and also the procedure for response prediction given in [44], could be useful for development of decision support systems.

Chapter 7

Automatic Response Selection

7.1 Introduction

As discussed in Section 4.3, selection of the optimum combination of ship responses for wave estimation is an important issue in the wave buoy analogy. Optimally, this selection should not be implemented manually in onboard applications. Therefore, availability of an automatic response selection procedure would be a great advantage for decision support.

As mentioned before, depending on the dimensions and also the loading conditions of a ship, the values of individual wave-induced responses and, consequently, the usefulness of them in wave estimation varies from one case to another. Therefore, the behaviour of transfer functions for available responses should be looked at first.

Andersen and Storhaug [1], and Lajic [30] have initiated studies on an automatic selection of responses, where sea state estimation is carried out using individual responses separately. Then, a proper combination of responses are those, for which the parameters or the wave spectral moments are closest to each other. This method can be applied in the traditional (parametric/non-parametric) wave buoy analogy, where the spectral density is optimised for the full range of frequencies.

In the moment-based sea state estimation, in order to apply the least squares

analysis, the number of responses that are used should be more than the number of wave parameters, as mentioned in Chapter 4. Therefore, estimation using one response is not feasible in the current approach. In this chapter, a more systematic and mathematically advanced method based on a local sensitivity analysis is applied to quantify the importance of individual responses in sea state estimates. As a case study, Rigoletto, which was studied in Chapters 4 and 5, is considered here.

7.2 Sensitivity measure

The method used here is adopted from [10] where a sensitivity analysis is used for importance ranking of the parameters to be estimated. Assuming that the estimated quantity, f, is a function of n input variables, i.e., $f = f(x_1, x_2, ..., x_n)$, the sensitivity of f to individual variables can be calculated using first order partial derivatives

$$sf_j = \frac{\partial f}{\partial x_j}, \quad j = 1, 2, ..., n \tag{7.1}$$

where the derivative of f with respect to the parameter x_j is evaluated at a point in the parameter space, where the sensitivity analysis is carried out. These derivatives form the sensitivity vector $SF = \{sf_j\}$. Here, since the wave estimation method in this project is based on spectral moments of responses, the variance of the j^{th} response, R_j, is used as x_j. The estimated wave spectrum is also represented in terms of the integrated wave parameters, p, such as the significant wave height, H_s, the peak period, T_p and the mean wave direction, μ. Those parameters are considered as f and Eq. (7.1) can be rewritten as

$$sf_{pj} = \frac{\partial p}{\partial R_j}. \tag{7.2}$$

For the sake of comparability between the different responses, the sensitivity factor should be scaled and non-dimensionalised. Therefore, this quantity is multiplied by $\frac{R_j}{p}$ so that the scaled sensitivity factor is given by

$$\overline{sf_{pj}} = \frac{\partial p}{\partial R_j}.\frac{R_j}{p}. \tag{7.3}$$

Eq. (7.3) expresses the sensitivity of a wave parameter to a change in the variance of the measured j^{th} response. A high $\overline{sf_{pj}}$ means that the value of the j^{th} response has an important influence on the wave parameter estimate and vice versa. $\frac{\partial R_j}{\partial p}$ can be evaluated as outlined in the following section.

7.3 Influence of wave parameters on the response spectra

As shown in Chapter 4, the transfer function of a particular response exhibits properties that typically change as the wave parameters (particularly the wave period and the wave direction) change. This means that spectral calculations, where transfer functions are combined with a wave spectrum, in general, lead to different outcomes depending on the wave parameters. In other words, the impact of varying one parameter of the wave spectrum, keeping the other parameters fixed, on the standard deviation of individual responses of a ship is usually notable [41].

As an example, Figures 7.1 and 7.2 show the influence of the peak period and the mean wave direction, respectively, on the response spectra, Φ, of pitch motion for Rigoletto. A long-crested JONSWAP spectrum is used for these illustrations. Similar plots have been presented in [41]. It can be seen in Figure 7.1 that the standard deviation of pitch motion, i.e. the square root of the area under the spectrum, has a very small magnitude if the wave energy is concentrated at high frequencies (low peak periods). As the peak period increases, this motion becomes considerable. Figure 7.2 shows that a shift of 90 degrees in wave direction from head/following sea towards beam sea results in a very small amplitudes of the pitch transfer function and, consequently, a small standard deviation in this motion.

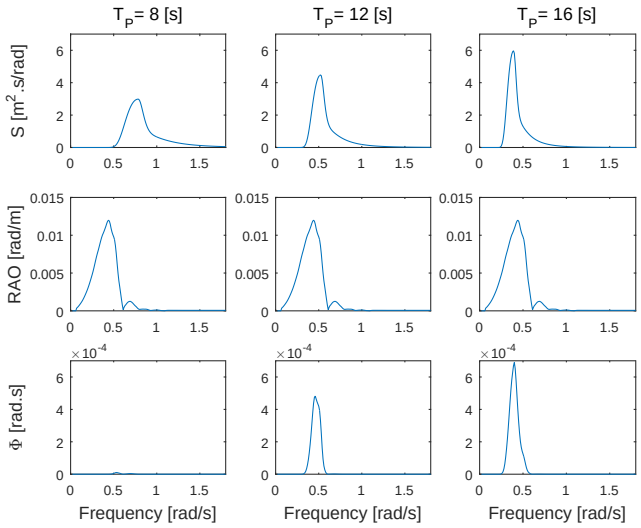

Figure 7.1: Effect of changing the peak period, T_p, on pitch motion at V=20 kn, H_s=4 m, μ=135 deg.

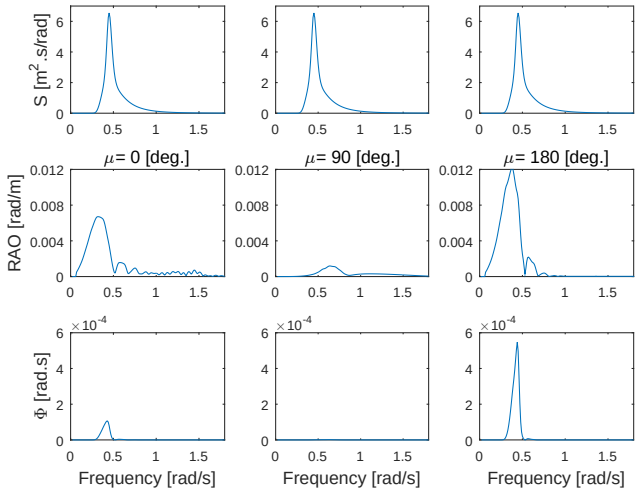

Figure 7.2: Effect of changing the relative wave direction, μ, on pitch motion at V=20 kn, H_s=4 m, T_p=14 s.

Using Eq. (6.13), the partial derivative of the variance with respect to a wave parameter, p, is achieved by

$$\frac{\partial R}{\partial p} = \int_0^\infty \int_{-\pi}^{\pi} \frac{\partial S}{\partial p} H^2(\omega, \theta) d\theta d\omega, \tag{7.4}$$

where $\frac{\partial S}{\partial p}$ can be obtained analytically or numerically. S is considered as a single short-crested unimodal wave modelled by the JONSWAP and a spreading factor as Eqs. (2.8) and (2.13). Substituting H_s for p and calculating the derivative, Eq. (7.4) can be written as

$$\begin{aligned}\frac{\partial R}{\partial H_s} =& 2 \times 5.061 \frac{H_s}{T_p^4}[1 - 0.287 ln(\gamma)] \int_0^\infty \int_{-\pi}^{\pi} \frac{g^2}{\omega^5} exp[-\frac{5}{4}(\frac{2\pi}{\omega T_p})^4] \times \\ & \gamma^{exp[\frac{-(\frac{\omega T_p}{2\pi}-1)^2}{2\sigma^2}]} H^2(\omega, \theta) N(s) cos^{2s}(\frac{\theta - \mu}{2}) d\theta d\omega. \end{aligned} \tag{7.5}$$

Consequently, the sensitivity factor, Eq. (7.3), for H_s is obtained using the inverse of Eq. (7.5)

$$\overline{sf_{H_s}} = (\frac{\partial R}{\partial H_s})^{-1} \frac{R}{Hs} = \frac{1}{2}. \tag{7.6}$$

This constant value of $\overline{sf_{H_s}}$ would be observed for any wave spectral description that is proportional to the square of the significant wave height. It means that regardless of the value of the significant wave height, all responses have the same importance in estimation of the significant wave height. This is quite

reasonable because the transfer function, by definition, does not depend on the wave height. Therefore, H_s is neglected in the sensitivity analysis here.

The derivative of the response variance with respect to the peak period is calculated by

$$\frac{\partial R}{\partial T_p} = \int_0^{\infty}\int_{-\pi}^{\pi}[\frac{-4}{T_p} + \frac{5}{{T_p}^5}(\frac{2\pi}{\omega})^4 - \frac{\omega}{2\pi\sigma^2\gamma}(\frac{\omega T_p}{2\pi} - 1)exp[\frac{-(\frac{\omega T_p}{2\pi} - 1)^2}{2\sigma^2}]]\times S(\omega,\theta)H^2(\omega,\theta)d\theta d\omega, \tag{7.7}$$

and, the sensitivity factor for T_p is:

$$\overline{sf_{T_p}} = (\frac{\partial R}{\partial T_p})^{-1}\frac{R}{T_p}. \tag{7.8}$$

Finally, the derivative of the response variance with respect to the mean wave direction is

$$\frac{\partial R}{\partial \mu} = 2s \times 5.061\frac{H_s}{T_p^4}[1 - 0.287ln(\gamma)]\int_0^{\infty}\int_{-\pi}^{\pi}\frac{g^2}{\omega^5}exp[-\frac{5}{4}(\frac{2\pi}{\omega T_p})^4]\times \gamma^{exp[\frac{-(\frac{\omega T_p}{2\pi}-1)^2}{2\sigma^2}]}H^2(\omega,\theta)N(s)cos^{2s}(\frac{\theta-\mu}{2})tan(\frac{\theta-\mu}{2})d\theta d\omega, \tag{7.9}$$

where μ is in rad. The sensitivity factor for μ is normalised by 2π:

$$\overline{sf_{\mu}} = (\frac{\partial R}{\partial \mu})^{-1}\frac{R}{2\pi}. \tag{7.10}$$

In order to get a visual understanding of the importance of individual responses, the variances of responses can be plotted for different wave periods and directions. Figures 7.3 to 7.7 show the variations of heave, pitch, vertical bending moment at midship section, sway and roll at V=20 kn and Draft=14.5 m. The steepness of these curves with respect to periods and directions represents the quantities of Eqs. (7.7) and (7.9), respectively.

It can be realized from Figures 7.3 and 7.4 that in head sea and following sea conditions, the energies of heave and pitch are negligible when the peak period falls in the wind sea range (e.g. $T_p < 10$ s). Therefore, in such conditions, other responses should be used for wave estimation. As seen in Figure 7.5, the wave bending moment responds to almost all wave conditions and since the inverse of steepness of variations are relatively high, the sensitivity of T_p and μ to this response is considerable for a large range of T_p and μ. The non-zero variances of pitch and bending moment in beam sea condition are due to the asymmetric geometry of the ship with respect to midship section. Sway motion is also

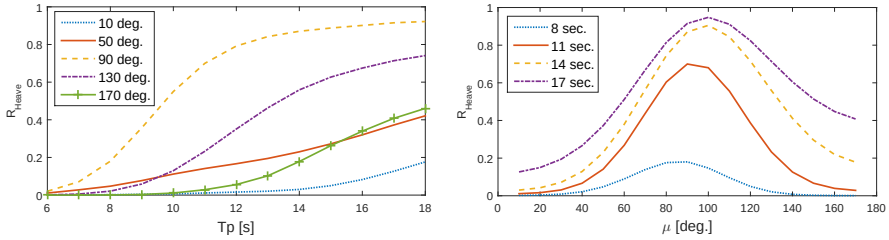

Figure 7.3: The variance of heave motion for different wave parameters. H_s=4 m.

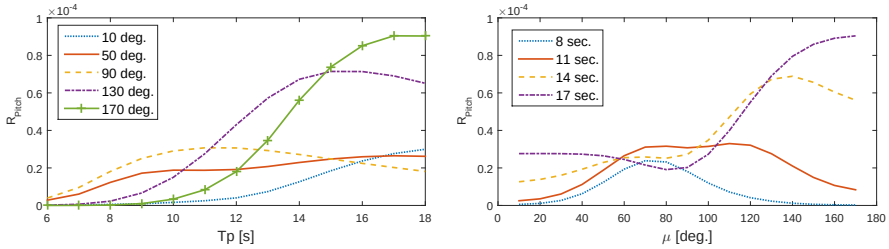

Figure 7.4: The variance of pitch motion for different wave parameters. H_s=4 m.

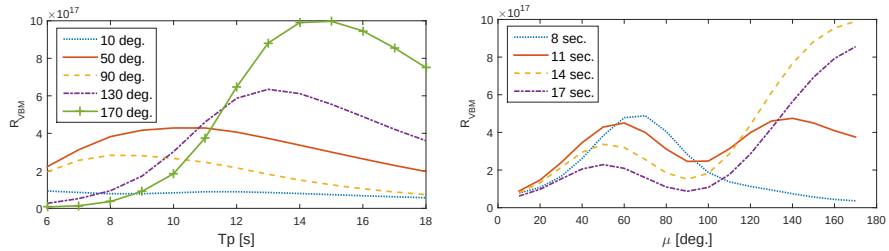

Figure 7.5: The variance of vertical bending moment for different wave parameters. H_s=4 m.

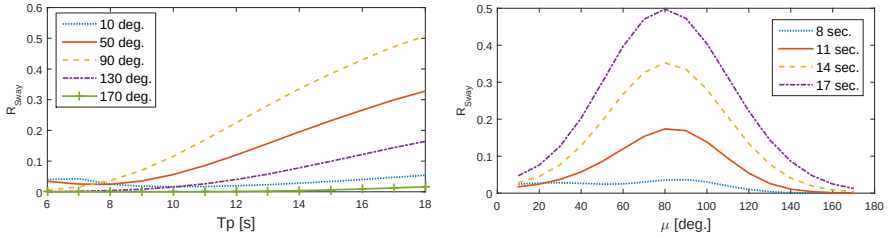

Figure 7.6: The variance of sway motion for different wave parameters. H_s=4 m.

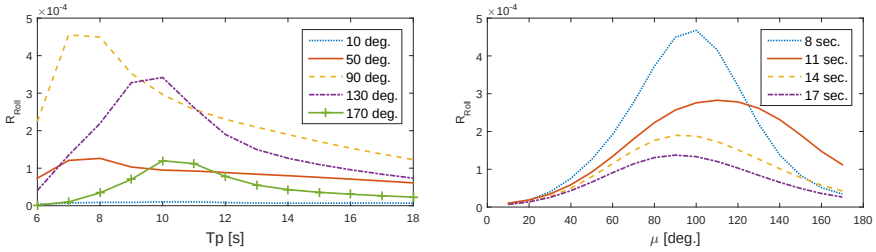

Figure 7.7: The variance of roll motion for different wave parameters. H_s=4 m.

useful in many wave conditions as shown in Figure 7.6. However, as expected, the variance of this response is very small in head sea and following sea. It can be seen in Figure 7.7 that the energy of roll motion is highly dependent on the wave condition. As inferred from Figures 7.3 to 7.7, the most critical condition for wave estimation is following sea condition, where all responses have small magnitudes.

7.4 Results and discussion

In the following, the sensitivity analysis is implemented for various waves with peak periods between 7 and 17 seconds, and mean wave directions from following sea to head sea. The loading condition of the ship is the same as Section 7.3. The significant wave height is fixed at 4 meters due to the constant sensitivity factor as discussed in Section 7.3. γ and s are also fixed at 3.3 and 25, respectively.

The sensitivity factors based on Eqs. (7.8) and (7.10) are calculated for heave, pitch, sway, roll and vertical bending moment at the midship section. It is assumed for calculation of the derivatives that the wave parameters are known. In practice, in order to perform the sensitivity analysis, the predicted wave parameters obtained, for instance, from the trend analysis in Chapter 6 can be used. The sensitivity factors can be calculated in real-time. As an alternative, for a specific ship, the procedure can be also pre-analysed at different loading and wave conditions so that the optimum combination of responses are determined over a range of probable conditions, and can be utilised during the operations. The latter approach is beneficial in the interest of time saving for real-time decision support applications.

Figures 7.8 and 7.9 show the values of $\overline{sf_{T_p}}$ and $\overline{sf_{\mu}}$, respectively, at different wave conditions. Both quantities should be considered simultaneously for response selection. In the case of $\mu = 10°$, since the energy amounts of the most

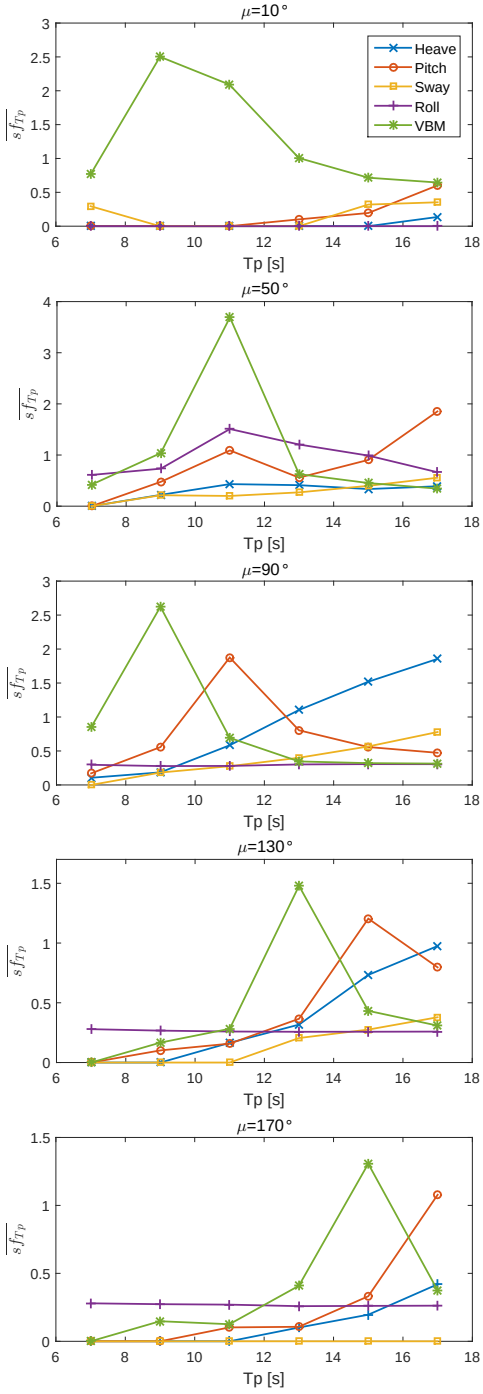

Figure 7.8: Normalised sensitivity factor for T_p, (The legends are identical in all plots).

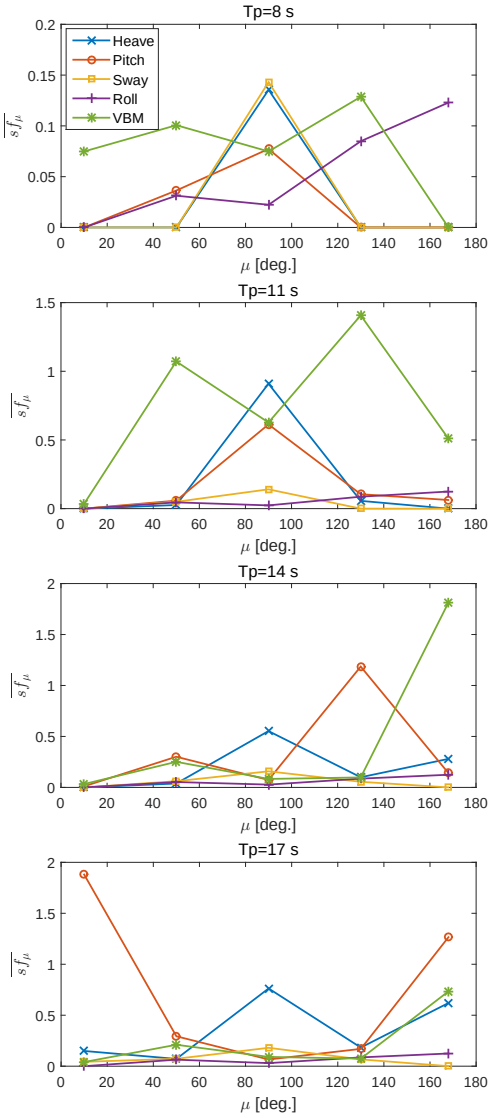

Figure 7.9: Normalised sensitivity factor for μ, (The legends are identical in all plots).

responses are very small as mentioned in Section 7.3, the sensitivity factors are very small or zero. However, the wave bending moment is an effective response for estimation of all peak periods in this case. When the peak period is long, e.g. $T_p > 16$ s, pitch could be useful for estimation of direction according to Figure 7.9. As seen in Figure 7.4, at $T_p = 17$ s, the differentiation of the variance of pitch with respect to direction is close to zero at both head sea and following sea, so the magnitude of $\overline{sf_\mu}$ becomes very large. When $\mu = 50°$, the bending moment, roll and pitch can have a big role in estimation of peak periods. This combination is also influential in estimation of wave directions in the stern-quartering sea condition.

In beam sea condition, $\mu = 90°$, for estimation of low peak periods, pitch and bending moment are proper responses. As the period increases, the importance of bending moment decreases whereas the importance of heave and sway motions increases based on Figure 7.8. Although the variance of roll motion is relatively large in beam sea condition (as seen in Figure 7.7), this response has the lowest sensitivity factor in terms of both wave parameters. Thus, it makes more sense to use sway motion instead of roll in this condition. In the case of $\mu = 130°$, both wave parameters have rather high sensitivities to wave bending moment and roll while $T_p < 14$ s. As the peak period increases, heave and pitch become more important than bending moment and roll.

When $\mu = 170°$, as seen in Figure 7.8, the impact of different responses on the peak period is similar to $\mu = 130°$. The sensitivity factor of the wave direction, on the other hand, depends very much on the value of the peak period (Figure 7.9). Bending moment, pitch, roll and heave could be useful in this case. As the sensitivity factor and the amount of energy of sway motion is almost zero, using this response in head sea condition is inefficient.

All in all, it can be inferred from this chapter that the wave bending moment is generally the most effective response for estimation of both the period and the wave direction. It is notable that the sensitivity analysis should be provided in different loading conditions in terms of speeds and drafts. However, the sensitivity factors are not expected to be subject to major changes. Because the magnitudes and the trends of transfer functions do not differ considerably at different loading conditions. It can also be expected that the importance of the responses are somewhat similar for other vessels of similar size and with a similar range of operational conditions.

It is noteworthy that this Chapter assumes the accuracy of different transfer functions to be the same. Therefore, beside the sensitivity analysis, any knowledge about uncertainty of transfer functions should be considered in response selection. This can be done through weighting the responses, as in Chapter 4, the sway motion is given less weight than heave, pitch and bending moment .

7.5 Conclusion

In this chapter, identification of an optimum combination of responses is carried out based on the sensitivity of the major wave parameters in a standard spectrum (e.g. JONSWAP) to the magnitudes of individual response variances. Those sensitivity calculations are simply obtained using first order derivatives of response variances with respect to the wave parameters. Although the response selection method is not implemented in the wave estimation approach in this thesis, it is believed that choosing the responses with higher importance at typical conditions can make the outcome of optimisation more efficient and reliable. It should be noted that this method can be used as a prior input to any response-based wave estimation method including parametric and non-parametric methods such as [38, 50, 58].

Chapter 8

Uncertainty Analysis

8.1 Introduction

The accuracy of wave data may vary widely and it is very much related to the estimation method. All methods that are used for estimation of waves and responses have a degree of uncertainty. In other words, the outcome of all methods is just an estimate and not the true wave spectrum. Even for wave buoys that are regarded as being highly accurate, during severe sea conditions, the presence of strong surface current or external forces on the buoy (e.g., breaking waves, mooring) may cause the buoy measurements to be biased (see also [46]). Before application of an estimated wave data set in planning and execution of marine operations, it is important to make sure that a data quality check has been carried out.

The systematic error (bias) of an estimator is determined by the difference between the expected value of the estimator and the true value. The precision of the quantity, on the other hand, refers to random variations and is usually summarised by the standard deviation. Normal (Gaussian) distribution is commonly adopted to describe random uncertainties. Any quantity should be quoted as a mean value, plus/minus a standard deviation. When the model involves several terms with associated errors, assuming that they are independent variables, it is possible to produce a single value over all uncertainties.

In general, there are two types of uncertainties: aleatory uncertainties and epistemic uncertainties. Aleatory uncertainties represent a natural randomness of a quantity, e.g. the variability in wave intensity over time. Aleatory uncertainties cannot be reduced or eliminated. Epistemic uncertainties represent

errors which can be reduced by collecting more information about a considered quantity and by improving the methods of measuring it. This uncertainty may be classified into: data uncertainty, statistical uncertainty and model uncertainty [8] as follows:

Data uncertainty is mainly due to the imperfection of an instrument used to measure a quantity. It is usually given by a manufacturer of the instrument. It can also be evaluated by a laboratory test or full-scale test. The constraints in positions of instrumentation and the synchronisation of measurements also contribute to data uncertainties.

Statistical uncertainty is due to limited information such as a limited number of observations of a quantity and also due to the estimation technique applied for evaluation of the distribution parameters. Statistical uncertainty can be determined by employing simulation techniques or by use of the maximum likelihood method as asymptotic results are available with this method. In the current wave estimation procedure, since short-term time series are utilised, they are affected by statistical uncertainty or sampling variability which may lead to under- or over-estimation of the responses.

Model uncertainty deals with imperfections, simplifications and idealisation in the mathematical formulation, transfer functions and optimisation method. For instance, the assumption that the standard wave model (i.e. JONSWAP spectrum here) perfectly represents the actual wave spectrum, is also imperfect. This has led to wave estimation studies based on nonparametric methods [38, 51, 57].

The aforementioned uncertainties are assessed quantitatively in this chapter using different methods.

8.2 Uncertainty Sources

As stated before, the optimisation problem in the standard response-based wave estimation is formulated based on Eq. (2.3). The model uncertainty can be evaluated by implementing a residual analysis, where the residual components between the two sides of this equation follow a normal distribution. In that way, the standard deviation of the residuals is usually regarded as the uncertainty measure. However, in this thesis, since the moment equations, Eq. (6.13), are used, the number of cost functions and, consequently, the number of residuals are limited, and residual analysis is not efficient in this method. The

moment-based cost function is shown here again:

$$R = \int_0^{\infty} \int_{-\pi}^{\pi} |H(\omega, \theta)|^2 \, S(\omega, \theta) \, d\theta d\omega. \tag{8.1}$$

Apart from the optimisation model, the main sources of errors in the estimation procedure are 1) the transfer function, H, and 2) the measured response, from which the variance, R, is obtained.

8.2.1 Uncertainty in the transfer functions

Various methods are used for evaluation of loadings and response functions (RAOs) of ships. These methods include model experiments, full-scale measurements and numerical methods. Depending on the method used, the parameters that cause uncertainties in the response evaluation are different. An overview of all uncertainty sources can be found in [54]. Accordingly, the uncertainties in full-scale tests are categorised as physical properties of fluid, environment, instrumentation and human factors. The uncertainties in experiments, in addition to the above parameters, are due to initial conditions, model definition and scaling. Quantification of experimental uncertainties have been suggested by the ITTC, which is presented in [28].

Numerical methods for hydrodynamic calculations have grown stronger during last decades. Strip theory has been traditionally very common for seakeeping calculations. However, 3D panel methods are becoming more advanced with adaptation of higher-order schemes, a Rankine panel, or a wave Green function. The application of CFD schemes with viscous modelling is also increasing. Therefore, transfer function calculations are more accurate than before. However, different mathematical models, modelling of boundary value problem, errors of body geometry modelling and inaccurate mass distribution, enforce epistemic uncertainties to these calculations.

Studies have been developed to quantify and minimise the errors in numerical models. One example is the so-called V&V (verification and validation) process, which is a comparative study of different computational programs typically implemented by the ITTC. Figure 8.1 shows an example of a set of RAOs for motions and structural loads of a container ship model, obtained from different computational programs in a bow-quartering sea condition [28]. As seen in the figure, quite large variations still exist between the results of different methods. Roll, yaw and horizontal bending moment seem to be the most uncertain responses in this figure. It can be concluded that uncertainty analysis is important during the analysis of structural loads and motions.

As observed in Figure 8.1, contrary to experimental and full-scale test methods,

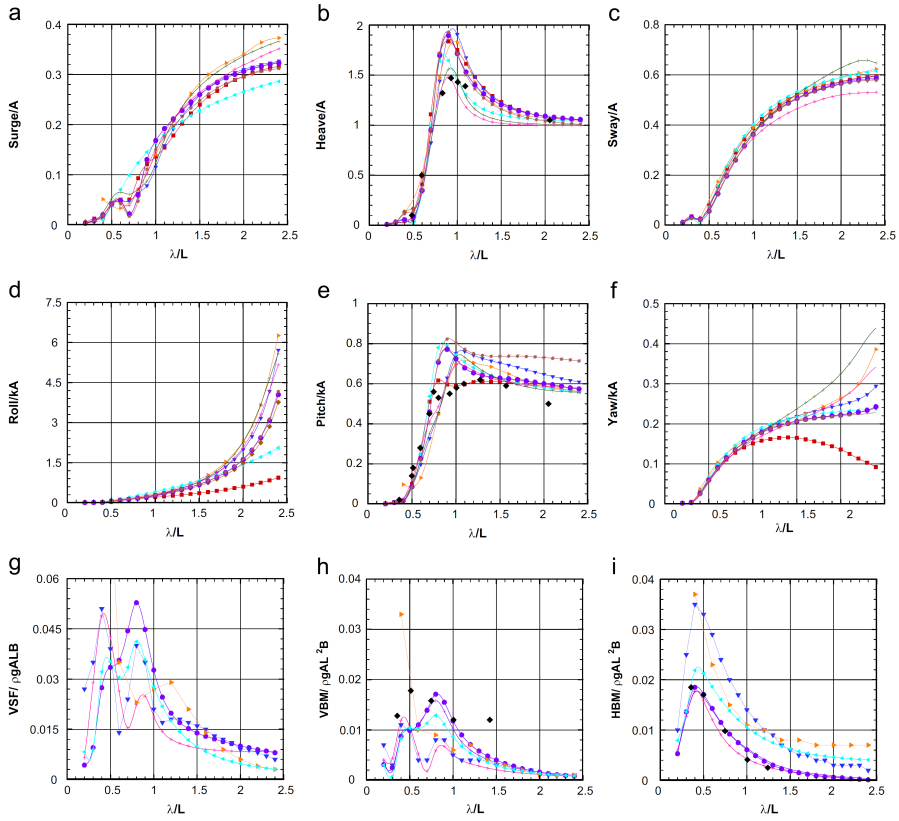

Figure 8.1: Amplitudes RAO for motions and structural loads using different computational methods, S175 container ship hull, Froude No=0.2 [28].

the uncertainties in numerical methods are not random, but only systematic bias as long as the input data are deterministic [17]. Modelling of those bias errors was introduced by Guedes Soares [17] based on comparisons between theoretical results and model experiments. Accordingly, the model error is represented as a factor, Ψ, which depends on frequency and multiplies the theoretical transfer function, $\hat{H}$:

$$H = \Psi(\omega)\hat{H}(\omega, \theta) + \epsilon(\omega), \tag{8.2}$$

where ϵ is the experimental error, which is a random frequency-dependent variable with zero mean and standard deviation σ_ϵ. Ψ is taken to be of the general form

$$\Psi(\omega) = a + b\omega + c\omega^2. \tag{8.3}$$

In an extended model, the coefficients a, b and c are dependent on the heading

of the ship relative to the waves, the ship speed and the block coefficient, C_B

$$\Psi(\mu, V, C_B, \omega) = a + b(\mu, V, C_B)\omega + c(\mu, V, C_B)\omega^2. \tag{8.4}$$

The parameters should be estimated using regression analysis. However, the higher the number of parameters to be estimated, the more data are required to provide statistical significance to the results. A similar regression approach is carried out by Bach [4] comparing full-scale derived transfer functions with theoretical calculations. Based on an estimate of Ψ, the calculated (theoretical) transfer functions can be calibrated to better fit with corresponding response measurements. Consequently, the calibrated theoretical transfer functions should (potentially) be better suited for sea state estimation. Another uncertainty analysis example is [20], where both systematic bias and random precision limits are estimated for experimental heave and pitch transfer functions.

8.2.2 Uncertainty in the measurements

The data uncertainty or the imperfection of the instruments should be considered prior to wave estimation. If random errors in response measurement are somehow available as standard deviations, the variance, R, in Eq. (8.1), can be considered as a normally distributed variable in the uncertainty analysis. This will be explained more in Section 8.3.2.

In wave estimation through numerical practices, in order to include measurement errors, it is usual to add noise to the generated signals. This is implemented on the studied cases in Chapter 4 using white noise with zero mean and standard deviations equal to 10 percent of the responses amplitudes. However, the changes in the estimated wave parameters were less than 3%. This is quite reasonable because the noise does not change the standard deviation or the variance of the time series significantly, and since the calculations are merely based on the spectral moments or the variances of the responses, it does not have considerable impact on the results. Nevertheless, bias errors might still be present in the full-scale measurements, which can be more important.

The common wind observations include mean wind speed, mean wind direction and maximum wind speed within the observation interval. The standard wind data represent measured or calibrated 10-minute average speed at 10 m above ground or mean sea level. Systematic errors in estimating mean wind speed and direction using wind instruments on buoys can be neglected [63], however, shipboard wind measurements are believed to be less accurate.

8.3 Uncertainty evaluation in sea state estimates

8.3.1 Wave estimation using different sets of RAOs

One way to assess the influence of transfer function errors in the wave estimation procedure is to consider different sets of transfer functions in the input and to measure the sampling variance of the wave parameters in the output. In this study, a different set of RAOs for the motions (heave, pitch and sway) are used to estimate the waves. Those transfer functions, called RAO2, are calculated using the in-house linear strip theory program, Iship.

Figure 8.2 shows the amplitudes of those transfer functions for the same operational condition as used in Chapter 4. Comparing the magnitudes of RAO2 with the original set of transfer functions, RAO1 in Figure 4.3, shows a difference of $10 - 15\%$ in the peak values of heave and pitch amplitudes. This range of errors is quite similar to those in Figure 8.1. The difference in sway motion, though, is higher particularly at low frequencies. When the relative directions of waves are 20-40 degrees, i.e. between following sea and stern-quartering sea condition, the calculation errors of sway can reach 75%.

The same estimation procedure as in Chapter 4 is applied on the same wave scenarios (Table 4.2) using RAO2. The new results are illustrated here in Figures 8.3-8.5 together with the results from Chapter 4. The standard deviations are included as the small-size pin bars. The average values and the standard deviations correspond to the 15 realisations. The quantities are compared in Tables C.1-C.4 in Appendix C. In unimodal wave cases, Figure 8.3, the estimations using RAO2 are very close to those from RAO1. This ensures the robustness of the method in such simple cases. In bimodal waves also, the new results match with RAO1 to some extent (Figures 8.4 and 8.5). However, particularly in wind-sea partitions, the significant wave heights are up to 1.3 meters different from the real values (case M). This could be due to the uncertainty in the high frequency part of the response functions. The peak periods also have notable errors in a few cases e.g. in stern-quartering swell partition; i.e. case O.

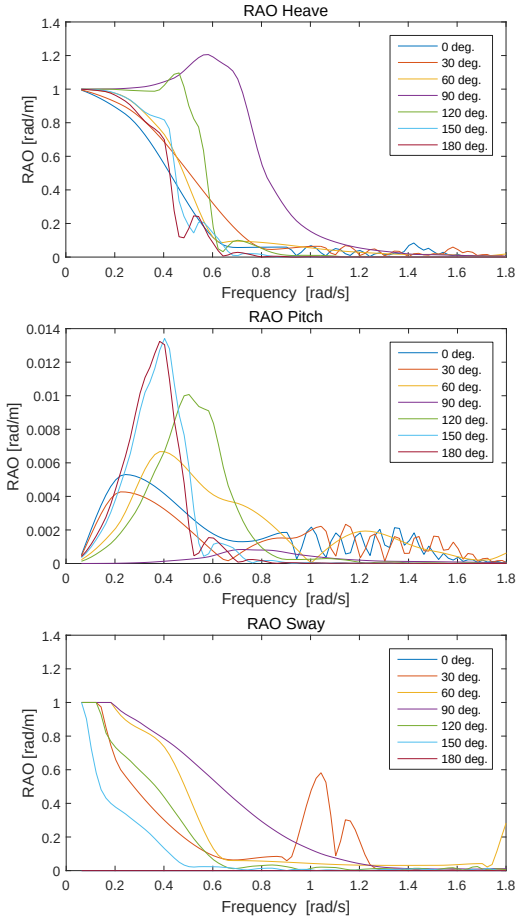

Figure 8.2: Amplitudes of RAO2 for different responses (V=20 kn, T=14.5 m).

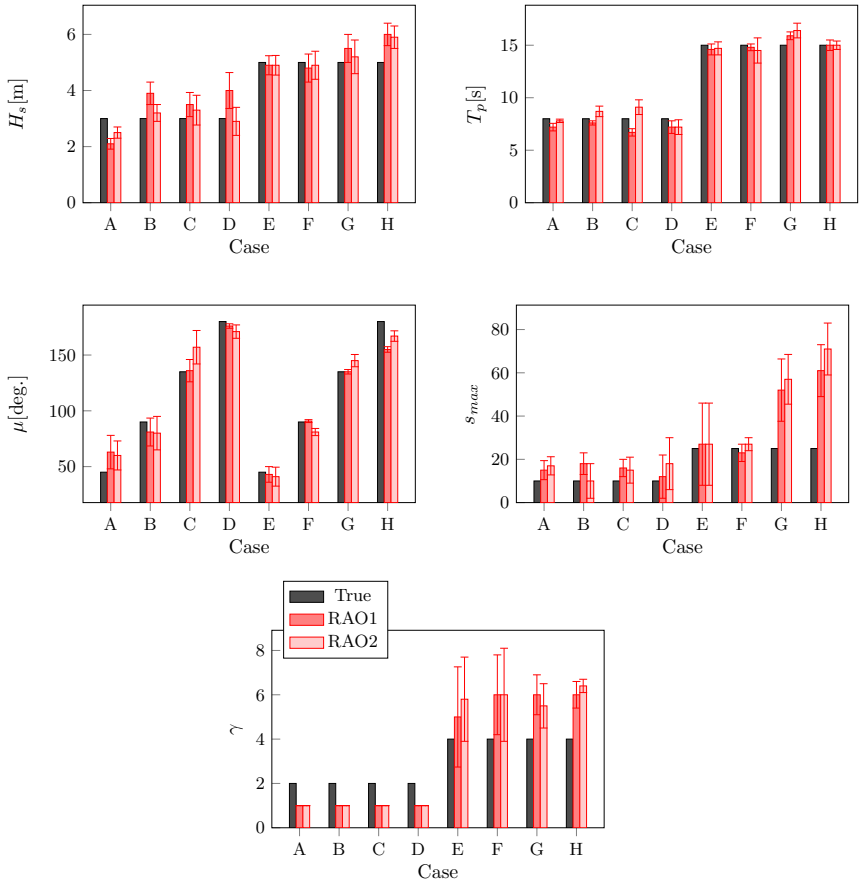

Figure 8.3: Estimated parameters for unimodal wave scenarios.

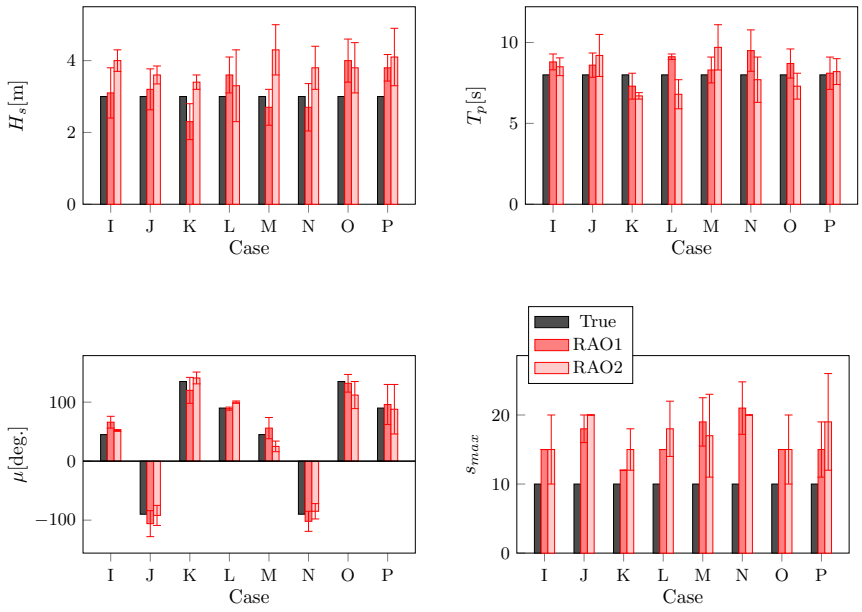

Figure 8.4: Estimated wind-sea parameters for bimodal wave scenarios.

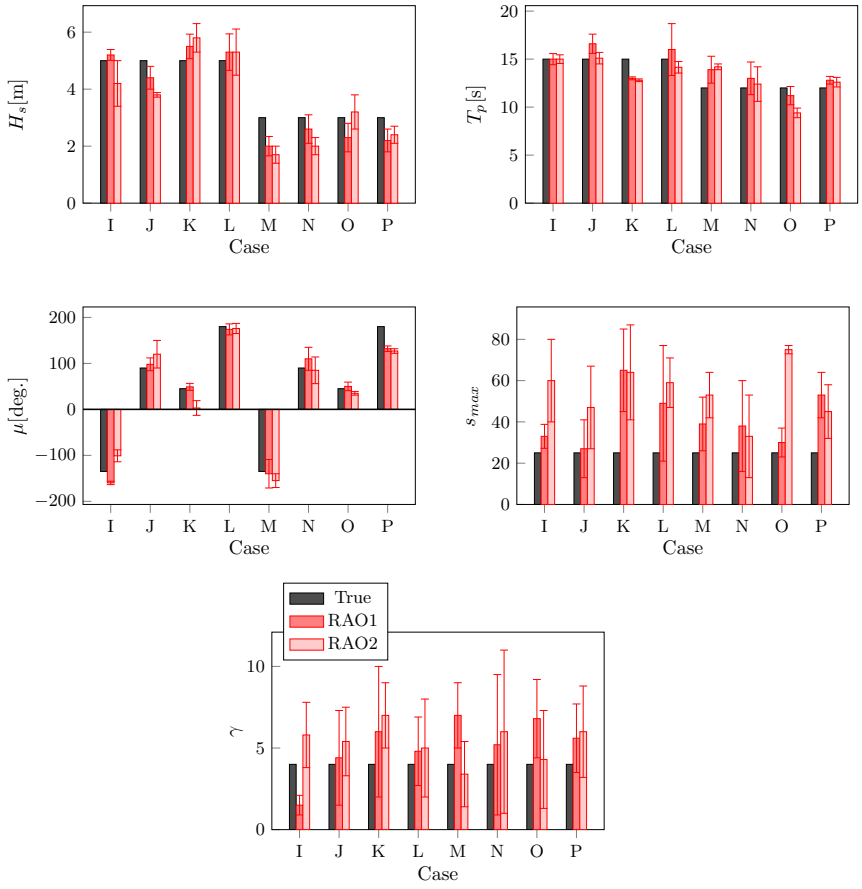

Figure 8.5: Estimated swell parameters for bimodal wave scenarios.

8.3.2 Linear error propagation

Uncertainty analysis can be run by propagating the input uncertainties through the model, all the way to the model output. This procedure follows the law of linear error propagation [5, 54]. Assuming that the value to be estimated, f, is a function of n input variables, x_n, i.e., $f = f(x_1, x_2, ..., x_n)$, the uncertainty in the output, u_f, can be calculated as

$$u_f^2 = (\frac{\partial f}{\partial x_1})^2 u_{x_1}^2 + (\frac{\partial f}{\partial x_2})^2 u_{x_2}^2 + ... + (\frac{\partial f}{\partial x_n})^2 u_{x_n}^2, \tag{8.5}$$

where $\frac{\partial f}{\partial x_n}$ denotes the partial derivative of the output f with respect to the variable x_n, which was utilised also in the sensitivity analysis in Chapter 7. u_{x_n} is the uncertainty in x_n that could be either bias or random error. However, uncertainty analysis usually assumes the variables to be normal processes as mentioned before. Thereby, all uncertainties (u) are considered here as standard deviations.

The variable, x_n, might be dependent on other variables, $y_1, ..., y_n$, which can be expressed as $x_n = g_n(y_1, y_2, ..., y_n)$. Then u_{x_n} can be found by:

$$u_{x_n}^2 = (\frac{\partial g_n}{\partial y_1})^2 u_{y_1}^2 + (\frac{\partial g_n}{\partial y_2})^2 u_{y_2}^2 + ... + (\frac{\partial g_n}{\partial y_n})^2 u_{y_n}^2. \tag{8.6}$$

In this chapter, the above method is utilised to evaluate the errors in the wave estimation procedure. The errors in a sea state estimate can be presented in terms of the errors in the wave integral parameters

$$u_p^2 = \frac{1}{K} \sum_{k=1}^{K} \Big(\frac{\partial p}{\partial R_k} \Big)^2 u_{R_k}^2, \tag{8.7}$$

where p stands for the main wave parameters: H_s, T_p and μ. Note that these parameters are assumed to be uncorrelated in Eq. (8.7). K is the number of responses used for wave estimation. The partial derivative of p with respect to the k^{th} response variance, $\frac{\partial p}{\partial R_k}$ is calculated as in Chapter 7. It is assumed in Eq. (8.7) that all uncertainties, either due to measurements or calculations, are reflected in the variance values.

Errors in response measurements, $u_{R_k}^{msr}$, may be provided by the sensors manufacturer as mentioned before. In the presented method in this project, the error in the theoretical variance, i.e. right hand side of Eq. (8.1), comes from 1) transfer function errors and 2) the separation frequency, ω_s, which is used for splitting the transfer functions. So, u_{R_k} in Eq. (8.7) can be expressed in general as

$$u_{R_k}^2 = (u_{R_k}^{msr})^2 + (u_{R_k}^{H_k})^2 + (u_{R_k}^{\omega_s})^2, \tag{8.8}$$

where $u_{R_k}^{H_k}$ represents the uncertainty in R due to transfer function error. The definition of this quantity assumes that an error in a transfer function is reflected in the magnitude of the corresponding theoretical response variance, Eq. (8.1). In the following, the way that $u_{R_k}^{H_k}$ is evaluated is described.

Apart from bias errors, that were discussed in Section 8.2.1, the precision (randomness) of a transfer function can be expressed as:

$$H(\omega) = \hat{H}(\omega)[1 + \epsilon(\omega)], \tag{8.9}$$

where $\hat{H}$ is the calculated transfer function and ϵ is a zero mean, normally distributed random error with standard deviation σ_ϵ. Although the transfer functions used in this project are obtained from hydrodynamic software, they are assumed here as random variables, just to show the applicability of the method for uncertainty analysis.

Substituting Eq. (8.9) into a discretised form of Eq. (8.1) gives

$$R_k = \sum_{j=1}^{m}\sum_{i=1}^{n} S_{ij}[\hat{H}_{ij,k}(1+\epsilon_j)]^2(\delta\omega)(\delta\theta), \tag{8.10}$$

where m and n are the number of frequencies and directions, respectively. Taking the variance of Eq. (8.10) yields $(u_{R_k}^{H_k})^2$ as

$$(u_{R_k}^{H_k})^2 = \sum_{j=1}^{m}\sum_{i=1}^{n} S_{ij}^2[2(\sigma_{\epsilon_j}\hat{H}_{ij,k})^4 + 4(\sigma_{\epsilon_j}\hat{H}_{ij,k})^2\hat{H}_{ij,k}^2](\delta\omega)^2(\delta\theta)^2. \tag{8.11}$$

For simplification, despite Eq. (8.2), σ_{ϵ_j} is considered constant and independent of frequency. $\sigma_\epsilon = 0.04$, obtained from [20, 54], is applied here for all responses. However, this assumption is not realistic since the accuracy of some responses (for instance roll and sway) are lower than the others (e.g. heave). Taking σ_ϵ out of the summations yields

$$(u_{R_k}^{H_k})^2 = (2\sigma_\epsilon^4 + 4\sigma_\epsilon^2)\sum_{j=1}^{m}\sum_{i=1}^{n} S_{ij}^2\hat{H}_{ij,k}^4(\delta\omega)^2(\delta\theta)^2. \tag{8.12}$$

The uncertainty of the response variance due to an error in separation frequency, $u_{R_k}^{\omega_s}$ in Eq. (8.8), can be written as

$$(u_{R_k}^{\omega_s})^2 = \left(\frac{\partial R_k}{\partial \omega_s}\right)^2 u_{\omega_s}^2, \tag{8.13}$$

where $\frac{\partial R_k}{\partial \omega_s}$ should be calculated numerically. Referring to Eq. (2.18), an error in ω_s could be due to the measured wind speed, U_w. So, Eq. (8.13) can be written as

$$(u_{R_k}^{\omega_s})^2 = \Big(\frac{\partial R_k}{\partial \omega_s}\Big)^2 \Big(\frac{\partial \omega_s}{\partial U_w}\Big)^2 u_{U_w}^2, \tag{8.14}$$

and based on Eq. (2.18),

$$(u_{R_k}^{\omega_s})^2 = \Big(\frac{\partial R_k}{\partial \omega_s}\Big)^2 \Big(\frac{-g}{\beta U_w^2}\Big)^2 u_{U_w}^2. \tag{8.15}$$

The absolute wind speed is derived using the relative wind speed, U_{rel}, and the relative wind direction, ν, which are both measured onboard the ship

$$U_w = U_{rel} + V cos(\nu). \tag{8.16}$$

Taking into account uncertainties in both measured parameters, the uncertainty of wind speed can be evaluated:

$$u_{U_w}^2 = \Big(\frac{\partial U_w}{\partial U_{rel}}\Big)^2 u_{U_{rel}}^2 + \Big(\frac{\partial U_w}{\partial \nu}\Big)^2 u_{\nu}^2. \tag{8.17}$$

The derivatives in Eq. (8.17) are obtained from Eq. (8.16) and finally

$$u_{U_w}^2 = u_{U_{rel}}^2 + [V sin(\nu)]^2 u_{\nu}^2. \tag{8.18}$$

The described formulations for uncertainty analysis are conceptually introduced here. Numerical examples of the method are limited to the wave parameters evaluated in the unimodal wave cases, i.e. cases A through H in Table 4.2, so uncertainty of the separation frequency is neglected since $\frac{\partial R_k}{\partial \omega_{e_s}}$ is close to zero in these cases.

Since random errors in response measurements do not have significant impact on the variance, as mentioned before, and information about any bias error in the sensors is not available here, $u_{R_k}^{msr}$ in Eq. (8.8) is also neglected. So, the uncertainty in the individual wave parameters depends only on the errors in the transfer functions:

$$u_p^2 = \frac{1}{K} \sum_{k=1}^{K} \Big(\frac{\partial p}{\partial R_k}\Big)^2 \Bigg|_{H_k = \hat{H}_k} (u_{R_k}^{H_k})^2. \tag{8.19}$$

The estimated parameters from Chapter 4 are used as input to the JONSWAP spectrum and the uncertainties are calculated from Eq. (8.19) using vertical motion, pitch, vertical bending moment and sway. The calculated uncertainties of the three main parameters are shown in Table 8.1. The coefficient of variation is defined as the ratio between the uncertainty and the mean value of the parameter:

$$COV_p = \frac{u_p}{p}. \tag{8.20}$$

Table 8.1: Uncertainties and coefficients of variations of wave parameter estimates, calculated by Eqs. (8.19) and (8.20).

Case		H_s(m)	T_p(s)	μ(deg.)
A	Value	3	8	45
	Uncertainty	0.21	0.44	17.2
	COV	0.07	0.05	0.05
B	Value	3	8	90
	Uncertainty	0.21	0.73	27.5
	COV	0.07	0.09	0.08
C	Value	3	8	135
	Uncertainty	0.21	0.13	4.3
	COV	0.07	0.02	0.01
D	Value	3	8	180
	Uncertainty	0.21	0.09	7
	COV	0.07	0.01	0.02
E	Value	5	15	45
	Uncertainty	0.35	1	11.3
	COV	0.07	0.07	0.03
F	Value	5	15	90
	Uncertainty	0.35	2.12	12.8
	COV	0.07	0.14	0.04
G	Value	5	15	135
	Uncertainty	0.35	1.55	7.6
	COV	0.07	0.1	0.02
H	Value	5	15	180
	Uncertainty	0.35	2.07	34.2
	COV	0.07	0.14	0.09

It should be noted that for the mean wave direction, the uncertainty is divided by 360° in Eq. (8.20), so the COV of the direction should not be used in comparison to the COV of the other parameters, but can be used only to assess the accuracy of the estimated wave direction in the individual cases (A, B, C, ...).

As seen in Table 8.1, the uncertainty in the significant wave height remains constant for varying wave directions. This happens because both $\frac{\partial R_k}{\partial p}$ and $u_{R_k}^{H_k}$ are proportional to the corresponding variance of the response with a constant coefficient according to Eqs. (7.5) and (8.12).

The highest uncertainties in the peak period are experienced in beam seas. This parameter is probably more reliable in low peak periods, A-D, compared to high peak periods, E-H, where the uncertainty reaches 2 seconds. The uncertainty in the wave direction estimation is quite low in most cases. However, for the head sea swell, i.e. case H, the estimated uncertainty is 34 degrees, which is rather high. This is due to the fact that when the peak period is longer than 14 seconds in head sea condition, the variations of directions with respect to heave, pitch and bending moment variances are high and, at the same time, the magnitudes of these responses are considerable. This is clear in Figures 7.3-7.5. It can be concluded that although lower derivatives of response variances give those responses greater importance in terms of response selection, the reliability of wave estimation based on those responses may decrease if the corresponding transfer functions are not accurate enough.

For directly recorded wave data (e.g. buoy measurements), for the JONSWAP and the Pierson-Moskowitz spectra, the sampling variability coefficient of variation of the significant wave height and zero upcrossing wave period are approximately 4-6 % and 1.5-2.5 % respectively for a 20-minute measurement interval [63]. Therefore, the coefficients of variations in Table 8.1 are relatively high compared to those wave data.

8.4 Uncertainty of Predicted Responses

In this section, the reliability of response estimation is assessed in terms of the zero order spectral moment (the variance) of a response spectrum, R, which is a very practical value for description of the response behaviour since it allows limit states and different probabilistic statements about the response. For instance,the probability of exceedance can be evaluated by the Rayleigh distribution as a function of R. Therefore, the uncertainty of a response estimate is directly related to the error in R [16]. An uncertainty modelling has also been conceptually included in operational guidance applications based on reliability theory and probability distribution models for wave parameters [45].

As described in Chapter 7, a sensitivity analysis can be carried out by using the derivatives of R to the wave parameters. This sensitivity measure can be used to estimate a change in the response variance (or failure probability) given a change in a parameter [7]:

$$R(p + \Delta p) \simeq R(p) + \frac{\partial R(p)}{\partial p} \Delta p, \tag{8.21}$$

where p is an operational/environmental variable that can be a fixed value or a parameter in a distribution function e.g. the mean value or the standard deviation.

Referring to Eq. (8.1) for evaluation of a response variance, the source of uncertainty refers to both the wave spectrum and the transfer function for that particular response. If uncertainties of the wave spectral ordinates are available, the wave spectral densities can be also expressed as random variables [16]:

$$S(\omega,\theta) = \hat{S}(\omega,\theta)[1+\zeta(\omega,\theta)], \tag{8.22}$$

where $\hat{S}$ is the estimated spectrum and ζ is a random error with zero mean and standard deviation σ_ζ. Using Eqs. (8.9) and (8.22), the statistical expression of R can be written as

$$R_l = \sum_{j=1}^{m}\sum_{i=1}^{n} \hat{S}_{ij}(1+\zeta_{ij})[\hat{H}_{ij,l}(1+\epsilon_j)]^2 \delta\omega\delta\theta, \tag{8.23}$$

where index l corresponds to the response to be estimated. Taking the variance of Eq. (8.23), where S and H_l are uncorrelated, leads to

$$\begin{aligned}(u_{R_l})^2 = &\sum_{j=1}^{m}\sum_{i=1}^{n} \hat{S}_{ij}^2 \hat{H}_{ij,l}^4 (\delta\omega)^2(\delta\theta)^2 \times \\ &(2\sigma_{\epsilon_j}^4 + 4\sigma_{\epsilon_j}^2 + \sigma_{\zeta_{ij}}^2 + 2\sigma_{\zeta_{ij}}^2\sigma_{\epsilon_j}^4 + 4\sigma_{\zeta_{ij}}^2\sigma_{\epsilon_j}^2).\end{aligned} \tag{8.24}$$

In this study, the sea states and the uncertainties are estimated in terms of integral parameters. Therefore, instead of applying uncertainties of wave spectral ordinates and using Eqs. (8.22)-(8.24), the wave parameters are considered as random variables with the mean values as estimated in Chapter 4 and the standard deviations as calculated in Section 8.3.2. The transfer functions are also considered random just as performed in Section 8.3.2. The uncertainties in the response variances are estimated using Monte-Carlo simulations based on Eq. (8.1).

The variability of the variance of individual responses is presented as the coefficient of variation of those responses, which is defined by

$$COV_{R_l} = \frac{std(R_l)}{mean(R_l)}, \tag{8.25}$$

Table 8.2 shows this quantity for different responses at the same wave cases as Table 8.1. It can be seen that the coefficients of variations of heave, pitch and bending moment are relatively low. For roll motion in beam sea cases, B and F, the coefficient of variation is very large, which implies a low reliability in estimation of this motion. The zero values correspond to the cases with negligible response variances (see Figures 7.3-7.7).

Table 8.2: Coefficient of variation for different responses.

Cases	Heave	Pitch	VBM	Sway	Roll
A	0.00	0.41	0.39	0.27	0.23
B	0.54	0.52	0.49	0.45	0.82
C	0.00	0.00	0.00	0.34	0.12
D	0.00	0.00	0.00	0.16	0.00
E	0.55	0.20	0.27	0.49	0.59
F	0.24	0.35	0.57	0.37	1.28
G	0.32	0.22	0.28	0.61	0.51
H	0.43	0.16	0.00	0.00	0.85

8.5 Conclusion

This chapter shows the applicability of different methods to assess uncertainties in the presented parametric wave estimation method and to evaluate the reliability of response predictions for decision support. Although the differences between computational methods for transfer function calculations can be quite large, the impact of this uncertainty on wave parameter estimates is not considerable in the studied cases.

Uncertainty analysis can be also carried out by using linear error propagation. In this method, propagation of the errors in the inputs, such as wind and response measurements, or transfer functions, to the estimates of wave parameters is evaluated.

The uncertainties of the predicted short-term responses are studied in terms of the coefficients of variations for the variances of those responses. This is implemented by taking both the estimated wave parameters and the transfer functions as random variables to the response estimator. The standard deviations in the response variances are evaluated using Monte-Carlo simulations.

The proposed methods in this chapter introduce possibilities for uncertainty evaluation. The practical examples are simplified and the results are limited. So, further studies are needed to evaluate reliability of the estimation methods.

Chapter 9

Conclusions and Recommendations

9.1 Conclusions

The main purpose of this thesis is to investigate possible improvement in real-time sea state estimation onboard ships and the predictability of ship responses. This is useful for developing decision support systems. A refined parametric modelling approach for the estimation of waves using measured ship responses is proposed. The method is based on the summation of two generalised JONSWAP models representing double-peaked directional wave spectra. The optimisation problem is formulated based on energy balance of the responses, in terms of spectral moments, being measured and theoretically calculated. This approach applies a sequential partitioning procedure, which is able to classify swell and wind-sea events. Real-time wind information is utilised to restrict the parameters to be fitted. This can overcome the lack of information in the high frequency part of the wave spectrum. The procedure is relatively simple and the computation time is reasonably short.

The wave characteristics that can be estimated by ship responses depend on the ship characteristics and operational/environmental conditions, e.g. the ship speed, the draft, and the relative direction of waves. Thus, in order to make sure that the selected responses are sufficiently sensitive to the waves, looking at the particular transfer functions is recommended. The responses are chosen in a way that the set of governing equations in the optimisation problem has a low uncertainty in terms of transfer function calculations. Additionally,

a systematic and efficient approach for automatic response selection is also presented by local sensitivity of wave parameters to different responses in a typical condition. This sensitivity analysis is based on first-order partial derivative calculations.

The wave estimation method is evaluated using simulated and full-scale data for two container ships as case studies. In the numerical simulation study, the procedure is examined for different wave scenarios including unimodal and bimodal spectra. Global optimisation is applied and the average values of estimated main parameters, i.e. the significant wave heights, the peak periods and the mean wave train directions are generally very close to the true values and the standard deviations are quite satisfactory. However, the shape parameters of the spectra, i.e. the spreading factors and the peakedness factors are sometimes erroneous. Thus, the current method, where only the moments of spectra are considered, is able to estimate the main integral parameters of individual systems, but it is not efficient as an estimator of the complete wave spectral shape. Nevertheless, the spectral shape of the waves may be unnecessary for onboard applications.

The estimations are also carried out using a different set of transfer functions from a different numerical model. This can address the impact of uncertainty of transfer function calculations on the wave estimation results. The robustness of the method for estimating the associated wave parameters is approved to some extent.

The results based on full-scale data of the same container ship (9400 TEU) strengthen the efficiency and robustness of the presented method particularly in unimodal waves. Comparing the results with other wave information sources such as radar and hindcast data, proves the validity of the method in general. Moreover, comparisons between the present method and the outcome of other response-based wave estimation methods are made in a few available cases. An increased accuracy is observed in the current method especially compared to the traditional parametric approach. In general, swell estimations based on parametric methods seem to be less accurate rather than wind seas, which is likely to be due to uncertainty in swell modelling. The comparisons between the results of full-scale data for another container ship and the hindcast data give a similar interpretation.

A dynamic trend model is fitted to the estimated wave parameters to track their evolution. This can provide a more efficient predictability during the voyage. The predictions are made in a time horizon of 20 minutes ahead of current measurements. The predictions and the confidence levels can also be used as initial guesses or constraints in the estimation procedures. The wave parameters are used to predict the future responses of the ship. The results show a good agreement between the predictions and the actual measurements.

In order to assess the reliability of the wave estimation method, uncertainty analysis is important. In that respect, random uncertainties of the transfer functions are considered using linear error propagation. Statistical inference of response variances is also dealt with using Monte-Carlo simulations, which can be useful for a reliability assessment of response predictions.

All in all, this study proves the maturity and reliability of the response-based sea state estimation method for ships with forward speed. However, it is inevitable that in reality, there might be a lack of accuracy in estimation procedure because of possible errors in acquiring data during measurements of responses and wind as well as evaluating spectra from a finite length of data. Therefore, further investigations should be carried out on real data to verify the applicability of the partitioning approach. The estimations are highly dependent on wind data, and unavailability or inaccuracy of this information onboard ships is not considered in this study.

9.2 Recommendation For Future Works

It is of interest to consider a wide range of wave scenarios numerically to extract the limiting wave characteristics that can be estimated by the method for a specific ship at different loading conditions. Since this limit depends highly on the length of the ship, larger-sized ships should be studied as well to see if the method is still valid for e.g. 18000 TEU container ships. As the ship size increases, ship motions become less significant since wave lengths are much shorter than ship length. However, for those vessels, decision support system is still important because hydroelastic vibrations (springing and whipping) can become critical for structural integrity.

It is noteworthy that initialisations are still critical in parametric methods, especially for wave direction estimation. In the swell systems, additional constraints using other sources of data may improve the results. For example, the local meteorological data can be utilised to provide proper limits for the wave parameters in a specific area, where the ship is operating. The wave spectral model can also be updated based on local information. Moreover, trend analysis of the estimations can be used as constraints to avoid outliers in the optimisation procedure. The impact of such conditioning on the results should be studied. If proper constraints are applied, the speed of optimisation can be increased 2-3 times.

As mentioned before, different models of wave spectra are used in the literature for parametric estimation of waves. It would be interesting to study the sensitivity of the estimates to the chosen model.

Most of the results in the different methods of wave buoy analogy, rely on numerical simulations. To validate the estimation processes, further studies on properly calibrated full-scale data or experimental data are still required. A data quality control is important to be developed to make the estimations more reliable.

It is difficult to state which estimation procedure, parametric modellings (the traditional version or the current version) or non-parametric methods (Bayesian method or Kalman filtering method) is the most efficient. The literature also reflects different opinions about this. In order to choose the optimum method, the associated results should be compared. In addition, a capability to merge data from different methods or sources would be helpful.

Apart from the method to be used, the optimum response selection is very important for wave estimation. The proposed method based on sensitivity analysis can be applied within the estimation procedure to see if it improves the results. In addition, the applicability and development of the introduced methods for uncertainty analysis could be investigated.

The wave estimation model in this thesis focuses on linear ship responses. It would be interesting to investigate the possibility of using nonlinear responses to estimate waves. For instance, the measured power and the estimated drift force, combined with the corresponding transfer functions may be useful for wave estimation. The measured upcrossing rate of high frequency sagging/hogging may also be used if empirical relations between those rates and significant wave heights and zero upcrossing periods are available. Other responses that are more commonly measured onboard ships are engine RPM and rudder angle. The latter responses are highly correlated with the wave period and the mean direction. Nevertheless, the nonlinearity and uncertainty of theoretical relations between waves and responses make the optimisation more complex and less accurate.

References

[1]. Andersen, I. M. and Storhaug, G. Dynamic selection of ship responses for estimation of on-site directional wave spectra. In *Proceedings of the 31th International Conference on Offshore Mechanics and Arctic Enginering*, 2012.

[2]. Andersen, I. M. V. *Full scale measurements of the hydro-elastic response of large container ships for decision support.* PhD thesis, Department of Mechanical Engineering, Technical University of Denmark, 2014.

[3]. Andersen, I. M. V., Jensen, J. J., and Nielsen, U. D. Evaluation of response prediction procedures using full scale measurements for a container ship. *Proceedings of the Prads 2013*, 2013.

[4]. Bach, K. F. Transfer functions of a large containership. Master thesis, Department of Mechanical Engineering, Technical University of Denmark, 2015.

[5]. BIPM, IEC, IFCC, ILAC, ISO, IUPAC, IUPAP, and OIML. Evaluation of measurement dataguide to the expression of uncertainty in measurement, JCGM 100: 2008 GUM 1995 with minor corrections, 2008.

[6]. Bitner-Gregersen, E. M., , and Hagen, O. Uncertainties in data for the offshore environment. *Structural Safety, Struct. Saf, Struct Saf*, 7(1): 11–34, 1990. ISSN 18793355, 01674730.

[7]. Bitner-Gregersen, E. M., Elzbieta, M., and Skjong, R. Concept for a risk based navigation decision assistant. *Marine Structures*, 22(2):275–286, 2009.

[8]. Bitner-Gregersen, E. M., Ewans, K. C., and Johnson, M. C. Some uncertainties associated with wind and wave description and their importance

for engineering applications. *Ocean Engineering*, 86:11–25, 2014.

[9]. Boukhanovsky, A. V. and Guedes Soares, C. Modelling of multipeaked directional wave spectra. *Applied Ocean Research*, (2):132–141, April . ISSN 01411187. doi: 10.1016/j.apor.2009.06.001.

[10]. Brun, R., Kühni, M., Siegrist, H., Gujer, W., and Reichert, P. Practical identifiability of asm2d parameters systematic selection and tuning of parameter subsets. *Water Research*, 36(16):4113–4127, 2002.

[11]. Davis, M. R., Watson, N. L., and Holloway, D. S. Measurement of Response Amplitude Operators for an 86 m High-Speed Catamaran. *Journal of ship researchShip Research*, 49(2):121–143, 2005.

[12]. Drouet, C., Cellier, N., Raymond, J., and Martigny, D. Sea state estimation based on ship motions measurements and data fusion. *Proceedings of the Asme 32nd International Conference on Ocean, Offshore and Arctic Engineering - 2013 - Vol 5*, 5:V005T06A049, 2013. doi: 10.1115/omae2013-10657.

[13]. Ewans, K. C., Bitner-Gregersen, E. M., and Guedes Soares, C. Estimation of Wind-Sea and Swell Components in a Bimodal Sea State. *Journal of Offshore Mechanics and Arctic Engineering*, 128(4):265, 2006. ISSN 08927219. doi: 10.1115/1.2166655. URL `http://offshoremechanics.asmedigitalcollection.asme.org/article.aspx?articleid=1456243`.

[14]. Ewans, K. C., Vanderschuren, L., and Tromans, P. S. FPSO Conference, Estimating Wind-Sea and Swell for FPSO Operability. *Journal of Offshore Mechanics and Arctic Engineering*, 128(4):314, 2006. ISSN 08927219. doi: 10.1115/1.2166653. URL `http://offshoremechanics.asmedigitalcollection.asme.org/article.aspx?articleid=1456271`.

[15]. Goda, Y. *Random Seas and Design of Maritime Structures*. University of Tokyo Press, 1985. ISBN 9780860083696.

[16]. Guedes Soares, C. Effect of spectral shape uncertainty in the short term wave-induced ship responses. *Applied Ocean Research*, 12(2):54–69, April 1990. ISSN 01411187. doi: 10.1016/S0141-1187(05)80030-6. URL `http://linkinghub.elsevier.com/retrieve/pii/S0141118705800306`.

[17]. Guedes Soares, C. Effect of transfer function uncertainty on short-term ship responses. *Ocean Engineering*, 18(4):329–362, 1991.

[18]. Guedes Soares, C. Representation of double-peaked sea wave spectra. *Ocean Engineering*, 11(2):185–207, 1984.

[19]. Hanson, J. L. and Phillips, O. M. Automated Analysis of Ocean Surface Directional Wave Spectra. *Journal of Atmospheric and Oceanic Technology*, 18(2):277–293, February 2001. ISSN 0739-0572. doi: 10.1175/1520-0426(2001)018⟨0277:AAOOSD⟩2.0.CO;2. URL `http://journals.ametsoc.org/doi/abs/10.1175/1520-0426\%282001\%29018\%3C0277\%3AAAOOSD\%3E2.0.CO\%3B2`.

[20]. Irvine, M., Longo, J., and Stern, F. Pitch and Heave Tests and Uncertainty Assessment for a Surface Combatant in Regular Head Waves. *Journal of Ship Research*, 52(2):146–163, 2008. ISSN 00224502.

[21]. Iseki, T. and Ohtsu, K. Bayesian estimation of directional wave spectra based on ship motions. *Control Engineering Practice, Control Eng. Practice, Con Eng Pr, Control Eng Pract, Control Eng Practice*, 8(2):215–219, 2000. ISSN 18736939, 09670661. doi: 10.1016/S0967-0661(99)00156-2.

[22]. Iseki, T. and Terada, D. Bayesian estimation of directional wave spectra for ship guidance system. *International Journal of Offshore and Polar Engineering, Int. J. Offshore Polar Eng, Int J Offsh, Int J Offshore Polar, Int J Offshore Polar Eng*, 12(1):25–30, 2002. ISSN 10535381.

[23]. Iseki, T., Baba, M., and Hirayama, K. Hybrid bayesian wave estimation for actual merchant vessels. *Marine Navigation and Safety of Sea Transportation: Maritime Transport and Shipping, Mar. Navig. Saf. Sea Transp.: Mar. Transp. Shipp*, pages 293–298, 2013.

[24]. Jacobi, G., Davis, M., and Davidson, G. Full-scale motions of a large high-speed catamaran: The influence of wave environment, speed and ride control system. *The Royal Institution of Naval Architects*, 2012.

[25]. Jensen, J. J. *Load and global response of ships*. Elsevier Ocean Engineering Book Series, 2001. ISBN 9780080439532.

[26]. Jensen, J. J. and Capul, J. Extreme response predictions for jack-up units in second order stochastic waves by FORM. *Probabilistic Engineering Mechanics*, 21(4):330–337, October 2006. ISSN 02668920. doi: 10.1016/j.probengmech.2005.11.007. URL `http://linkinghub.elsevier.com/retrieve/pii/S0266892005000834`.

[27]. Kerbiriou, M., Prevosto, M., and Maisondieu, C. Influence of an improved sea-state description on a wave energy convertor production. In *Proceedings*

of the 26th International Conference on Offshore Mechanics and Arctic Enginering, 2007.

[28]. Kim, Y. and Hermansky, G. Uncertainties in seakeeping analysis and related loads and response procedures. *Ocean Engineering*, 86:68–81, 2014.

[29]. Kitagawa, G. *Introduction to time series modeling*. Chapman, 2010. ISBN 1584889217, 9781584889212.

[30]. Lajic, Z. *Fault-tolerant Onboard Monitoring and Decision Support Systems*. PhD thesis, Department of Mechanical Engineering, Technical University of Denmark, December 2010.

[31]. Madsen, H. *Time Series Analysis*. CRC Press, 2007.

[32]. McCormick, M. E. *Ocean engineering mechanics: with applications*. Cambridge University Press, 2009.

[33]. Montazeri, N. and Nielsen, U. D. Parametric estimation in the wave buoy analogy - an elaborated approach based on energy considerations. In *Proceedings of the ASME 2014 33rd International Conference on Ocean, Offshore and Arctic Engineering (OMAE 2014)*, 2014.

[34]. Montazeri, N., Nielsen, U. D., and Jensen, J. J. Estimation of wind sea and swell using shipboard measurements a refined parametric modelling approach. *Applied Ocean Research*, 54:73–86, 2016. ISSN 18791549, 01411187. doi: 10.1016/j.apor.2015.11.004.

[35]. Nielsen, J. K., Pedersen, N. H., Michelsen, J., Nielsen, U. D., Baatrup, J., Jensen, J. J., and Petersen, E. S. SeaSense - Real-time Onboard Decision Support. In *Proc. of WMTC2006*, London, UK, 2006.

[36]. Nielsen, U. D. *Estimation of Directional Wave Spectra from Measured Ship*. PhD thesis, Technical University of Denmark, 2005.

[37]. Nielsen, U. D. Estimations of on-site directional wave spectra from measured ship responses. *Marine Structures*, 19(1):33–69, January 2006. ISSN 09518339. doi: 10.1016/j.marstruc.2006.06.001. URL `http://linkinghub.elsevier.com/retrieve/pii/S0951833906000529`.

[38]. Nielsen, U. D. Response-based estimation of sea state parameters- Influence of filtering. *Ocean Engineering*, 34(13):1797–1810, September 2007. ISSN 00298018. doi: 10.1016/j.oceaneng.2007.03.002. URL `http:`

//linkinghub.elsevier.com/retrieve/pii/S0029801807000625.

[39]. Nielsen, U. D. The wave buoy analogy estimating high-frequency wave excitations. *Applied Ocean Research*, 30(2):100–106, April 2008. ISSN 01411187. doi: 10.1016/j.apor.2008.07.002. URL http://linkinghub.elsevier.com/retrieve/pii/S014111870800031X.

[40]. Nielsen, U. D. Introducing two hyperparameters in Bayesian estimation of wave spectra. *Probabilistic Engineering Mechanics*, 23(1): 84–94, January 2008. ISSN 02668920. doi: 10.1016/j.probengmech.2007.10.007. URL http://linkinghub.elsevier.com/retrieve/pii/S0266892007000458.

[41]. Nielsen, U. D. *Ship Operations -Engineering Analyses and Guidance*. Lecture notes, Technical University of Denmark, 2010.

[42]. Nielsen, U. D. and Iseki, T. A Study on Parametric Wave Estimation Based on Measured Ship Motions. *Journal of Japan Institute of Navigation*, 126, 2012.

[43]. Nielsen, U. D. and Iseki, T. Blind estimation of a ship's relative wave heading. In *Proceedings of the ASME 2012 31st International Conference on Ocean, Offshore and Arctic Engineering*, pages 1–9. ASME, 2012.

[44]. Nielsen, U. D. and Iseki, T. Prediction of First-Order Vessel Responses with Applications to Decision Support Systems. In *Proc. of 5th WMTC (to appear in)*, Providence, RI, USA, 2015.

[45]. Nielsen, U. D. and Jensen, J. J. A novel approach for navigational guidance of ships using onboard monitoring systems. *Ocean Engineering*, 38(2-3):444–455, February 2011. ISSN 00298018. doi: 10.1016/j.oceaneng.2010.11.024. URL http://linkinghub.elsevier.com/retrieve/pii/S0029801810002696.

[46]. Nielsen, U. D. and Stredulinsky, D. C. Sea state estimation from an advancing ship A comparative study using sea trial data. *Applied Ocean Research*, 34:33–44, January 2012. ISSN 01411187. doi: 10.1016/j.apor.2011.11.001. URL http://linkinghub.elsevier.com/retrieve/pii/S0141118711000873.

[47]. Nielsen, U. D., Jensen, J. J., Pedersen, P. T., and Ito, Y. Onboard monitoring of fatigue damage rates in the hull girder. *Marine Structures*, 24:182–206, 2011.

[48]. Nielsen, U. D., Andersen, I. M. V., and Koning, J. Comparisons of Means for Estimating Sea States from an Advancing Large Container Ship. In *Proceeding of the PRADS 2013*. PRADS, 2013.

[49]. Ochi, M. K. and Hubble, E. N. Six-parameter wave spectra. *Coastal Engineering Proceedings*, 1(15), 1976.

[50]. Pascoal, R. and Guedes Soares, C. Non-parametric wave spectral estimation using vessel motions. *Applied Ocean Research*, 30(1):46–53, February 2008. ISSN 01411187. doi: 10.1016/j.apor.2008.03.003. URL `http://linkinghub.elsevier.com/retrieve/pii/S0141118708000163`.

[51]. Pascoal, R. and Guedes Soares, C. Kalman filtering of vessel motions for ocean wave directional spectrum estimation. *Ocean Engineering*, 36 (6-7):477–488, May 2009. ISSN 00298018. doi: 10.1016/j.oceaneng.2009.01.013. URL `http://linkinghub.elsevier.com/retrieve/pii/S0029801809000183`.

[52]. Pascoal, R., Guedes Soares, C., and Sorensen, A. Ocean Wave Spectral Estimation Using Vessel Wave Frequency Motions. *Journal of Offshore Mechanics and Arctic Engineering*, 129(2):90, 2007. ISSN 08927219. doi: 10.1115/1.2426986. URL `http://offshoremechanics.asmedigitalcollection.asme.org/article.aspx?articleid=1456353`.

[53]. Portilla, J., Ocampo-Torres, F. J., and Monbaliu, J. Spectral Partitioning and Identification of Wind Sea and Swell. *Journal of Atmospheric and Oceanic Technology*, 26(1):107–122, January 2009. ISSN 0739-0572. doi: 10.1175/2008JTECHO609.1. URL `http://journals.ametsoc.org/doi/abs/10.1175/2008JTECHO609.1`.

[54]. Qiu, W., Sales Junior, J., Lee, D., Lie, H., Magarovskii, V., Mikami, T., Rousset, J., Sphaier, S., Tao, L., and Wang, X. Uncertainties related to predictions of loads and responses for ocean and offshore structures. *Ocean Engineering*, 86:58–67, 2014. ISSN 00298018. doi: 10.1016/j.oceaneng.2014.02.031. URL `http://dx.doi.org/10.1016/j.oceaneng.2014.02.031`.

[55]. Rodriguez, G., Guedes Soares, C., Pacheco, M., and Perez-Martell, E. Wave Height Distribution in Mixed Sea States. *Journal of Offshore Mechanics and Arctic Engineering*, 124(1):34, 2002. ISSN 08927219. doi: 10.1115/1.1445794. URL `http://offshoremechanics.asmedigitalcollection.asme.org/article.aspx?articleid=1475388`.

[56]. Simos, A. N., Sparano, J. V., Tannuri, E. A., and Matos, V. L. F.

Directional Wave Spectrum Estimation Based on a Vessel 1 st Order Motions : Field Results. In *Proceedings of the Seventeenth Internaional Offshore and Polar Engineering Conference*, pages 1938–1944, Lisbon, Portugal, 2007. ISOPE. ISBN 9781880653685.

[57]. Simos, A. N., Tannuri, E. A., Sparano, J. V., and Matos, V. L. F. Estimating wave spectra from the motions of moored vessels: Experimental validation. *Applied Ocean Research*, 32(2):191–208, April 2010. ISSN 01411187. doi: 10.1016/j.apor.2009.10.004. URL `http://linkinghub.elsevier.com/retrieve/pii/S0141118709000923`.

[58]. Tannuri, E. A., Sparano, J. V., Simos, A. N., and Da Cruz, J. J. Estimating directional wave spectrum based on stationary ship motion measurements. *Applied Ocean Research*, 25(5):243–261, October 2003. ISSN 01411187. doi: 10.1016/j.apor.2004.01.003. URL `http://linkinghub.elsevier.com/retrieve/pii/S0141118704000070`.

[59]. Tannuri, E. A., Simos, A. N., Sparano, J. V., and Matos, V. L. F. Motion-based wave estimation: Small-scale tests with a crane-barge model. *Marine Structures*, 28(1):67–85, August 2012. ISSN 09518339. doi: 10.1016/j.marstruc.2012.05.002. URL `http://linkinghub.elsevier.com/retrieve/pii/S0951833912000366`.

[60]. Tannuri, E. A., da Silva Bispo, I. B., Simos, A. N., Filho, A. N. Q., da Cruz, J. J., and Carvalho, R. C. A. Development of an on-board wave estimation system based on the motions of a moored FPSO: Preliminary assessments from a field campaign. In *Proceedings of the ASME 2013 32nd International Conference on Ocean, Offshore and Arctic Engineering*, pages 1–8, Nantes, France, 2013. ASME.

[61]. Torsethaugen, K. and Haver, S. Simplified double peak spectral model for ocean waves. In *The Fourteenth International Offshore and Polar Engineering Conference*. International Society of Offshore and Polar Engineers, 2004.

[62]. Tutorial, W. A matlab toolbox for analysis of random waves and loads. *WAFO group, Lund institute of technology centre of mathematical science*, 2000.

[63]. Veritas, D. N. Modelling and analysis of marine operations. *Offshore Standard*, 2011.

[64]. Wang, D. W. and Hwang, P. A. An Operational Method for Separating Wind Sea and Swell from Ocean Wave Spectra. *Journal of Atmospheric and Oceanic Technology*, 18(2001):2052–2062, 2001.

Appendix A

Examples of spectral estimations of waves based on numerical studies in Chapter 4.

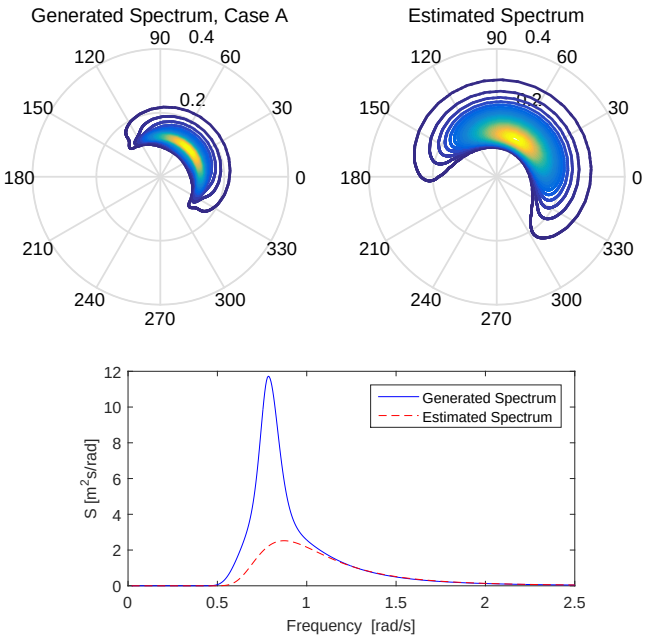

Figure A.1: Case A.

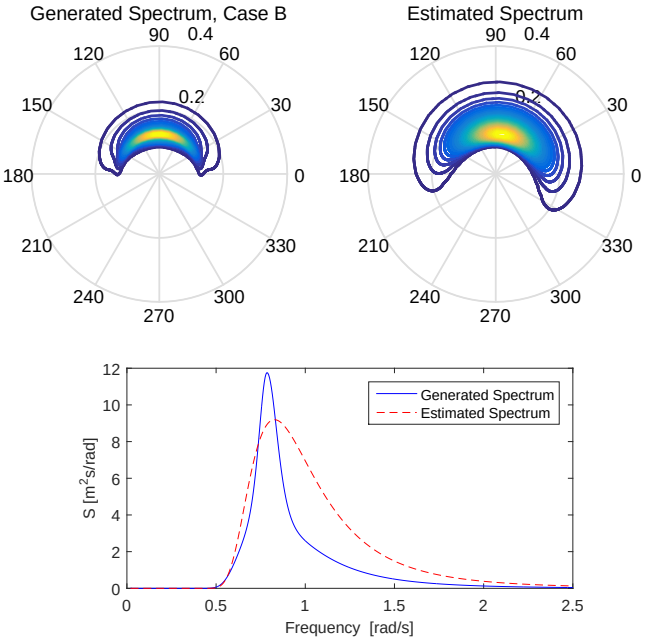

Figure A.2: Case B.

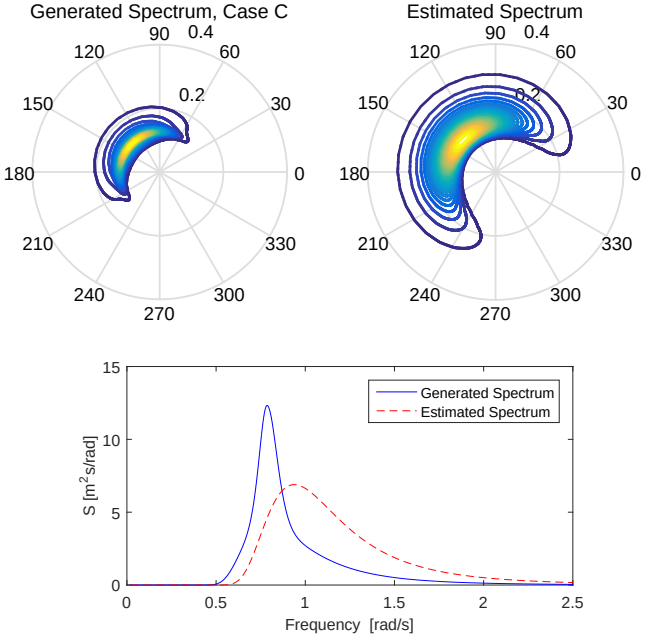

Figure A.3: Case C.

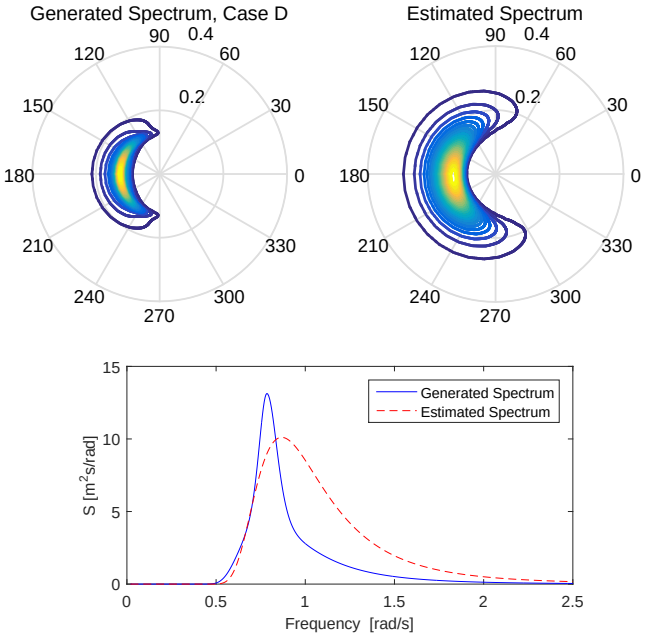

Figure A.4: Case D.

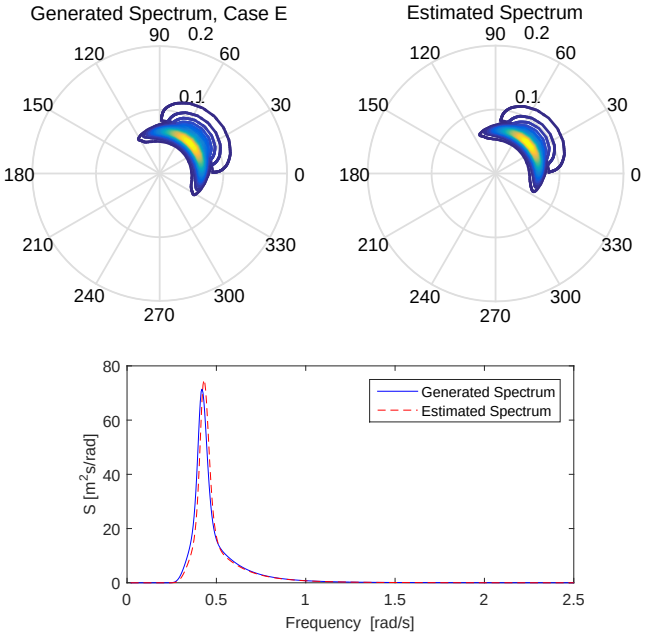

Figure A.5: Case E.

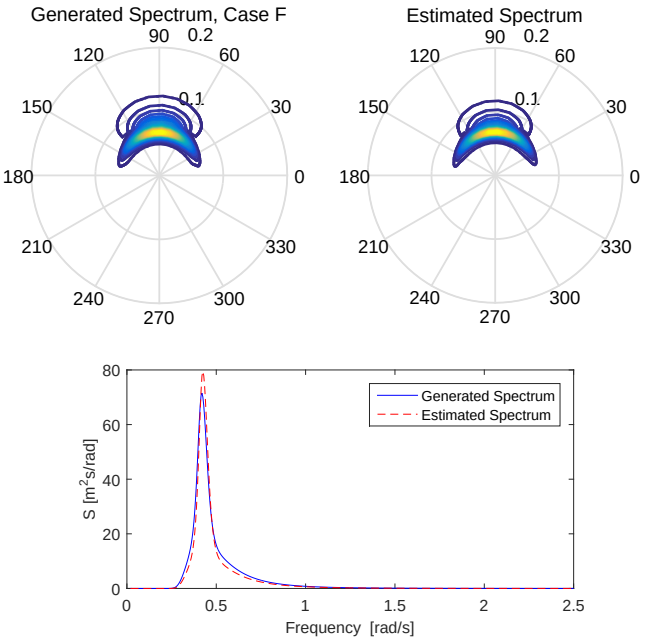

Figure A.6: Case F.

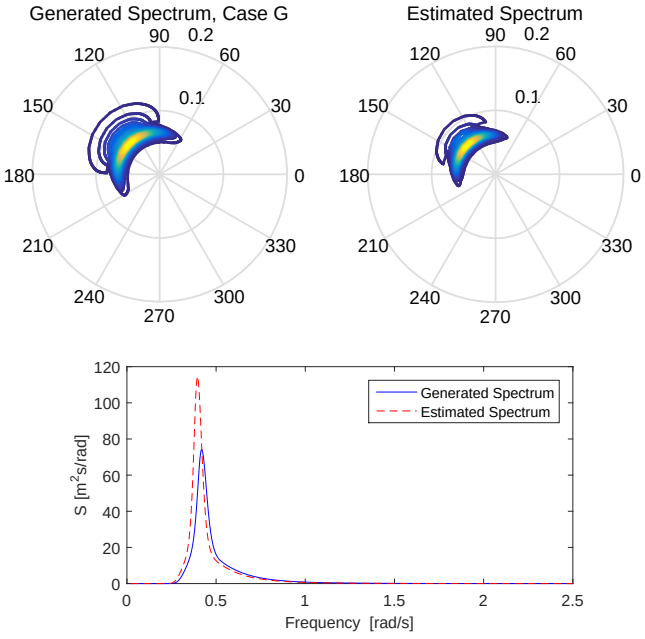

Figure A.7: Case G.

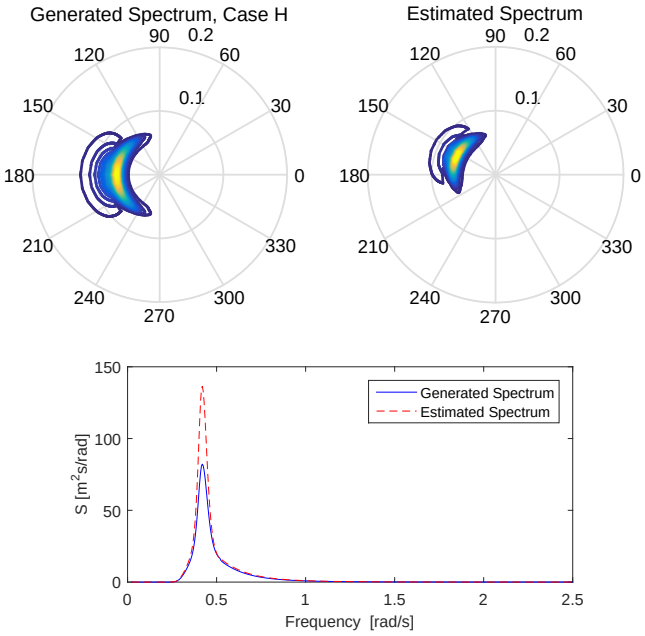

Figure A.8: Case H.

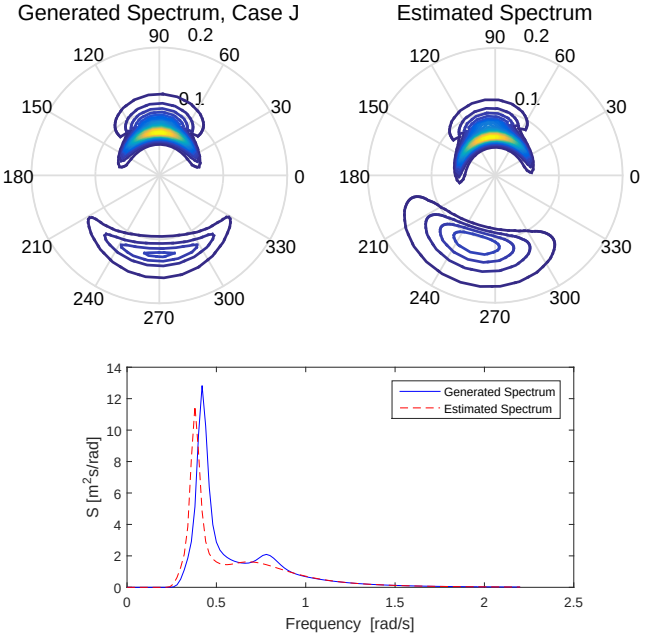

Figure A.9: Case J.

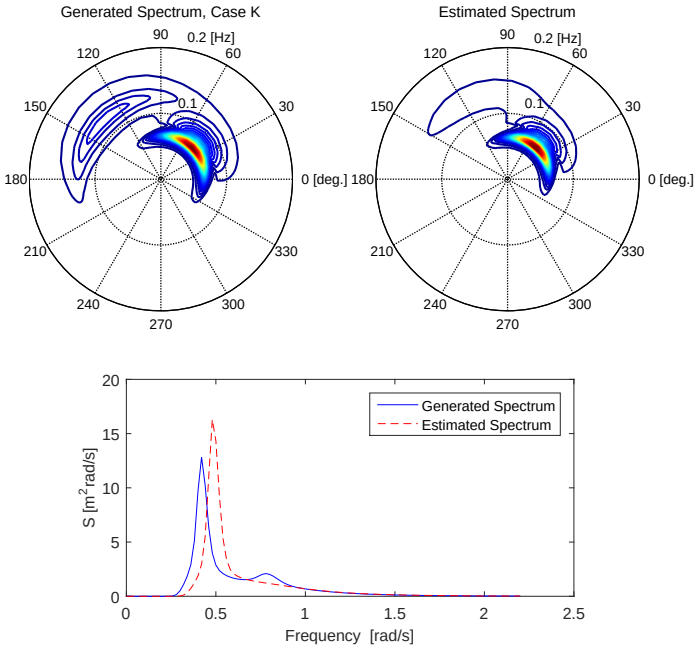

Figure A.10: Case K.

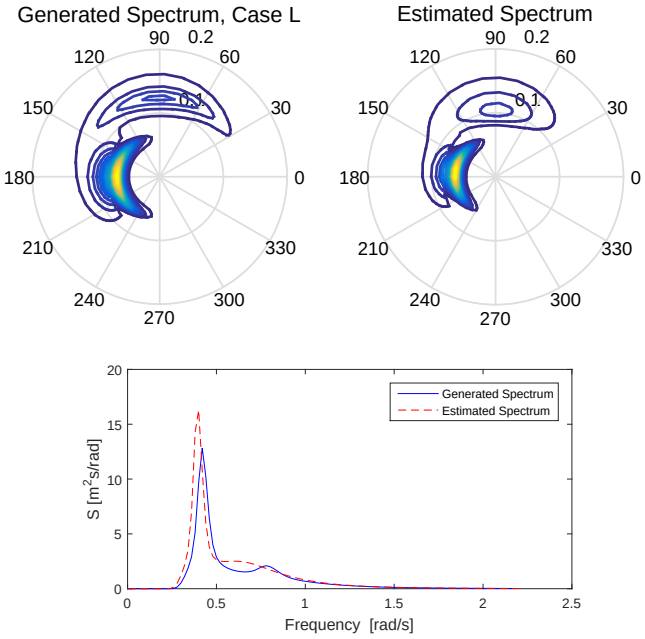

Figure A.11: Case L.

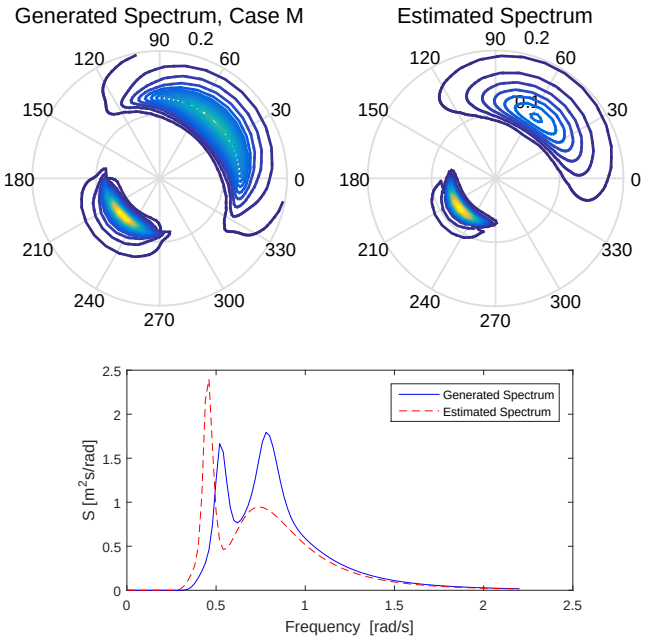

Figure A.12: Case M.

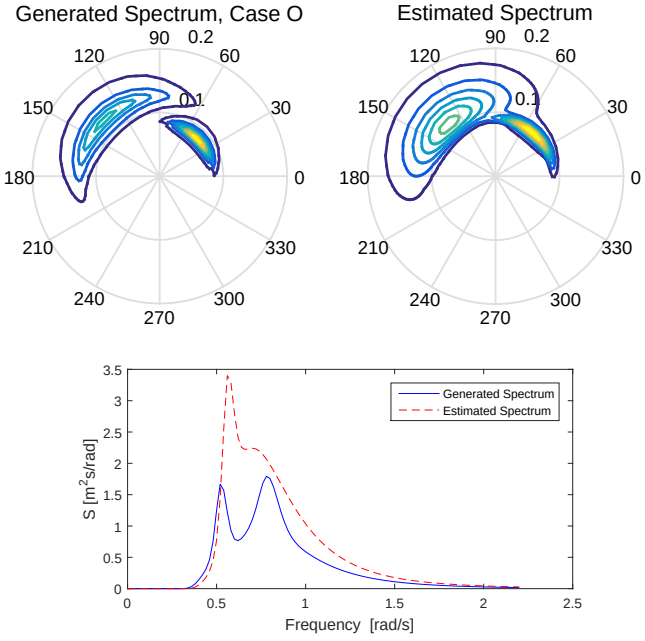

Figure A.13: Case O.

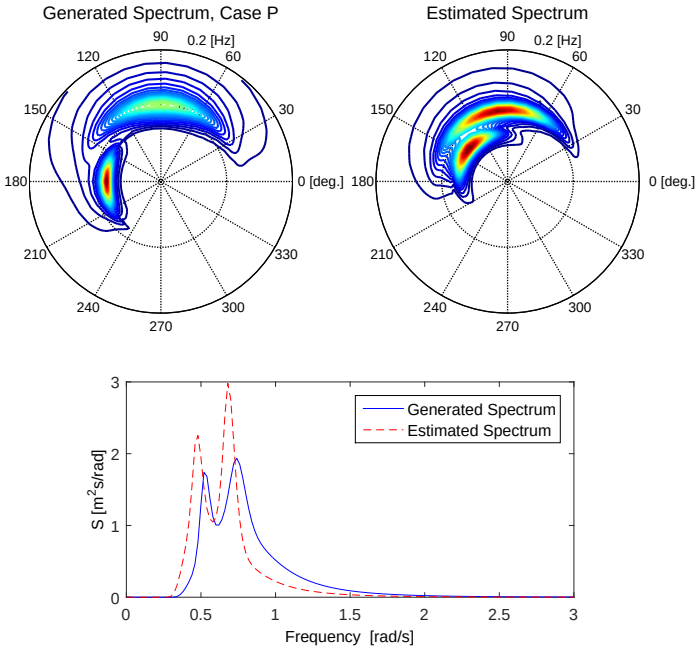

Figure A.14: Case P.

Appendix B

Table B.1: Coverage factors for t-distribution.

ν	60.0%	66.7%	75.0%	80.0%	87.5%	90.0%	95.0%	97.5%	99.0%	99.5%	99.9%
1	0.325	0.577	1.000	1.376	2.414	3.078	6.314	12.706	31.821	63.657	318.31
2	0.289	0.500	0.816	1.061	1.604	1.886	2.920	4.303	6.965	9.925	22.327
3	0.277	0.476	0.765	0.978	1.423	1.638	2.353	3.182	4.541	5.841	10.215
4	0.271	0.464	0.741	0.941	1.344	1.533	2.132	2.776	3.747	4.604	7.173
5	0.267	0.457	0.727	0.920	1.301	1.476	2.015	2.571	3.365	4.032	5.893
6	0.265	0.453	0.718	0.906	1.273	1.440	1.943	2.447	3.143	3.707	5.208
7	0.263	0.449	0.711	0.896	1.254	1.415	1.895	2.365	2.998	3.499	4.785
8	0.262	0.447	0.706	0.889	1.240	1.397	1.860	2.306	2.896	3.355	4.501
9	0.261	0.445	0.703	0.883	1.230	1.383	1.833	2.262	2.821	3.250	4.297
10	0.260	0.444	0.700	0.879	1.221	1.372	1.812	2.228	2.764	3.169	4.144
11	0.260	0.443	0.697	0.876	1.214	1.363	1.796	2.201	2.718	3.106	4.025
12	0.259	0.442	0.695	0.873	1.209	1.356	1.782	2.179	2.681	3.055	3.930
13	0.259	0.441	0.694	0.870	1.204	1.350	1.771	2.160	2.650	3.012	3.852
14	0.258	0.440	0.692	0.868	1.200	1.345	1.761	2.145	2.624	2.977	3.787
15	0.258	0.439	0.691	0.866	1.197	1.341	1.753	2.131	2.602	2.947	3.733
16	0.258	0.439	0.690	0.865	1.194	1.337	1.746	2.120	2.583	2.921	3.686
17	0.257	0.438	0.689	0.863	1.191	1.333	1.740	2.110	2.567	2.898	3.646
18	0.257	0.438	0.688	0.862	1.189	1.330	1.734	2.101	2.552	2.878	3.610
19	0.257	0.438	0.688	0.861	1.187	1.328	1.729	2.093	2.539	2.861	3.579
20	0.257	0.437	0.687	0.860	1.185	1.325	1.725	2.086	2.528	2.845	3.552

Appendix C

Comparisons of the wave estimation results based on RAO1 and RAO2.

Table C.1: Parameters of unimodal spectrum (Wind Sea).

Case		H_s(m)	T_p(s)	μ(deg.)	s_{max}
A	real	3	8	45	10
	mean (RAO1)	2.1	7.2	63	15
	mean (RAO2)	2.5	7.8	60	17
	std (RAO1)	0.19	0.36	15	4.4
	std (RAO2)	0.2	0.16	13	4.2
B	real	3	8	90	10
	mean (RAO1)	3.9	7.6	81	18
	mean (RAO2)	3.2	8.7	80	10
	std (RAO1)	0.4	0.2	12.5	5
	std (RAO2)	0.45	0.5	15	8
C	real	3	8	135	10
	mean (RAO1)	3.5	6.7	136	16
	mean (RAO2)	3.3	9.1	157	15
	std (RAO1)	0.43	0.35	10	4
	std (RAO2)	0.53	0.7	15	6
D	real	3	8	180	10
	mean (RAO1)	4	7.2	-176	12
	mean (RAO2)	2.9	8.5	171	18
	std (RAO1)	0.64	0.6	2	10
	std (RAO2)	0.5	0.7	6	12

Table C.2: Parameters of unimodal spectrum (Swell).

Case		H_s(m)	T_p(s)	μ(deg.)	s_{max}	γ
E	real	5	15	45	25	4
	mean (RAO1)	4.9	14.6	43	27	5
	mean (RAO2)	4.9	14.7	41	27	5.8
	std (RAO1)	0.34	0.52	7	19	2.26
	std (RAO2)	0.35	0.62	8.5	19	1.9
F	real	5	15	90	25	4
	mean (RAO1)	4.8	14.8	90.8	23	6
	mean (RAO2)	4.9	14.5	81	27	6
	std(RAO1)	0.5	0.32	1.3	4	1.8
	std(RAO2)	0.5	1.2	3.2	3	2.1
G	real	5	15	135	25	4
	mean (RAO1)	5.5	15.9	135	52	6
	mean (RAO2)	5.2	16.4	145	57	5.5
	std (RAO1)	0.5	0.37	2	14.4	0.9
	std (RAO2)	0.6	0.7	5.5	11.5	1
H	real	5	15	180	25	4
	mean (RAO1)	6	15	155	61	6
	mean (RAO2)	5.9	15	167	71	6.4
	std (RAO1)	0.4	0.5	2.5	12	0.6
	std (RAO2)	0.4	0.4	4.7	12	0.3

Table C.3: Parameters of bimodal spectrum (1).

Case		Wind sea				Swell				
		H_s(m)	T_p(s)	μ(deg.)	s_{max}	H_s(m)	T_p(s)	μ(deg.)	s_{max}	γ
I	real	3	8	45	10	5	15	-135	25	4
	mean (RAO1)	3.1	8.8	66	15	5.2	15	-160	33	1.5
	mean (RAO2)	4	8.5	52	15	4.2	15	-101	60	5.8
	std (RAO1)	0.7	0.49	10	0	0.65	0.58	12	5.8	0.6
	std (RAO2)	0.3	0.55	1.5	5	0.8	0.45	13	20	2
J	real	3	8	-90	10	5	15	90	25	4
	mean (RAO1)	3.2	8.6	-106	18	4.4	16.6	98	27	4.4
	mean (RAO2)	3.6	9.2	-92	20	3.8	15.1	120	47	5.4
	std (RAO1)	0.57	0.75	22	2	1.3	1	7.6	14	2.9
	std (RAO2)	0.25	1.3	17	0	0.08	0.6	30	20	2.1
K	real	3	8	135	10	5	15	45	25	4
	mean (RAO1)	2.3	7.3	120	12	5.5	13	49	65	6
	mean (RAO2)	3.4	6.7	141	15	5.8	12.8	3	64	7
	std (RAO1)	0.5	0.8	13	0	0.4	0.15	14	20	4
	std (RAO2)	0.2	0.2	10	3	0.5	0.14	16	23	2
L	real	3	8	90	10	5	15	180	25	4
	mean (RAO1)	3.6	9.12	89	15	5.3	16	174	49	4.8
	mean (RAO2)	3.3	6.8	100	18	5.8	14.15	176	59	5
	std (RAO1)	0.5	0.17	2	0	0.93	2.7	4	28	2.1
	std (RAO2)	1	0.9	2	4	0.81	0.6	11	12	3

Table C.4: Parameters of bimodal spectrum (2).

Case		Wind sea				Swell				
		H_s(m)	T_p(s)	μ(deg.)	s_{max}	H_s(m)	T_p(s)	μ(deg.)	s_{max}	γ
M	real	3	8	45	10	2	12	-135	25	4
	mean (RAO1)	2.7	8.3	56	19	2	13.9	-140	39	7
	mean (RAO2)	4.3	9.7	25	17	1.7	14.2	-155	53	3.4
	std (RAO1)	0.5	0.8	18.6	3.5	0.3	1.4	31	13	2
	std (RAO2)	0.7	1.4	9	6	0.3	0.3	15	11	2
N	real	3	8	-90	10	2	12	90	25	4
	mean (RAO1)	2.7	9.5	-102	21	2.6	13	110	38	5.2
	mean (RAO2)	3.8	7.7	-85	20	2	12.4	85	33	6
	std (RAO1)	0.66	1.28	17	3.8	0.19	1.7	25	22	4.3
	std (RAO2)	0.6	1.4	13	0	0.3	1.8	29	20	5
O	real	3	8	135	10	2	12	45	25	4
	mean (RAO1)	4	8.7	132	15	2.3	11.2	50	30	6.8
	mean (RAO2)	3.8	7.3	112	15	3.2	9.4	35	75	4.3
	std (RAO1)	0.6	0.9	15	0	0.18	0.95	9.3	7	2.4
	std (RAO2)	0.7	0.8	23	5	0.6	0.5	4	2	3
P	real	3	8	90	10	2	12	180	25	4
	mean (RAO1)	3.8	8.1	96	15	2.2	12.8	132	53	5.6
	mean (RAO2)	4.1	8.2	88	19	2.4	12.6	127	45	6
	std (RAO1)	0.37	1	34	4	0.3	0.4	6	11	2.1
	std (RAO2)	0.8	0.8	42	7	0.3	0.5	5	13	2.8